ELUCIDATING THE NEUROINFLAMMATORY SIGNALING ROLES OF HEME IN ALZHEIMER'S DISEASE ENVIRONMENTS

A Dissertation
Presented to
The Academic Faculty

by

Sitara Bala Sankar

In Partial Fulfillment
of the Requirements for the Degree
Doctor of Philosophy in Biomedical Engineering

Georgia Institute of Technology and Emory University
May 2020

ELUCIDATING THE NEUROINFLAMMATORY SIGNALING ROLES OF HEME IN ALZHEIMER'S DISEASE ENVIRONMENTS

Approved by:

Dr. Levi B. Wood, Advisor
George W. Woodruff School of Mechanical Engineering
Georgia Institute of Technology

Dr. Manu O. Platt
Wallace H. Coulter Department of Biomedical Engineering
Georgia Institute of Technology

Dr. Yulia Grishchuk
Center for Genomic Medicine
Massachusetts General Hospital

Dr. Amit R. Reddi
School of Chemistry and Biochemistry
Georgia Institute of Technology

Dr. Michelle C. LaPlaca
Wallace H. Coulter Department of Biomedical Engineering
Georgia Institute of Technology

Date Approved: December 13, 2019

ACKNOWLEDGEMENTS

This work would not have been possible without the guidance and support of so many wonderful people in my life. I would like to acknowledge them here.

First, I would like to thank my advisor, Dr. Levi Wood, for taking a chance on me right at the beginning of his career, back when I didn't know how to do anything. His mentorship gave me the direction to develop into a confident and rigorous scientist and encouraged my enthusiasm for scientific discovery. I will always be grateful for all that he has taught me.

I owe many thanks to the members of the Wood Lab, who have provided me with the support, guidance, and feedback necessary to conquer many research roadblocks over the years. Special thanks go to Alyssa Pybus and Kristie Garza, who have been my pillars of support, both experimentally and emotionally, and made the workplace a fun place to be. I am fortunate to have had colleagues I could so readily rely on, but mostly I am thankful that we are friends.

I am incredibly grateful for the undergraduate students I have had the opportunity to mentor, Kajol Shah, Mary Catherine Bryant, and Andres Begazo. Their hard work has been pivotal in driving the progress of this project and their presence in the lab has made my days so much brighter. Watching them grow into independent researchers has been one of the most rewarding aspects of graduate school.

I wish to acknowledge my committee members, Dr. Amit Reddi, Dr. Manu Platt, Dr. Michelle LaPlaca, and Dr. Yulia Grishchuk, who not only contributed their time and

expertise to help steer this project, but have also served as strong role models for what a scientist should be.

I have been extremely fortunate to work with incredible collaborators on this project. I owe much gratitude to Dr. Rebecca Donegan and Dr. David Hanna, who taught me everything I know about heme and made numerous scientific contributions to this work. So much of this project would not have been possible without their expertise and assistance.

I wish to thank Kathryn Murray, who I met day one at Georgia Tech, for her constant friendship and for always lifting my spirits when I needed it. So much in our lives has changed over the years, but I am glad that we haven't.

I owe much gratitude to my parents, Asha and Subra, and my sister Ankita for their support over the years and their encouragement of my scientific career. Their love and support has been critical to my success.

Finally, I wish to thank Ilya Kolb, my best friend and biggest fan, whose belief in me over the years has been unwavering, even in those moments when I most doubted myself. I am lucky to have a found a partner to share in all my hardship and happiness, both in this journey and beyond.

TABLE OF CONTENTS

LIST OF TABLES

LIST OF FIGURES

heme, were incubated with pH sensitive pHrodo beads to assess phagocytic capacity. The percentage of total cells uptaking beads, quantified by fluorescence microscopy and ImageJ, was significantly reduced upon treatment with Hb (n=32 images; $p<0.0001$; vehicle vs. 50 nM heme and vehicle vs. 25 μM heme). C. Representative fluorescent microscopy images of pHrodo bead (red) phagocytosis by control, 50 nM heme, and 25 μM heme treated SIM-A9 microglia co-stained for phalloidin (green) and DAPI (blue). Scale bars: 50 μm. *This figure was originally published in the Journal of Biological Chemistry. Sankar et al. Heme and hemoglobin suppress amyloid β–mediated inflammatory activation of mouse astrocytes. J. Biol. Chem. 2018; 293: 11358-11373. © the American Society for Biochemistry and Molecular Biology*

LIST OF SYMBOLS AND ABBREVIATIONS

a.u.	Arbitrary units
Aβ	Amyloid beta
$A\beta_{1-42}$	Amyloid beta (1-42)
AD	Alzheimer's disease
Akt	Protein kinase B
ALA	Aminolevulinic acid synthase
ANOVA	Analysis of variance
APP	Amyloid precursor protein
ATCC	American Type Culture Collection
BACE1	Beta secretase 1
BBB	Blood brain barrier
BCA	Bicinchoninic acid
BSA	Bovine serum albumin
CCL	C-C motif ligand
CD	Cluster of differentiation
CO	Carbon monoxide
CSF	Cerebrospinal fluid
CXCL	C-X-C motif ligand
DAPI	4′,6-diamidino-2-phenylindole
DMEM	Dulbecco's modified Eagle Medium
DPBS	Dulbecco's phosphate-buffered saline
EGFP	Enhanced green fluorescent protein

FBS	Fetal bovine serum
GFAP	Glial fibrillary acidic protein
GM-CSF	Granulocyte-Macrophage Colony Stimulating Factor
Hb	Hemoglobin
HBSS	Hank's balanced salt solution
HD	Heme depleted
HFIP	Hexafluoroisopropyl alcohol
HMW	High molecular weight
HS1	Heme sensor 1
IGF1R	Insulin-like growth factor 1 receptor
IL	Interleukin
IP	Intraperitoneal
IP-10	Interferon-inducible protein-10
IR	Insulin receptor (IR)
Jak	Janus kinase
KC	Keratinocyte chemoattractant
LMW	Low molecular weight
LOOCV	Leave one out cross validation
LTP	Long-term potentiation
LV	Latent variable
M-CSF	Macrophage Colony Stimulating Factor
MAPK	Mitogen-activated protein kinase
MCI	Mild cognitive impairment
MCP	Monocyte Chemoattractant Protein
mRNA	Messenger ribonucleic acid

mTOR	Mammalian target of rapamycin
NF-κB	Nuclear factor kappa-light-chain-enhancer of activated B cells
OBB	Odyssey blocking buffer
p-	Phosphorylated
PBS	Phosphate-buffered saline
PFA	Paraformaldehyde
PLSDA	Partial least squares discriminant analysis
PI3K	Phosphatidylinositol 3-kinase
PMSF	Phenylmethylsulfonyl fluoride
PSD95	Postsynaptic density 95
RANTES	Regulated on Activation, Normal T Cell Expressed and Secreted
RT	Room temperature
SA	Succinylacetone
SDS	Sodium dodecyl sulfate
SEM	Standard error of the mean
STAT	Signal transducer and activator of transcription
TBST	Tris-buffered saline + Tween 20
TGF	Transforming growth factor
TLR4	Toll-like receptor 4
TNF-α	Tumor necrosis factor-α
VEGF	Vascular endothelial growth factor
WT	Wild Type

SUMMARY

The prevalence of Alzheimer's disease (AD) is rapidly increasing, yet there are currently no effective therapies to halt or slow disease progression. In light of the vast failures of therapies targeting traditional AD hallmarks, such as amyloid beta (Aβ), it is becoming increasingly recognized that a combination of many complex pathological events, including neuroinflammation, contributes to AD. Thus, it is necessary to pursue novel therapeutic strategies to address multiple pathological aspects of AD.

Recent findings of vascular permeability early in AD implicate blood-derived factors in AD pathology. Indeed, hemoglobin (Hb) and its co-factor, heme, are upregulated in AD brain tissue and physically bind Aβ, suggesting a role for these molecules in AD pathogenesis. However, to date there is little understanding of how these factors affect disease progression. Although less appreciated than their roles in oxygen transport, heme and Hb have potent immunomodulatory signaling functions, but these functions have not been established in the context of the brain immune cells, astrocytes and microglia. Given the importance of neuroinflammation to AD pathology, the objective of this work is to elucidate the contribution of heme to neuroinflammatory signaling in AD environments.

The present work accomplishes this by using *in vitro* and *in vivo* models to determine the effects of heme, Hb, and their interactions with Aβ on glial immune function and to interrogate heme-mediated intracellular signaling mechanisms. Our findings suggest that heme and Hb suppress a myriad of critical glial immune functions, including cytokine expression, expression of scavenger receptors, and clearance of Aβ. Furthermore, we found that heme exerts these effects through modulation of the PI3K/AKT/mTOR signaling

pathway. This work is the first to identify mechanisms through which heme contributes to glial dysfunction in AD environments and suggests that heme could serve as a novel therapeutic target for AD.

CHAPTER 1. INTRODUCTION

1.1 Current Alzheimer's disease landscape

Alzheimer's disease (AD) is a chronic, neurodegenerative disease which affects more than 40 million people worldwide and is the most common cause of dementia [1, 2]. With an aging population, the prevalence of AD is rapidly increasing, with AD currently affecting twice as many people as in 1990 [3]. By 2050, the prevalence of AD is projected to more than triple to affect 130 million people globally [1]. Symptoms of AD are debilitating, including gradual loss of memory, language, and cognitive abilities, which affect a patient's ability to perform everyday tasks [2]. In the advanced stages of AD, patients lose the ability to carry out even basic bodily functions such as walking and swallowing, and ultimately the disease is fatal [2]. Although decades of research have gone into uncovering the mechanisms underlying AD, there is still no effective therapy to halt or slow disease progression. In fact, in the United States, AD is the only leading cause of death that cannot be prevented, cured, or slowed, and deaths due to AD have increased by 89% since the year 2000 [2]. Furthermore, the worldwide cost of AD is over $800 billion, and is expected to surpass $1 trillion in the coming years [1]. Thus, AD presents a formidable challenge for healthcare and society globally, urging the rapid development of effective therapies.

While numerous efforts have been made towards therapeutic intervention in AD, there are several major roadblocks inhibiting their success. AD is unlike many other modern diseases in that the mechanisms defining it are incredibly multifaceted and remain poorly understood. While familial AD is well-characterized by mutations in the amyloid

precursor protein (APP), presenilin1, and presenilin2 genes, more common is sporadic AD, which still lacks a clear etiology and is likely caused by a combination of genetic and environmental factors [4]. AD is comorbid with a diverse array of other medical conditions spanning from psychiatric disorders, (ie. chronic depression [5]), acute traumatic brain injuries [6], vascular disorders (ie. hypertension [7], ischemia [8], and diabetes mellitus [9]), osteoporosis [10], and glaucoma [11], again suggesting complexity in the molecular factors contributing to its onset and progression. Further complicating therapeutic development is delivery across the blood brain barrier (BBB), which typically protects the brain from circulating molecules and limits cross talk between the brain and the periphery [12]. Added to these complexities, AD molecular pathology can begin years, sometimes decades before symptoms are apparent, making early intervention and optimal drug evaluation difficult [13]. Taken together, it is clear that there are still major challenges to overcome in the face of treating AD, but further unraveling the molecular underpinnings associated with the disease is necessary to inform therapeutic development.

1.2 Pathological hallmarks of Alzheimer's disease

1.2.1 Amyloid beta

For the past twenty years, the amyloid cascade hypothesis has dominated AD research and therapeutic development [14]. This hypothesis postulates that the primary causative factor driving AD pathogenesis is the accumulation of amyloid beta (Aβ) protein deposits in the brain parenchyma and on cerebral vasculature [14-16]. Specifically, the Aβ isoform $A\beta_{1\text{-}42,}$ which is formed by sequential processing of amyloid precursor protein (APP) by β- and γ-secretases aggregates extracellularly to form oligomers and plaques [15].

This triggers a cascade which is hypothesized to involve downstream activation of brain immune cells, dysregulation of neuronal homeostasis, and formation of hyperphosphorylated tau tangles, ultimately leading to neuronal death and dementia [14] (**Figure 1-1**).

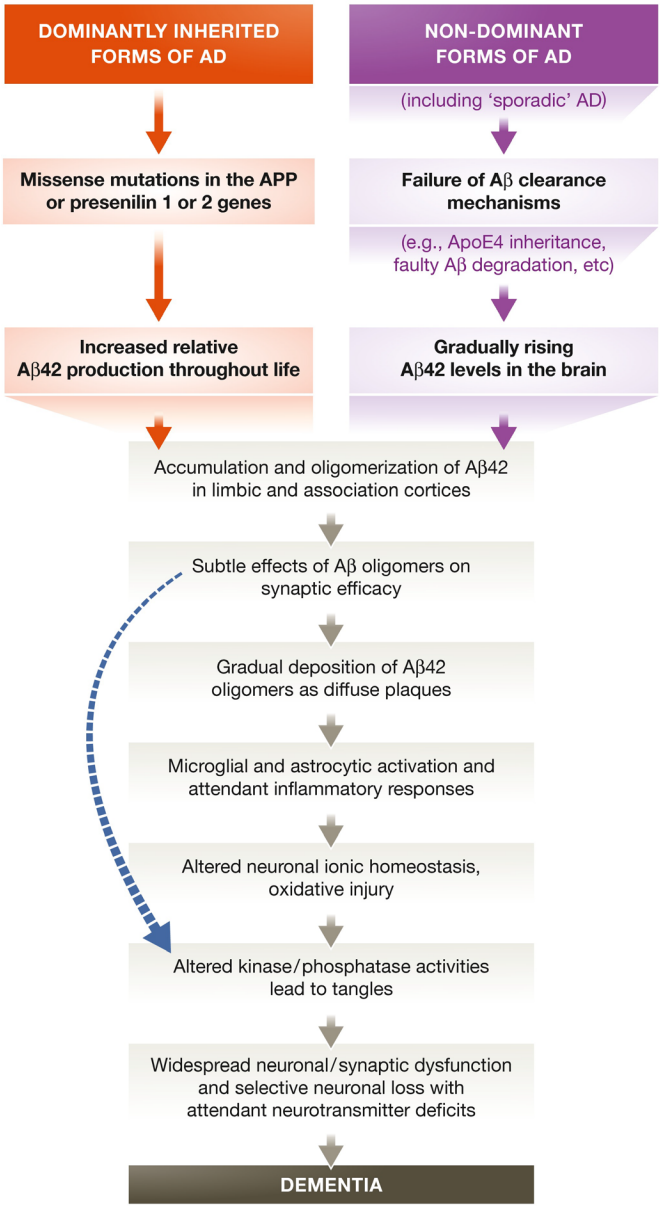

Figure 1-1. The amyloid cascade hypothesis. The amyloid cascade hypothesis suggests that $A\beta_{1\text{-}42}$ aggregates in the brain and ultimately triggers the formation of tau tangles and neuronal dysfunction and death in AD. This figure was originally published open access in

Indeed, the vast contributions of Aβ pathology on neurodegeneration in AD have been well established. *In vitro* studies have found that Aβ can trigger neuronal apoptotic cell death [18] and alter neuronal calcium homeostasis, rendering cells susceptible to calcium-dependent neurotoxicity [19]. Aβ also induces mitochondrial dysfunction and degeneration in neurons, resulting in decreased adenosine triphosphate production and impairment of neuronal energetics [20, 21]. Furthermore, studies of both humans with AD and mouse models transgenic for human APP have found that Aβ drastically disrupts neuronal networks and synapses, which ultimately leads to cognitive impairment [22].

Despite the clear involvement of Aβ in neurodegeneration in AD, targeting Aβ processing and clearance as a therapeutic strategy has proven to be troublesome. In the last decade, dozens of once-promising drugs targeting Aβ processing or clearance have proven to be futile in clinical trials [23-25]. In 2012, Pfizer and Johnson and Johnson both ran phase III clinical trials for the anti-Aβ antibody, bapineuzumab, which specifically targeted Aβ oligomers and plaques [25]. Both trials failed due to lack of efficacy in improving cognition, despite bapineuzumab having successfully reduced amyloid burden, total tau, and phosphorylated tau in cerebrospinal fluid [26-28]. Soon after, Eli Lilly launched a phase III clinical trial for solanezumab, another anti-Aβ monoclonal antibody, this time targeting monomeric Aβ with hopes that intervening earlier in AD progression may be the answer [25]. However, solanezumab again failed to improve cognition in patients with mild AD [23]. More recently, in 2017, Merck disbanded its phase III clinical trial for verubecestat, a β-secretase 1 (BACE1) inhibitor, after concluding that the drug may

actually worsen cognitive function [29]. Earlier this year, Biogen and Eisai ended a pair of parallel phase III trials for aducanumab, another monoclonal antibody targeting Aβ, which had proven to be successful in clearing Aβ in AD mouse models and an earlier human clinical trial [30, 31]. In fact, AD therapeutic development has been so devastating that it is has ultimately led to the closure of several prominent neuro-pharmaceutical research and development programs, including those of Pfizer and Eli Lilly [32, 33].

In light of the repeated failures of such clinical trials, it is becoming increasingly recognized that AD is multifaceted, and that Aβ is only one of many complex pathological events that contributes to AD pathogenesis. Along these lines, recent studies of postmortem human brain tissue have identified "resilient" individuals with high Aβ loads who did not experience neuronal death or dementia, revealing that Aβ burden on its own may not be sufficient for driving neurodegeneration [34]. Furthermore, similar studies have shown that there are distinct, molecular signatures associated with patients demonstrating this "resilience" to AD, suggesting that a combination of Aβ and other molecular factors may be necessary for neurodegeneration to occur [35].

1.2.2 Neuroinflammation

As per the traditional amyloid cascade hypothesis (**Figure 1-1**), neuroinflammation, characterized by the activation of microglia and astrocytes, is hypothesized to be a mere consequence of $A\beta_{1-42}$ extracellular deposition. However, it is becoming increasingly recognized that neuroinflammation may play a causal role in AD pathogenesis. Whether glial activation is protective or deleterious remains a matter of

debate, and it is likely that in reality, glial immune activity carries a range of positive to negative implications to AD pathology.

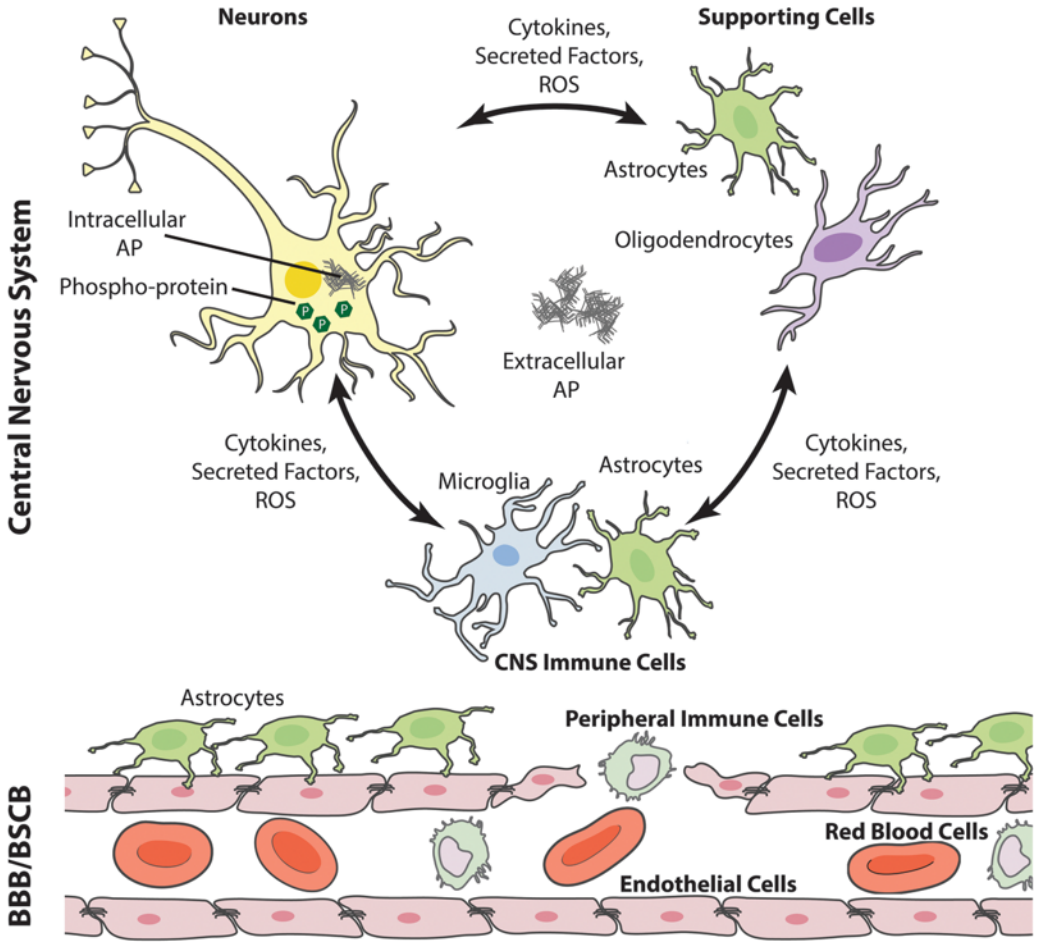

Figure 1-2. Alzheimer's disease pathology is multifaceted. Alzheimer's disease is complex, involving the combination of many pathologies. This includes the formation of extracellular Aβ plaques, intra-neuronal hyper-phosphorylated tau, immune activity of microglia and astrocytes, and dysregulation of the BBB. This figure was originally published in Integrative Biology and was reproduced with permission from Oxford University Press [36]. Wood et al. Systems biology of neurodegenerative diseases. Integr. Biol. 2015; 7: 758-775. © Oxford University Press

1.2.2.1 Cytokines and chemokines

Expression of a wide range of cytokines and chemokines by both astrocytes and microglia is one of the key neuroinflammatory phenotypes observed in AD environments.

In Aβ transgenic mouse models, pro-inflammatory cytokine expression (ie. TNF-α, IL-6, IL-12p40, IL-1β, IL-1α and GM-CSF) is upregulated and correlates with Aβ load [37]. The chemokine interferon-inducible protein-10 (IP-10) is upregulated and co-localizes with Aβ plaques in Tg2576 mice [38]. Such findings are mirrored *in vitro*, with Aβ upregulating a vast array of pro-inflammatory cytokines in both astrocyte and microglial cultures [39, 40]. *In vitro,* Aβ also upregulates microglia and astrocyte expression of chemokines including C-C motif ligand (CCL) 2, CCL3, C-X-C motif ligand (CXCL) 8, and MCP-1 [41-43]. Conversely, Aβ also induces the expression of anti-inflammatory cytokines, including transforming growth factor (TGF)-β and IL-10 [44]. Ultimately, AD pathological severity correlates with upregulation of profiles of cytokines including both pro- and anti-inflammatory factors [45].

Further work has shown that cytokine upregulation is not exclusively a consequence of Aβ deposition. Studies of patients with only mild cognitive impairment (MCI) have found upregulation of TNF-α and TGF-β protein in cerebrospinal fluid (CSF) when no significant changes in CSF Aβ levels were yet detectable [46]. Similar studies of cytokine messenger ribonucleic acid (mRNA) expression from postmortem human brain tissue found upregulation of IL-1, IL-2, IL-6, IL-8, Macrophage-Colony Stimulating Factor (M-CSF), TNF-α, and TGF-β upregulated prior to clinical manifestation of AD [47]. Moreover, analysis of cultured human peripheral blood mononuclear cells found that cells derived from MCI patients more robustly expressed a panel of cytokines than those derived from patients with AD [48]. Together, these data suggest that neuroinflammation could be an early pathological event rather than merely consequential, and that neuroinflammation can actually modulate the transition from MCI to overt AD and dementia.

Upregulation of pro- and anti- inflammatory cytokines and chemokines has multifaceted consequences to AD pathogenesis. For example, the pro-inflammatory TNF-α has been shown to have a myriad of neurodegenerative effects, suppressing long-term potentiation (LTP) of synaptic transmission [49] and correlating with increased risk of progression from MCI to dementia [46]. Conversely, overexpression of TNF- α has been shown to decrease Aβ plaque burden, suggesting an ameliorative role in AD [50]. Similarly, IL-10, a traditionally anti-inflammatory cytokine has been shown to enhance neurogenesis and improve spatial learning in the APP/PS1 Aβ mouse model [51], while simultaneously worsening Aβ plaque burden and cognitive function in the TgCRND8 Aβ mouse model [52]. Numerous other factors such as VEGF [45, 53] and IL-4 [54, 55] have also been shown to impart seemingly contradictory effects in the context of AD. Taken together, it is clear that upregulation of cytokines and chemokines is an important aspect of neuroinflammation in AD, and likely contributes both positively and negatively to disease progression.

1.2.2.2 Scavenger activity

Uptake and clearance of pathogens through scavenger activity is an important function of astrocytes and microglia, which becomes particularly relevant in an AD environment. Notably, activated glial cells are important mediators in the clearance of Aβ plaques. Reactive astrocytes are known to migrate towards and co-localize with Aβ plaques *in vitro* and *in vivo* [56, 57] and contribute to Aβ clearance by internalizing and degrading it [58, 59]. This suggests that scavenger activity concomitant with astrocyte activation can improve AD pathology. However, it is debated as to whether these functions are net beneficial and whether they translate to human AD pathology. Analysis of postmortem

human AD brain tissue has revealed that although astrocytes uptake Aβ, they can selectively lyse and deposit their Aβ loads, resulting in astrocyte-derived Aβ plaques and worsening amyloid pathology [60]. Furthermore, astrocytic Aβ clearance may ultimately contribute to "fatigue," meaning that over time, important physiological astrocyte functions may be lost in exchange for Aβ clearance functions [61]. Like so, a subset of reactive astrocytes, called A1 astrocytes, which are prevalent in AD, have been reported to lose phagocytic function, particularly in their abilities to uptake synaptosomes and myelin debris [62].

Similar dichotomous findings are paralleled in microglia. *In vivo*, activated microglia are recruited to Aβ plaques and eliminate Aβ deposits through phagocytosis [63]. However, as animals age and the disease progresses, microglia can also become fatigued, with expression of genes involved in Aβ clearance becoming downregulated, resulting in increased Aβ accumulation [64]. Furthermore, important physiological microglial functions such as phagocytic capacity and directed process motility are impaired in AD mice and loss of function correlates with Aβ burden [65]. In summary, reactive glia in AD environments experience changes to scavenger capacity, which contribute to most neuroprotection and neurodegeneration.

1.2.3 Blood brain barrier dysregulation

Although previously unappreciated, BBB dysregulation is emerging as an early pathological event in AD. The BBB, which refers to the blood vessels that vascularize the brain, typically functions to regulate the transport of cells, molecules, and ions between the blood and the brain, selectively permitting transport of factors that are required for

maintaining brain homeostasis [66, 67]. BBB dysfunction can contribute to unregulated extravasation of cells and molecules into the brain, resulting in a myriad of pathological consequences (**Figure 1-3**).

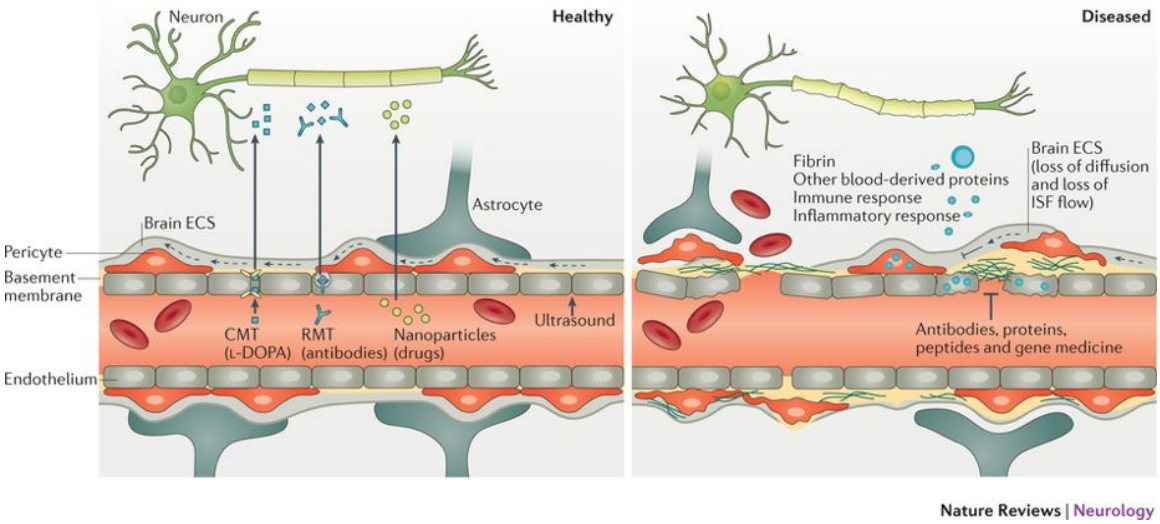

Figure 1-3. The blood-brain barrier is dysregulated in Alzheimer's disease. Blood-brain barrier dysregulation in Alzheimer's disease results in extravasation of blood-derived factors into the parenchyma and initiation of an inflammatory response. This figure was originally published in Nature Reviews Neurology and was reproduced with permission from Springer Nature [68]. Sweeney et al. Blood-brain barrier breakdown in Alzheimer disease and other neurodegenerative disorders. Nat. Rev. Neurol. 2018; 14:133-150. © Springer Nature

Studies of human AD patients have identified BBB breakdown to be an early feature of AD. Dynamic contrast-enhanced magnetic resonance imaging studies have found altered blood–brain–CSF compartmental kinetics and increased BBB leakage in patients with even early AD [69, 70]. BBB leakage rates also correlated with cognitive decline [70]. Furthermore, temporal studies of CSF biomarkers in humans with AD identified biomarkers associated with vascular dysfunction to manifest early in disease, prior to cognitive impairment and amyloid deposition [71]. These data suggest that BBB dysfunction can precede amyloid deposition, potentially contributing as a causal aspect of

AD. Cerebral amyloid angiopathy, or deposition of Aβ on the walls of brain vasculature, has also been reported to contribute to BBB leakage, suggesting that leakage may start early in AD but worsen with disease progression [72]

1.3 Relevance of heme and hemoglobin to Alzheimer's disease

1.3.1 Heme and hemoglobin are implicated in AD

The aforementioned findings of vascular permeability in AD have implicated blood-derived cells and proteins as important contributors to disease progression. Indeed, the blood protein hemoglobin (Hb) and its cofactor heme, are gaining attention for their implications in AD. Hb is predominantly known for its role as the oxygen-carrying protein abundant in red blood cells [73]. One Hb molecule is composed of four subunits: two alpha subunits and two beta subunits, each of which contains one heme group [73]. Each heme group contains one iron atom which can bind one oxygen molecule [74]. In instances of vascular permeability, such as in AD, red blood cells can extravasate through the disrupted BBB and lyse, resulting in accumulation of Hb and Hb-derived free heme in the brain [75].

Indeed, increased brain tissue levels of both Hb and heme are characteristic of AD, in both human disease and AD mouse models [76-79]. Analysis of postmortem human AD tissue has shown increased heme in the temporal lobe [78] and increased Hb mRNA and protein in the inferior temporal gyrus and parietal gray and white matter [79], respectively. Furthermore, Hb-derived peptides have been shown to be elevated and preferentially localized to blood vessels in the cerebellum of AD patients [80]. Similar findings have been observed in the APP/PS1 AD mouse model, which also presents vascular permeability

[81]. Specifically, APP/PS1 mice have elevated levels of Hb protein in the primary motor cortex, entorhinal cortex, and hippocampus [76].

In addition to being elevated in AD, heme and Hb are highly relevant to AD due to their well-established physical interaction with Aβ. In the brains of humans with AD, heme has been found to physically bind Aβ [78]. In APP/PS1 mice, Hb binds with Aβ in a heme-dependent manner [76]. *In vitro* studies also demonstrate heme and Hb binding with Aβ, and in the case of heme, this binding results in an Aβ-heme complex with unique peroxidase activity [76, 82, 83]. This peroxidase activity can result in oxidation of neurotransmitters, thus contributing to neurodegeneration in AD [82, 84].

While vascular permeability is likely a strong contributor to elevated levels of heme and Hb in AD, mounting evidence suggests that other pathological events may further contribute to this environment. Although red blood cells are the predominant cell type for Hb localization, Hb is also expressed in non-erythroid cells [85]. Of particular relevance to AD are findings of Hb expression by rodent and human neuronal cells [85-88] and astrocytes [85, 87]. Along these lines, in APP/PS1 mice with upregulated levels of Hb, Hb protein expression co-localizes with neurons, and to a lesser extent, glia, suggesting that neurodegenerative and neuroinflammatory processes could be affected by excess Hb synthesis [76, 79] (**Figure 1-4**).

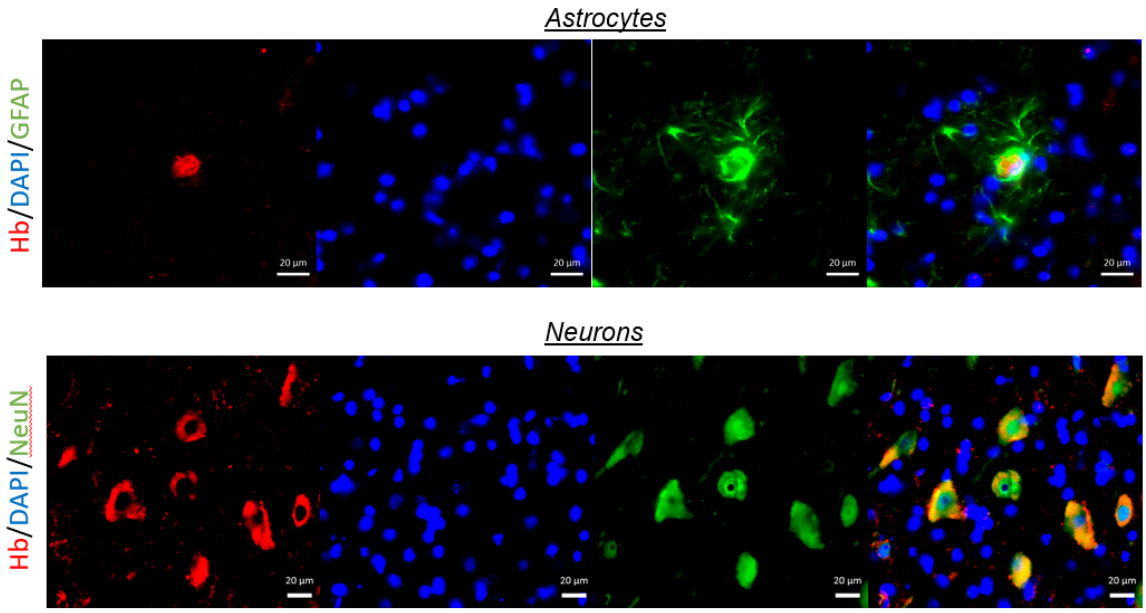

Figure 1-4. Hb colocalizes with astrocytes and neurons in APP/PS1 mice. Twelve month old APP/PS1 mice exhibit Hb (red) colocalization with astrocytes (top) and neurons (bottom), which are identified by GFAP and NeuN immunoreactivity, respectively. Scale bars, 20 µM.

With regards to heme, Hb-derived heme is not the only source of heme which is relevant to AD pathology. Heme is synthesized endogenously in almost all tissues, including the brain, and is an essential molecule for numerous living organisms [89]. Indeed, given its involvement in protein complex assembly and signal transduction, deficits in heme function and synthesis adversely affect numerous body systems, including the nervous system [89]. Heme regulates processes such as gene expression, RNA processing, energy production, and ion transport, all of which are relevant to neurodegeneration [90, 91]. Disrupted heme metabolism, through a combination of defects in heme import, export, and synthesis have been linked to several neurodegenerative conditions, including AD [90]. Additional hypotheses suggest that neuronal loss in AD may contribute to excess free heme in the brain, for example as a result of cytochrome c release [75]. It is also plausible that

excess heme is biosynthesized by neuronal cells, which also produce Aβ in AD, thus resulting in Aβ-heme complexes in AD brains [84].

Concomitant with these reports are findings that heme oxygenase pathway activity, which is responsible for heme degradation, may also be implicated in AD pathology. Heme oxygenase 1 (HO-1) correlates with cognitive decline in AD [92, 93], and both HO-1 and heme oxygenase 2 are elevated in APP/PS1 mouse brains [94]. Taken together, these findings suggest multiple mechanisms through which heme and Hb may become elevated in AD and contribute to AD pathology.

1.3.2 Heme and hemoglobin have immunomodulatory and cell signaling functions

Although less appreciated than their roles in oxygen transport, heme and Hb have potent immunomodulatory functions and can act on a number of cellular targets, contributing both pro- and anti-inflammatory effects. These functions have been widely studied in peripheral macrophages and endothelial cells [95, 96]. With regards to pro-inflammatory effects, extracellular heme binds toll-like receptor 4 (TLR4), resulting in inflammatory cytokine expression and cell activation [95-97]. Heme has also been shown to enhance chemokine expression and chemotaxis of immune cells [98]. Pro-inflammatory activity is mediated by activation of intracellular signaling pathways, including mitogen activated protein kinases (MAPKs) [97, 99, 100], protein tyrosine kinases [101, 102], and the nuclear factor kappa-light-chain-enhancer of activated B cells (NF-κB) [97] (**Figure 1-5**). Heme further exerts pro-inflammatory effect through activating inflammatory transcription factors, including p53 [103, 104], and Rev-erbα [105-110] (**Figure 1-5**).

Moreover, independently of heme, Hb has been shown to activate pro-inflammatory genes through the NF-κB pathway [111].

With respect to anti-inflammatory effects, catabolism of heme by the inducible enzyme, HO-1, generates anti-inflammatory byproducts [112]. These include carbon monoxide (CO) and bilirubin, which suppress pro-inflammatory cytokine expression and upregulate anti-inflammatory cytokine expression, among many other anti-inflammatory activities [112-116]. HO-1 anti-inflammatory activity is also mediated by canonical phospho-signaling cascades, including MAPK [112, 113], NF-κB [112, 117], Janus kinase - Signal Transducer and Activator of Transcription proteins (Jak-STAT) [112, 118] and phosphatidylinositol 3-kinase/Protein Kinase B (PI3K/Akt) [112, 119].

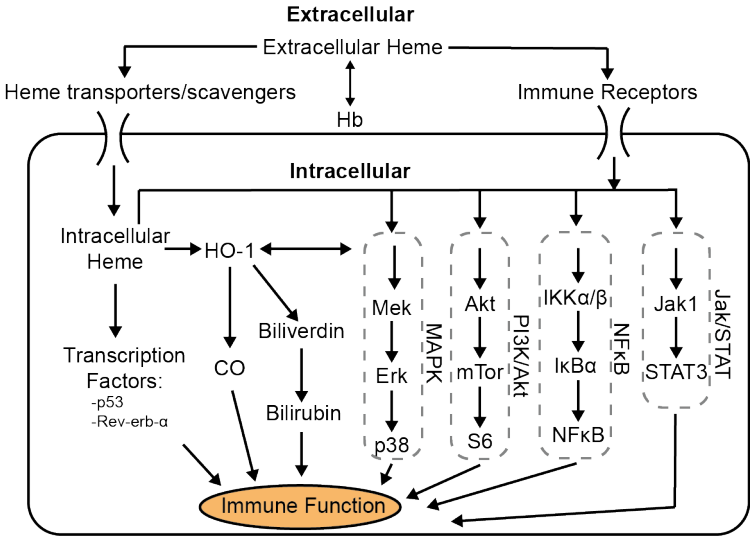

Figure 1-5. Heme is a potent immunomodulatory signaling molecule. Heme can drive immunomodulatory signaling through numerous intracellular and extracellular mechanisms. Heme can activate transcription factors and phospho-signaling pathways that regulate immune function. Heme can also be degraded by HO-1 into its by-products, carbon monoxide, biliverdin, and bilirubin, which have immunomodulatory functions.

Further complicating heme signaling are the differential action mechanisms for extra- and intra-cellular heme. For example, extracellular heme and Hb can trigger

signaling cascades by binding to cell surface receptors [96, 97], while cellular internalization of heme is required for direct activation of the HO-1 pathway via heme binding of the transcription repressor Bach1 [120]. A number of heme and Hb scavenger receptors and transporters, including Cluster of Differentiation (CD)163 [121-123], CD91 [123, 124], heme responsive gene protein 1 (HRG-1) [125], and feline leukemia virus subgroup C cellular receptor family, member 2 (FLVCR2) [126], mediate the import and export of extra- and intracellular heme, respectively.

Taken together, the mechanisms for heme and Hb signaling are intricate, and consist of both pro- and anti-inflammatory signaling. However, it is clear that there are numerous signaling mechanisms that they could contribute to neuroinflammation and neurodegeneration characteristic of AD. Identifying pathological perturbations in heme signaling in AD presents a formidable challenge, but is critical to therapeutic development.

1.4 Scope and organization of this thesis

Although heme and Hb are well established in their relevance to AD, there is very little understanding of how they may contribute to AD pathogenesis. Moreover, heme and Hb are potent immunomodulatory signaling molecules, but these functions have not been characterized in the context of the brain. Since glial immune activity is a prominent aspect of AD, heme and Hb may exert glial immunomodulatory functions that drive AD pathogenesis. The goal of this thesis is to address this gap by elucidating the role heme may play in modulating the neuroimmune system in AD environments. As such, the overarching hypothesis is that heme and Hb impair glial immune function through modulation of intracellular signaling pathways.

The subsequent chapters investigate this hypothesis using both *in vitro* and *in vivo* model systems. Chapter 2 of this thesis examines how heme and Hb affect inflammatory activation of astrocytes and microglia *in vitro,* in both Aβ-dependent and Aβ-independent contexts. Chapter 3 hones in on astrocytes to identify intracellular immune signaling mechanisms dysregulated by heme. Finally, Chapter 4 extends these studies *in vivo*, examining how heme affects neuroinflammation in wild type (WT) mice, with and without the presence of Aβ.

CHAPTER 2. DETERMINING THE EFFECTS OF HEME, HEMOGLOBIN, AND THEIR INTERACTIONS WITH AMYLOID BETA ON GLIAL INFLAMMATORY ACTIVATION *IN VITRO*

This chapter was adapted from [127] Sankar et al. (2018). J. Biol. Chem., 293(29):11358-11373. © the American Society for Biochemistry and Molecular Biology

2.1 Introduction

Neuroinflammation is becoming increasingly recognized as an important aspect of AD pathology, but whether glial activity promotes pathogenesis [128] or is neuroprotective [129] remains contested. Glial activity plays an important role in neuroprotection and maintaining tissue homeostasis by regulating metabolism [130], pruning neurites and synapses [131], secreting neuroprotective cytokines [44], and clearing pathogens such as Aβ, the hallmark protein of AD [56, 57, 132]. However, glial inflammatory activity can also promote a neurotoxic microenvironment via overexpression of neurotoxic cytokines [62, 133] and reactive oxygen species [134], among other factors. Moreover, there is increasing evidence that glia efficiently clear Aβ early in AD but that they become dysfunctional with time, perhaps due to changes in environmental factors and immunomodulatory signaling during AD progression [56, 64, 65]. As both astrocytes and microglia have been reported to migrate toward Aβ plaques and uptake and degrade Aβ [56, 63, 135-137], deficits in glial immune function may contribute to AD pathogenesis. Furthermore, both astrocytes and microglia secrete chemokines, which function in further recruiting immune cells to Aβ plaque sites [138, 139]. Expression patterns of chemokines

can vary with disease progression, and loss of chemokine expression could further contribute to impaired clearance mechanisms [140].

Increased brain tissue levels of the blood-derived factors, Hb and heme, are characteristic of AD [76-79] and are associated with a number of AD risk factors, including age, brain injury, and stroke [141, 142]. Notably, analysis of post-mortem human AD tissue has shown increased heme in the temporal lobe [78] and increased Hb mRNA and protein in the inferior temporal gyrus and parietal gray and white matter [76], respectively. In fact, heme has been shown to colocalize with Aβ deposits in AD tissue [143], and Hb has been found within senile plaques and cerebral amyloid angiopathy [79]. Furthermore, both heme and Hb have been reported to bind Aβ and alter its aggregation state [78, 79].

Although traditionally known for their oxygen carrying properties [73], both heme and Hb have diverse immunomodulatory capabilities. Studies in macrophages and endothelial cells indicate that heme stimulates the immune response via TLR4 signaling [97]. Moreover, Hb can promote inflammation independently of heme [111]. However, the immunomodulatory potential of heme and Hb on immune cells of the brain, namely astrocytes and microglia, remain uncharacterized. Despite the aforementioned observations pointing to potential roles for heme and Hb in modulating AD pathogenesis, the effects of heme and Hb on Aβ-mediated inflammatory response and the physiologic consequences of heme and Hb interactions with Aβ remain unknown.

Herein, we elucidate the effects of heme and Hb on astrocyte and microglial immune function *in vitro* and delineate how heme and Hb specifically affect astrocyte and microglial inflammatory response to Aβ. Surprisingly, our data reveal that heme and Hb,

which are pro-inflammatory in macrophages [97, 144, 145], largely suppress the Aβ-mediated astrocyte expression of a broad collection of pro-inflammatory cytokines. In microglia, we observed dose-dependent responses, resulting in suppression of cytokines in some contexts and upregulation of cytokines in others. Our data further show that differences in Aβ speciation contribute to differences in cytokine expression in astrocytes, and that physical interaction between heme/Hb with Aβ and resulting immunomodulatory effects are Aβ species dependent. Moreover, we determined that heme and Hb exert immunomodulatory effects via Aβ-independent mechanisms, as evident by suppression of scavenger activity of both astrocytes and microglia without the presence of Aβ. Taken together, these data suggest that heme and Hb modulate immune function in astrocytes and microglia through both Aβ-dependent and Aβ-independent mechanisms. Graphical representations of the experimental designs and approaches in this chapter are depicted in **Figure 2-1** and **Figure 2-2**.

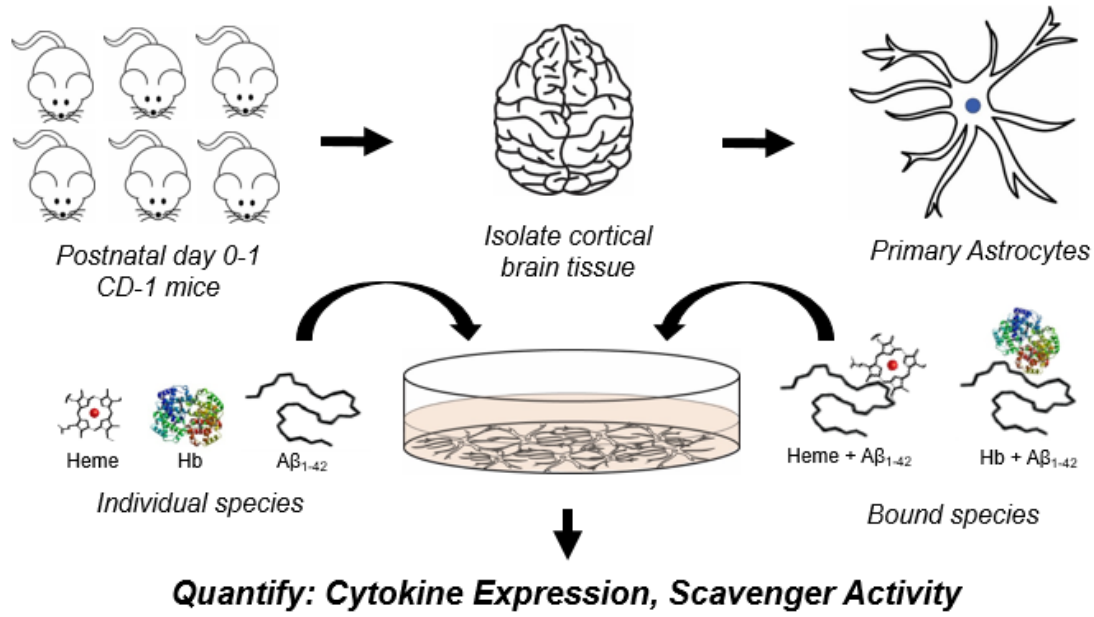

Figure 2-1. Experimental design for determining the effects of heme, hemoglobin, and amyloid beta on astrocyte immune function *in vitro*. Experimental strategy consists of deriving primary mouse astrocyte cultures and quantifying their immune activity in response to individual species of heme, Hb, and Aβ as well as physically bound species of heme or Hb with Aβ. Astrocyte immune activity is quantified in terms of cytokine expression and scavenger activity.

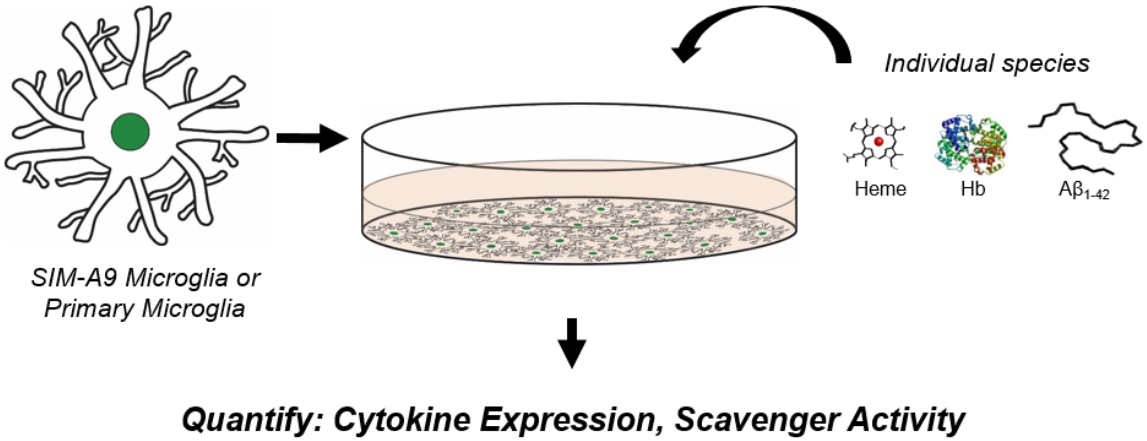

Figure 2-2. Experimental design for determining the effects of heme, hemoglobin, and amyloid beta on microglial immune function *in vitro.* Experimental strategy consists of deriving both SIM-A9 and primary mouse microglial cultures and quantifying their immune activity in response to individual species of heme, Hb, and Aβ. Microglial immune activity is quantified in terms of cytokine expression and scavenger activity.

2.2 Materials and Methods

2.2.1 Recombinant $A\beta_{1-42}$ preparation

For all experiments, hexafluoroisopropyl alcohol (HFIP)-pretreated $A\beta_{1-42}$ (rPeptide, Watkinsville, GA) was diluted from stocks of 50 or 500 μM Aβ in 1% NH_4OH that were stored at −80 °C. Before reconstitution, $A\beta_{1-42}$ was retreated with 500 μl HFIP per milligram of $A\beta_{1-42}$ overnight to prevent pre-aggregation. HFIP was evaporated before dilution in 1% NH_4OH.

2.2.2 Primary mouse astrocyte cultures

Astrocyte cultures were derived from postnatal day 0–1 CD1 mice (Charles River Laboratories) under a protocol approved by the Georgia Institute of Technology Institutional Animal Care and Use Committee. Cortices were isolated following an existing protocol [146] and triturated in plating medium with a 1-ml sterile pipette tip. Plating medium consisted of minimum essential medium (Thermo Fisher Scientific) with 10% horse serum (Sigma), 1% antibiotic/antimycotic solution (Sigma), and 0.3% glucose solution (Sigma). Cells were left to attach overnight to T-75 flasks coated in 0.1 mg/ml poly-D-lysine (Sigma). After 24 h, flasks were knocked to remove debris and rinsed with PBS, and plating medium was replaced with astrocyte medium (ScienCell) with 2% fetal bovine serum (ScienCell), 1% penicillin/streptomycin solution (ScienCell), and 1% astrocyte growth serum (ScienCell), in which cultures were maintained for up to four passages for conditioning. Cultures were maintained in a 37 °C, 5% CO_2 humidified incubator.

2.2.3 SIM-A9 microglial cultures

SIM-A9 cells (American Type Culture Collection (ATCC), Manassas, VA) were cultured in Dulbecco's modified Eagle's medium (DMEM)/F-12 (ATCC) supplemented with 10% heat-inactivated bovine serum (Thermo Fisher Scientific) and 5% heat-inactivated horse serum (Thermo Fisher Scientific). Cultures were maintained in a 37 °C, 5% CO_2 humidified incubator.

2.2.4 Primary mouse microglial cultures

Microglial cultures were derived from postnatal P0-3 CD1 mice (Charles River Laboratories) under a protocol approved by the Georgia Institute of Technology Institutional Animal Care and Use Committee. Brains were harvested from pups and triturated in trypsin-ethylenediaminetetraacetic acid solution, then incubated for 15 min at 37 °C. DMEM with 10% FBS was added to halt enzymatic digestion. Tissue was resuspended, then cell suspension was centrifuged at 800xg for 5 min at 15 °C. Debris was removed using a pipette, and remaining cell suspension was filtered through a 40 µm cell strainer. Cell suspension was again centrifuged at 800xg for 5 min at 15 °C, washed with PBS, and re-centrifuged to pellet cells. The cell pellet was resuspended in PBS and then incubated with CD11b+ magnetic microbeads (Miltenyi Biotec, Bergisch Gladbach, Germany) at 4 °C for 15 min. Meanwhile, a miniMACS® CD11b+ purification column (Miltenyi Biotec) was washed with PBS and fixed in a miniMACS® magnetic separator (Miltenyi Biotec). The cell suspension was then added to the column. After elution, the column was washed twice with DMEM, then detached from the magnet. Cells were dispensed into a collection tube and plated in DMEM + 10% FBS in 96 well plates coated

with 0.1 mg/ml poly-D-lysine (Sigma). After 24 h, half the media was replaced with fresh DMEM + 10% FBS. Cultures were maintained in a 37 °C, 5% CO_2 humidified incubator.

2.2.5 RAW 264.7 macrophage cultures

RAW 264.7 cells (ATCC) were cultured in Dulbecco's modified Eagle's medium (Lonza, Walkersville, MD) supplemented with 10% fetal bovine serum (Thermo Fisher Scientific) and 1% antibiotic/antimycotic solution (Sigma). Cultures were maintained in a 37 °C, 5% CO_2 humidified incubator.

2.2.6 Cell conditioning and lysis

For cytokine expression, phosphoprotein signaling, and Western blot analyses, primary astrocytes were plated in 6-well plates and conditioned with combinations of hemin chloride (50 nM; EMD Millipore), human hemoglobin (50 nM; Sigma), rapamycin (10 nM; Selleck Chemicals, Houston, TX), and $A\beta_{1\text{-}42}$ (50 nM; rPeptide) in 1% (w/v) NH_4OH. For CD36 analysis, cells co-conditioned with rapamycin were first preconditioned with rapamycin for 1 h. Conditions were applied at 75% confluence for 24 h, after which conditioning medium was collected for cytokine analysis, and cell lysates were collected for phosphoprotein signaling and Western blotting analyses using the Bio-Plex cell lysis kit (Bio-Rad), with the addition of one cOmplete mini protease inhibitor tablet (Roche, Basel, Switzerland) and 20 µl of phenylmethylsulfonyl fluoride (PMSF) (Sigma) per 5 ml of lysis buffer. Lysates were placed in microcentrifuge tubes and inverted at 4 °C for 10 min. Lysates and medium were centrifuged at 4 °C for 10 min at 13,200 rpm, and supernatant was collected and stored at −80 °C until analysis.

2.2.7 Multiplexed cytokine signaling analysis

For cytokine signaling analysis, conditioned medium was thawed on ice and centrifuged at 4 °C for 10 min at 13,200 rpm. All samples were diluted 2:3 (conditioned medium/assay buffer), because this dilution fell within the linear range of bead fluorescence intensity versus protein concentration for detectable analytes. Multiplex cytokine analysis was conducted by adapting the protocol provided for the Milliplex® MAP mouse cytokine/chemokine 32-Plex kit, with beads for Eotaxin, G-CSF, GM-CSF, interferon-γ, IL-1α, IL-1β, IL-2, IL-3, IL-4, IL-5, IL-6, IL-7, IL-9, IL-10, IL-12p40, IL-12p70, IL-13, IL-15, IL-17, IP-10, KC, LIF, LIX, MCP-1, M-CSF, MIG, MIP-1α, MIP-1β, MIP-2, RANTES, tumor necrosis factor-α (TNF-α), and vascular endothelial growth factor (VEGF). Beads were read on a MAGPIX® system (Luminex, Austin, TX).

2.2.8 Western blot

Cell lysates, obtained as described above, were thawed on ice and then centrifuged for 10 min at 10,000 rpm and 4 °C. Protein concentration was determined using a Pierce BCA protein assay and equal amounts of protein were dissolved in reducing sample buffer, boiled, and loaded onto sodium dodecyl sulfate (SDS)-polyacrylamide gels. Following separation by electrophoresis, proteins were transferred to a Hybond P 0.45-µm polyvinylidene fluoride membrane (GE Healthcare). Membranes were blocked at room temperature (RT) for 1 h with 5% milk in Tris-buffered saline containing 0.01% Tween 20 (TBST). Membranes were probed at 4 °C overnight with rabbit anti-CD36 (1:500; Novus Biologicals, Littleton, CO) and mouse anti-α-tubulin (1:2000; Sigma). Membranes were then incubated with Alexa Fluor–conjugated secondary antibodies (1:2000; Thermo Fisher

Scientific) for 2 h at RT. Imaging of blots was performed using an Odyssey CLx imager (LI-COR Biosciences, Lincoln, NE). Protein quantification was performed using Image Studio Lite version 5.2 (LI-COR Biosciences).

2.2.9 $A\beta_{1-42}$ internalization assay

Primary astrocytes were plated in 0.1 mg/ml poly-D-lysine–treated half-area 96-well, glass-bottom plates at a density of 10,000 cells/well and maintained in a 37 °C, 5% CO2 humidified incubator. At 75% confluence, cells were conditioned with either 50 nM $A\beta_{1-42}$, 50 nM $A\beta_{1-42}$ plus 50 nM hemin chloride, or 50 nM $A\beta_{1-42}$ plus 50 nM human hemoglobin in astrocyte medium for 24 h. Cells were fixed with 4% paraformaldehyde (PFA), permeabilized for 10 min at RT with 0.1% Triton X-100, and blocked with a 5% bovine serum albumin (BSA), 3% goat serum (Sigma) solution for 1 h. Primary antibody incubation was performed overnight at 4 °C, using the 6E10 antibody (1:200; BioLegend) in 0.5% BSA wash buffer. After washing with wash buffer, fixed cells were incubated with Alexa Fluor 488 goat anti-mouse secondary antibody (1:200; Thermo Fisher Scientific) for 2 h at RT. Cells were co-stained with 4′,6-diamidino-2-phenylindole (DAPI) (100 ng/ml; Thermo Fisher Scientific) for nuclei and Alexa Fluor 555 phalloidin (1:40; Thermo Fisher Scientific) for actin.

Confocal microscopy was performed on a Zeiss LSM 700 laser-scanning inverted microscope to obtain 15–30 optical sections with 1-μm interval thickness. Orthogonal projections were rendered using Zen version 2.3 software (Zeiss, Oberkochen, Germany).

2.2.10 E. coli particle internalization assay

Primary astrocytes or SIM-A9 microglia were plated on 96-well plates at a density of 10,000 cells/well and left to adhere overnight in a 37 °C, 5% CO2 humidified incubator. Cells were treated with either control, 50 nM hemin chloride, or 50 nM human hemoglobin conditions for 4 h. Conditioning medium was aspirated, and cells were incubated with the E. coli fluorescent BioParticle suspension from the Vybrant™ phagocytosis assay kit (Thermo Fisher Scientific) for 1 h. Extracellular fluorescence was quenched with trypan blue. Fluorescence was read on a SpectraMax M3 microplate reader (λex = 480 nm; λem = 520 nm) (Molecular Devices, Sunnyvale, CA).

2.2.11 Phagocytosis assay

Primary astrocytes or SIM-A9 microglia were plated in 0.1 mg/ml poly-D-lysine–treated half-area 96-well, glass-bottom plates at a density of 10,000 cells/well and left to adhere overnight in a 37 °C, 5% CO2 humidified incubator. Cells were treated with either control, 50 nM hemin chloride, or 50 nM human hemoglobin conditions for 24 h. Conditioning medium was aspirated, and cells were incubated with a fluorescent pHrodo™ Red Zymosan BioParticle suspension (Thermo Fisher Scientific) diluted in astrocyte medium for 2 h. After removing BioParticle suspension, cells were fixed with 4% paraformaldehyde, permeabilized for 10 min at RT with 0.1% Triton X-100, and blocked with a 5% BSA, 3% goat serum (Sigma) solution for 1 h. Primary antibody incubation was performed overnight at 4 °C, with rabbit anti-glial fibrillary acidic protein (GFAP) (1:1000; Novus Biologicals). After washing with wash buffer, fixed cells were incubated with Alexa Fluor 488 goat anti-mouse secondary antibody (1:200; Thermo Fisher Scientific) for 2 h at RT. Cells were co-stained with DAPI (1 ng/ml; Thermo Fisher Scientific) for nuclei.

Fluorescence microscopy was performed on a Zeiss Axio Observer Z.1 inverted microscope and quantified using ImageJ.

2.2.12 Partial least squares discriminant analysis

Partial least squares discriminant analysis (PLSDA) was performed in MATLAB using the partial least squares algorithm by Cleiton Nunes available on the Mathworks File Exchange. All data were z-scored before inputting into the algorithm. For all analyses, an orthogonal rotation in the latent variable (LV) 1-LV2 plane was performed to identify LVs that best separated conditions.

2.2.13 Statistics

All statistical analyses were performed using GraphPad Prism version 7 (GraphPad Software, La Jolla, CA). Values are presented as mean ± standard error of the mean (SEM). Statistical significance was determined, as appropriate, using Student's t test, ordinary one-way analysis of variance (ANOVA) followed by Dunnett's or Sidak's post hoc test, or Kruskal–Wallis ANOVA followed by Dunn's post hoc test. Normality of data was tested using the Shapiro–Wilk test of normality. Levels of significance were set as follows: $*p < 0.05$; $**p < 0.01$; $****p < 0.0001$.

2.3 Results

2.3.1 Heme and hemoglobin modulate $A\beta_{1-42}$-induced astrocyte inflammatory cytokine expression

Canonical markers of astrocyte activation, such as glial fibrillary acidic protein (GFAP) [147, 148], are not reliable activation markers in culture due to high baseline expression. Therefore, we used a multiplexed immunoassay to robustly quantify astrocyte activation in terms of protein expression of 32 cytokines into the culture medium. As expected, astrocytes conditioned for 24 h with $A\beta_{1-42}$ increased expression of numerous pro-inflammatory cytokines, including Interleukin (IL)-1β [149], Regulated on Activation, Normal T Cell Expressed and Secreted (RANTES) [39], and Granulocyte-Macrophage Colony Stimulating Factor (GM-CSF) [37] (**Figure 2-3A**). Because we measured a total of 32 cytokines, we aimed to create a cytokine profile that could be used to discern differences between groups. To do so, we utilized a PLSDA [150], an approach which has previously used to identify a cytokine profile distinguishing post-mortem human control and AD brain tissues [45]. Applying this analysis here identified an axis called a latent variable (LV1) that distinguished $A\beta_{1-42}$ conditioned wells from all other conditions (**Figure 2-3B**). The LV1 axis consisted of a profile of cytokines that were most different between groups (**Figure 2-3C**), whereas LV2 defined a second axis of cytokines that were most different in the heme + $A\beta_{1-42}$ condition (**Figure 2-3D**). By plotting each sample in terms of its score on LV1 (representing a composite indicator of cytokine expression), we found that $A\beta_{1-42}$ induced cytokine expression was significantly increased compared with controls or $A\beta_{1-42}$ wells that were co-treated with heme or Hb (**Figure 2-3E**). Plotting of selected individual cytokines revealed a trend where certain pro-inflammatory cytokines, such as RANTES and GM-CSF [151], were downregulated by heme and Hb, whereas others, such as keratinocyte chemoattractant (KC) [152] and Monocyte Chemoattractant

Protein (MCP)-1 [153], were not substantially modulated (**Figure 2-3F**), reflecting our multivariate analysis (**Figure 2-3,B-E**).

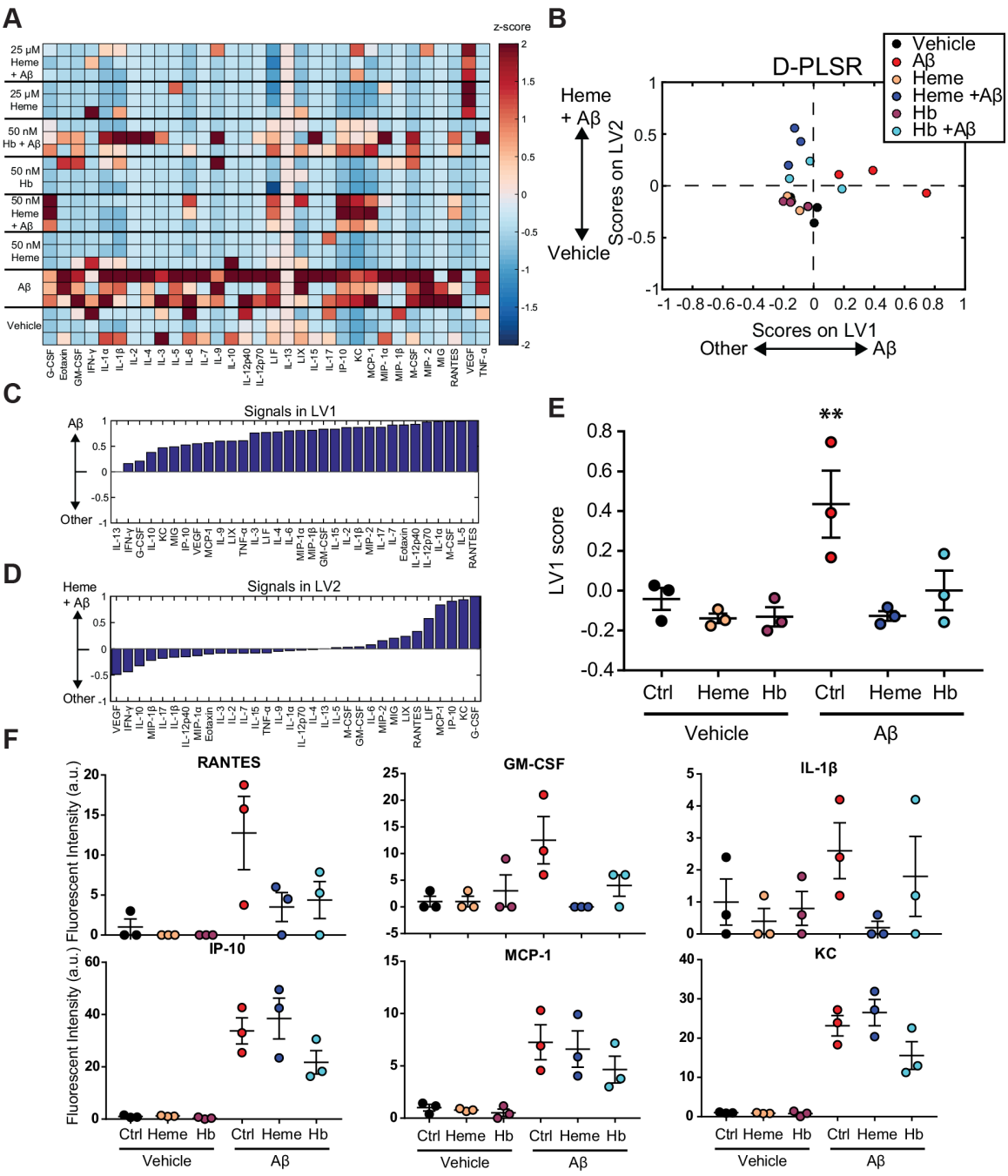

Figure 2-3. Heme and Hb suppress Aβ1–42-induced cytokine protein expression in primary mouse astrocytes. A. Quantification of 32 cytokines expressed into the medium of primary mouse astrocyte cultures via Luminex analysis. Each column is z-scored. Compared with vehicle control (0.001% NH4OH), cytokine expression is increased in response to 50 nM Aβ1-42. Moreover, co-conditioning of $A\beta_{1–42}$ with either 50 nM heme or 50 nM Hb suppressed cytokine expression (n = 3 wells). B. A partial least squares discriminant analysis, generated from the cytokine expression data set, identified a latent variable (LV1), based on cytokine expression, which separates Aβ1–42-only treated astrocytes from all other conditions along the horizontal axis. C. LV1 depicts a linear

combination of cytokines that correlate with the $A\beta_{1-42}$ only condition and identifies RANTES as the top correlate with $A\beta_{1–42}$ treated astrocytes in the panel of 32 cytokines. D. LV2 depicts a linear combination of cytokines that correlate with the heme + $A\beta_{1–42}$ condition. E. Plotting LV1 scores for each group shows that the LV1 profile segregates $A\beta_{1–42}$ treated astrocytes from all other conditions (**$p < 0.01$; ordinary one-way ANOVA with Dunnett's post hoc test). F. Plotting cytokine expression for six consistently measured cytokines, RANTES, M-CSF, IL-1β, IP-10, KC, and MCP-1, reveals that heme and Hb suppress expression of some, but not all, cytokines. Data are presented as mean ± SEM. This figure was originally published in the Journal of Biological Chemistry. Sankar et al. Heme and hemoglobin suppress amyloid β–mediated inflammatory activation of mouse astrocytes. J. Biol. Chem. 2018; 293: 11358-11373. © the American Society for Biochemistry and Molecular Biology

2.3.2 Inflammatory activation of astrocytes by soluble $A\beta_{1-42}$ aggregates is reversed by association with heme or hemoglobin

Recent studies of isolated Aβ from post-mortem human tissues have revealed that different species have distinct cytotoxicities and ligand affinities [154, 155]. We therefore sought to identify the inflammatory effects of various $A\beta_{1–42}$ species assess the effect that heme or Hb association with these species had on inflammatory activation of astrocytes. Toward this end, we conditioned astrocytes with 50 nM preparations of three distinct $A\beta_{1–42}$ species, which were isolated through a combination of centrifugation and size exclusion chromatography [127]. These species included a soluble >75-kDa high molecular weight (HMW) oligomer, a soluble <6.5 kDa low molecular weight (LMW) oligomer, and a fibrillar pellet [127]. Astrocytes were conditioned with these species for 24 h and assayed for their ability to stimulate the expression of inflammatory cytokines relative to a 50 nM concentration of the unseparated, $A\beta_{1–42}$ stock mixture and vehicle control. Most interestingly, we found that application of the soluble >75-kDa oligomer is highly inflammatory and comparable with that of the application of the unseparated $A\beta_{1–42}$ stock mixture (**Figure 2-4**). In marked contrast, preparations of the $A\beta_{1–42}$ pellet or the soluble

LMW species yielded minimal cytokine expression in astrocytes compared with the unseparated $A\beta_{1-42}$ stock mixture (**Figure 2-6**).

Since heme and Hb have been reported to physically interact with $A\beta_{1-42}$ [76, 78, 82], we next sought to determine what role heme and Hb association play in mediating $A\beta_{1-42}$ inflammatory activation. Since the HMW $A\beta_{1-42}$ oligomer was discovered to be the only species capable of physically binding heme and Hb [127], we assessed the effects of either heme or Hb binding with this species on astrocyte cytokine expression. Strikingly, we found that upon binding with heme, the pro-inflammatory response of the HMW $A\beta_{1-42}$ oligomer was almost entirely suppressed (**Figure 2-4**). A similar trend was observed, although to a lesser extent, with Hb-bound oligomer (**Figure 2-5**). Together these data suggest that heme and Hb may be downregulating astrocyte inflammatory activity through physically modifying $A\beta_{1-42}$.

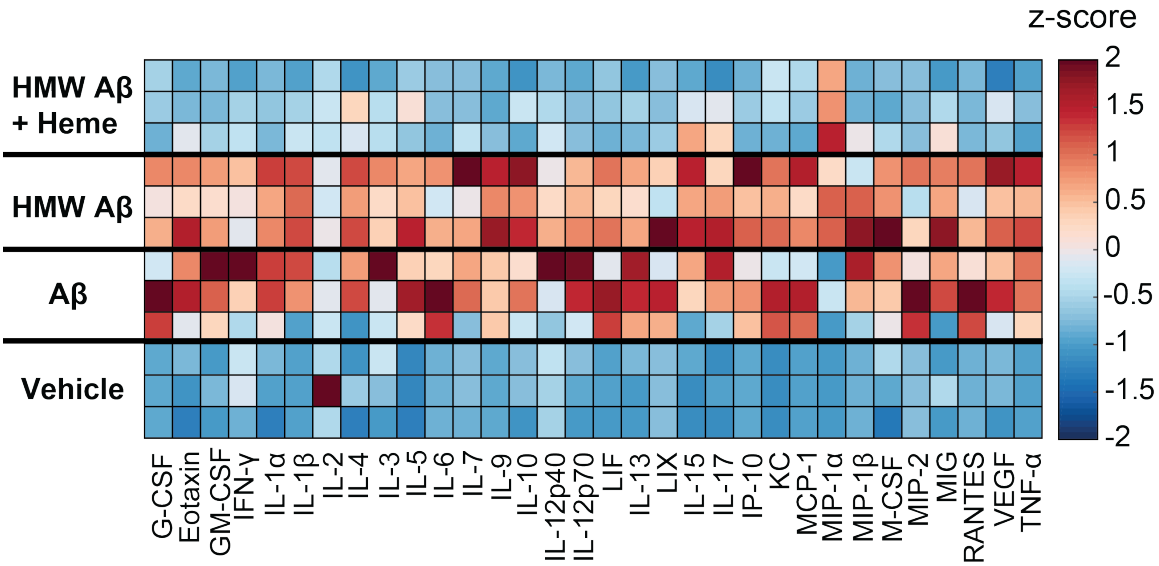

Figure 2-4. Heme binding suppresses inflammatory capacity of HMW Aβ$_{1–42}$. Heatmap of z-scored cytokine expression by primary mouse astrocytes upon incubation with 50 nM unseparated, stock Aβ$_{1–42}$, HMW Aβ$_{1–42}$, and Heme-bound HMW Aβ$_{1–42}$. *This figure was originally published in the Journal of Biological Chemistry. Sankar et al. Heme and hemoglobin suppress amyloid β–mediated inflammatory activation of mouse astrocytes. J. Biol. Chem. 2018; 293: 11358-11373. © the American Society for Biochemistry and Molecular Biology*

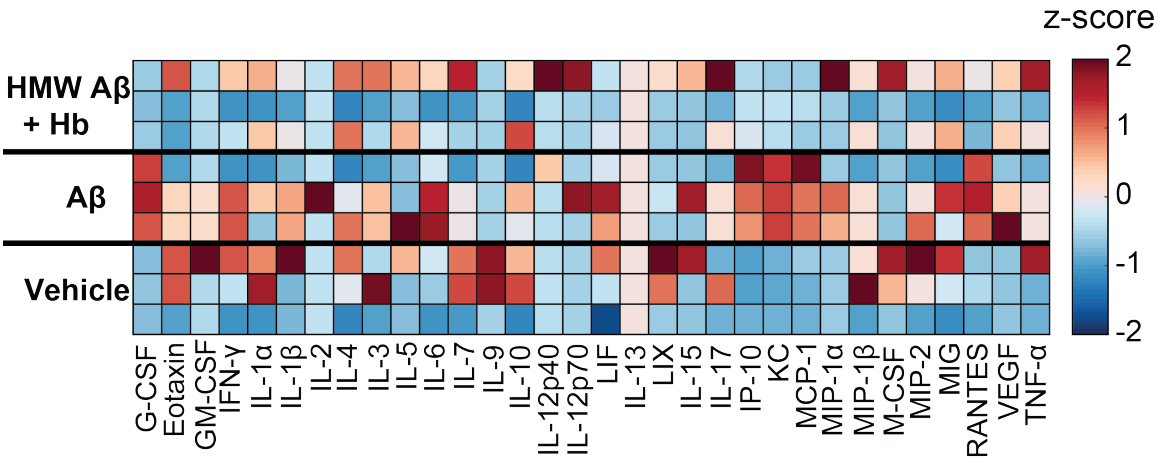

Figure 2-5. Hb binding suppresses inflammatory capacity of HMW Aβ$_{1–42}$. Heatmap of z-scored cytokine expression by primary mouse astrocytes upon incubation with 50 nM unseparated, stock Aβ$_{1–42}$ and Hb-bound HMW Aβ$_{1–42}$. *This figure was originally published in the Journal of Biological Chemistry. Sankar et al. Heme and hemoglobin suppress amyloid β–mediated inflammatory activation of mouse astrocytes. J. Biol. Chem. 2018; 293: 11358-11373. © the American Society for Biochemistry and Molecular Biology*

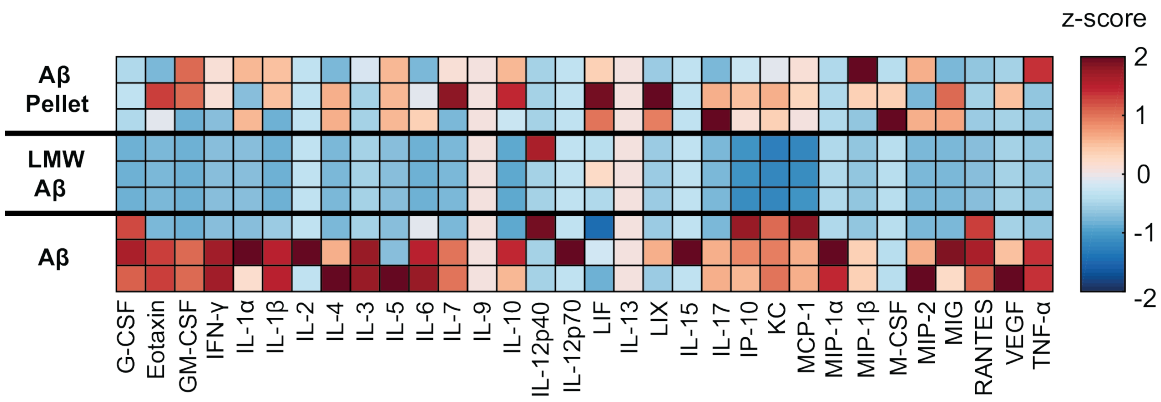

Figure 2-6. LMW and pellet Aβ$_{1-42}$ are minimally inflammatory. Quantification of 32 cytokines (expressed as z-scored cytokine expression) secreted from primary mouse astrocytes shows that 50 nM soluble LMW Aβ$_{1-42}$ is not inflammatory and that the insoluble 50 nM Aβ$_{1-42}$ pellet is minimally inflammatory compared to the unseparated 50 nM Aβ$_{1-42}$ stock. *This figure was originally published in the Journal of Biological Chemistry. Sankar et al. Heme and hemoglobin suppress amyloid β–mediated inflammatory activation of mouse astrocytes. J. Biol. Chem. 2018; 293: 11358-11373. © the American Society for Biochemistry and Molecular Biology*

2.3.3 Heme and hemoglobin reduce astrocyte scavenger activity

Since heme and Hb reduced Aβ$_{1-42}$-induced expression of multiple inflammatory cytokines (**Figure 2-3**), we next investigated their effects on astrocytic capacity to scavenge Aβ$_{1-42}$ and other substrates. First, we conditioned astrocytes with 50 nM Aβ$_{1-42}$, either alone or together with heme or Hb. We then used immunocytochemistry to stain for Aβ$_{1-42}$ using the 6E10 antibody (1:1000; BioLegend, San Diego, CA). Astrocytes treated with Aβ$_{1-42}$ alone showed Aβ$_{1-42}$ localized within the plane of the cell (**Figure 2-7A, arrows**). In contrast, astrocytes co-conditioned with heme, and to a lesser extent Hb, showed little Aβ$_{1-42}$ within the plane of the cell and substantial labeling on the cell surface, suggesting that heme and Hb suppress Aβ$_{1-42}$ internalization (**Figure 2-7A, arrows**).

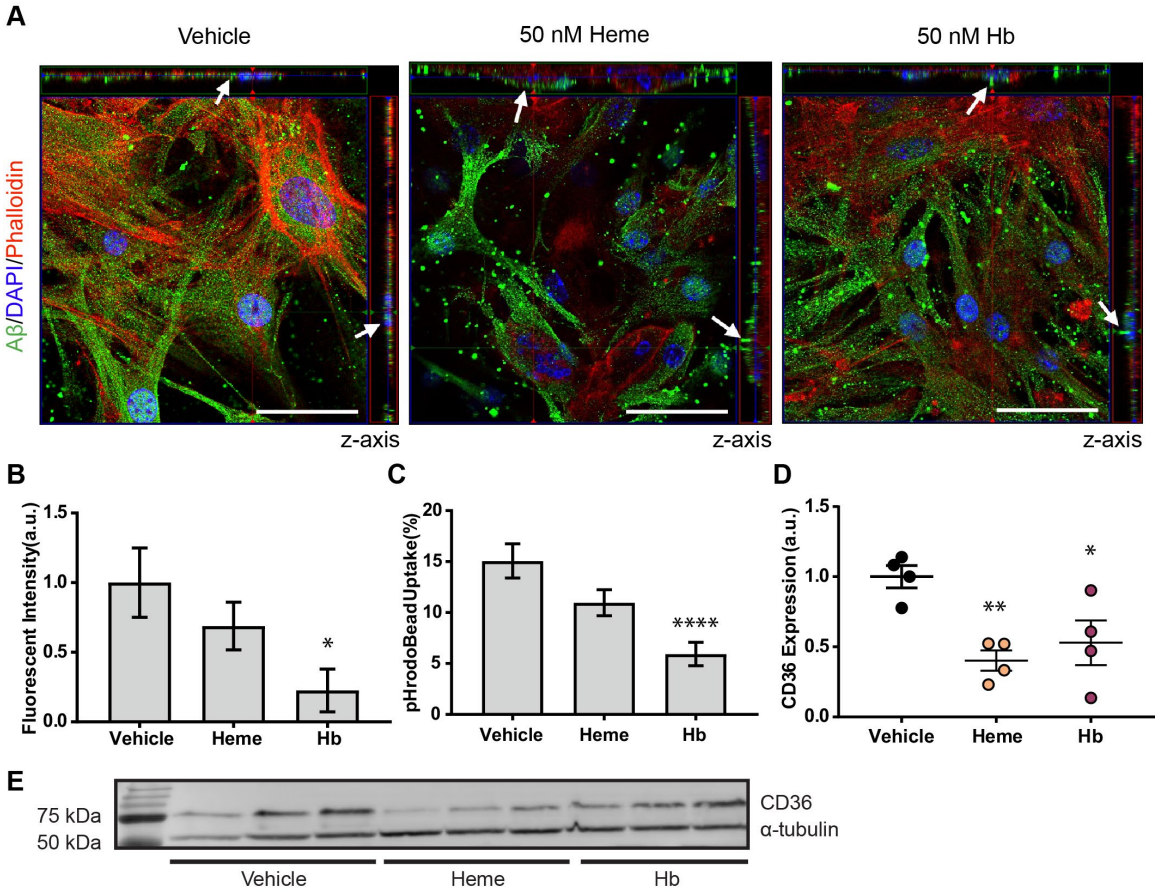

Figure 2-7. Heme and Hb suppress astrocyte internalization of Aβ$_{1–42}$ and phagocytic capacity. A. Confocal imaging of primary astrocytes incubated with 50 nM Aβ$_{1–42}$ (left) stained with DAPI (blue), Alexa Fluor 555 phalloidin (red), and anti-Aβ 6E10 (green) reveals Aβ$_{1–42}$ within the plane of the cell. Co-incubation with 50 nM heme (center) or 50 nM Hb (right) reduced Aβ$_{1–42}$ internalization. Arrows indicate Aβ$_{1–42}$ localization inside the cell (left) or on the cell surface (center, right). B. Primary astrocytes, preincubated with 50 nM heme or 50 nM Hb, were incubated with trypan-quenched, fluorescein-labeled, killed E. coli particles. Particle internalization, measured by fluorescence intensity using a microplate reader, significantly decreased upon incubation with 50 nM Hb (n = 28 wells; *p < 0.05; ordinary one-way ANOVA with Dunnett's post hoc test, vehicle versus Hb). C. Primary astrocytes, preincubated with 50 nM heme or 50 nM Hb, were incubated with pH-sensitive pHrodo beads to assess phagocytic capacity. The percentage of total cells uptaking beads, quantified by fluorescence microscopy (Figure 2-8), was significantly reduced upon treatment with Hb (n = 30-33 images; ****p < 0.0001; Kruskal-Wallis ANOVA with Dunn's post hoc test; vehicle versus Hb). D. Primary astrocytes conditioned with vehicle control, 50 nM heme, and 50 nM Hb were lysed and analyzed via Western blotting for CD36 expression. Quantification, normalized by α-tubulin, reveals that both heme and Hb down-regulate expression of CD36 (n = 4 wells; *p < 0.05; **p < 0.01; ordinary one-way ANOVA with Dunnett's post hoc test). E. Western blotting depicting CD36 expression. Data are presented as mean ± SEM. Scale bars, 50 μm. *This figure was originally published in the Journal of Biological Chemistry. Sankar et al. Heme and*

hemoglobin suppress amyloid β–mediated inflammatory activation of mouse astrocytes. J. Biol. Chem. 2018; 293: 11358-11373. © the American Society for Biochemistry and Molecular Biology

To determine if heme or Hb affected scavenger activity for other substrates, we next interrogated their effects on astrocyte internalization of killed E. coli particles. We treated astrocyte cultures with killed E. coli microparticles that were labeled with a trypan-quenched fluorescein (Thermo Fisher). Fluorescent intensity (λ_{ex} = 480 nm; λ_{em} = 520 nm) was quantified on a microplate reader and revealed that Hb, and to a lesser extend heme, reduced microparticle internalization compared to control (**Figure 2-7**). To determine if these effects also modulated phagocytosis, we incubated astrocytes with pH-sensitive pHrodo® Zymosan particles, which fluoresce in phagosomes. Quantification of phagocytic cells using fluorescence microscopy (**Figure 2-8**) demonstrated a significant reduction of phagocytosis in Hb-treated astrocytes and a non-significant reduction by heme (**Figure 2-7C**), mirroring our observations with killed E. coli particles.

Since heme and Hb appeared to have similar effects, though to differing degrees, we next wanted to determine if these effects were associated with changes in astrocyte phagocytic receptor expression. Key astrocyte scavenger receptors include CD36, RAGE, and CD47 [156]. Of these, we chose to quantify CD36 expression since it mediates both phagocytosis and inflammatory signaling in astrocytes [157]. Indeed, western blot analysis revealed decreased CD36 expression in the presence of heme or Hb (**Figure 2-7D-E**). This finding is consistent with heme and Hb mediated modulation of Aβ-induced inflammation (**Figure 2-3**), since CD36 is required for astrocyte activation [157] and mediates Aβ-induced inflammatory signaling [158].

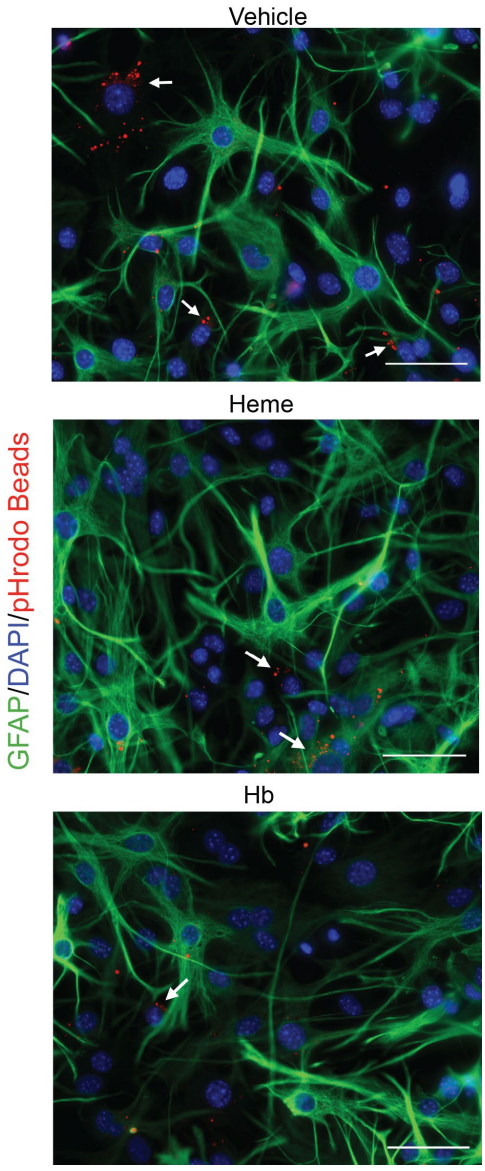

Figure 2-8. Representative fluorescent microscopy images of pHrodo bead (red) phagocytosis by control, heme, and Hb treated primary astrocytes. Astrocytes are co-stained for GFAP (green) and DAPI (blue). Arrows indicate cells with internalized beads. Scale bars: 50 µm. This figure was originally published in the Journal of Biological Chemistry. *Sankar et al. Heme and hemoglobin suppress amyloid β–mediated inflammatory activation of mouse astrocytes. J. Biol. Chem. 2018; 293: 11358-11373. © the American Society for Biochemistry and Molecular Biology*

2.3.4 Heme modulates $A\beta_{1-42}$ induced microglial cytokine expression and suppresses microglial scavenger activity

In order to assess the effects of heme and Hb on microglial immune function, we performed a similar analysis on the SIM-A9 spontaneously immortalized microglial cell line. While primary microglia provide the most physiologically relevant *in vitro* platform, they do not readily proliferate in culture and thus require large animal numbers for experiments of this nature [159]. Therefore, we initially performed these experiments with the SIM-A9 cell line. The SIM-A9 cell line is suitable for this study because it is expected to behave more comparably to primary microglia than virally transformed lines, as it is well characterized to phagocytose Aβ, express key activation markers (CD68, Iba-1), and undergo M1/M2 polarization as assessed via inducible nitric oxygen synthase and Arginase-1 expression [160].

Using similar methodology to the primary astrocytes, we conditioned cells with combinations of 50 nM recombinant $A\beta_{1-42}$, equimolar (50 nM) heme or Hb, and high (25 μM) dose heme, and used a multiplexed immunoassay to quantify protein expression of a panel of 32 cytokines into the culture medium. Similar to primary astrocytes, application of $A\beta_{1-42}$ broadly increased expression of numerous pro-inflammatory cytokines, while neither Hb nor high or low doses of heme significantly modulated cytokine expression compared to control (**Figure 2-9A-D**). Although to a lesser degree than primary astrocytes, low doses of heme and Hb suppressed expression of several cytokines, including IL-4, IL-10, and IL-2 (**Figure 2-9E**). Furthermore, in stark contrast to astrocytes, 25 μM heme applied together with $A\beta_{1-42}$ significantly amplified expression of certain cytokines, including TNF-α, IL-6, and MIP-1α, compared to treatment with $A\beta_{1-42}$ alone (**Figure**

2-9E). Repeating this experiment using primary microglia derived from mouse pups yielded a very similar cytokine expression panel in response to all conditions (**Figure 2-10**). Lastly, cytokine expression in response to just 25 μM heme was compared between primary mouse microglia and RAW 264.7 macrophages, which have been previously reported to express pro-inflammatory factors in response to heme [97, 145]. Consistent with these prior findings, heme on its own was robustly inflammatory in the RAW 264.7 macrophages, but only upregulated few analytes (ie. IP-10, KC), in microglia (**Figure 2-11**), a surprising finding given the similar developmental lineage between astrocytes and microglia [161].

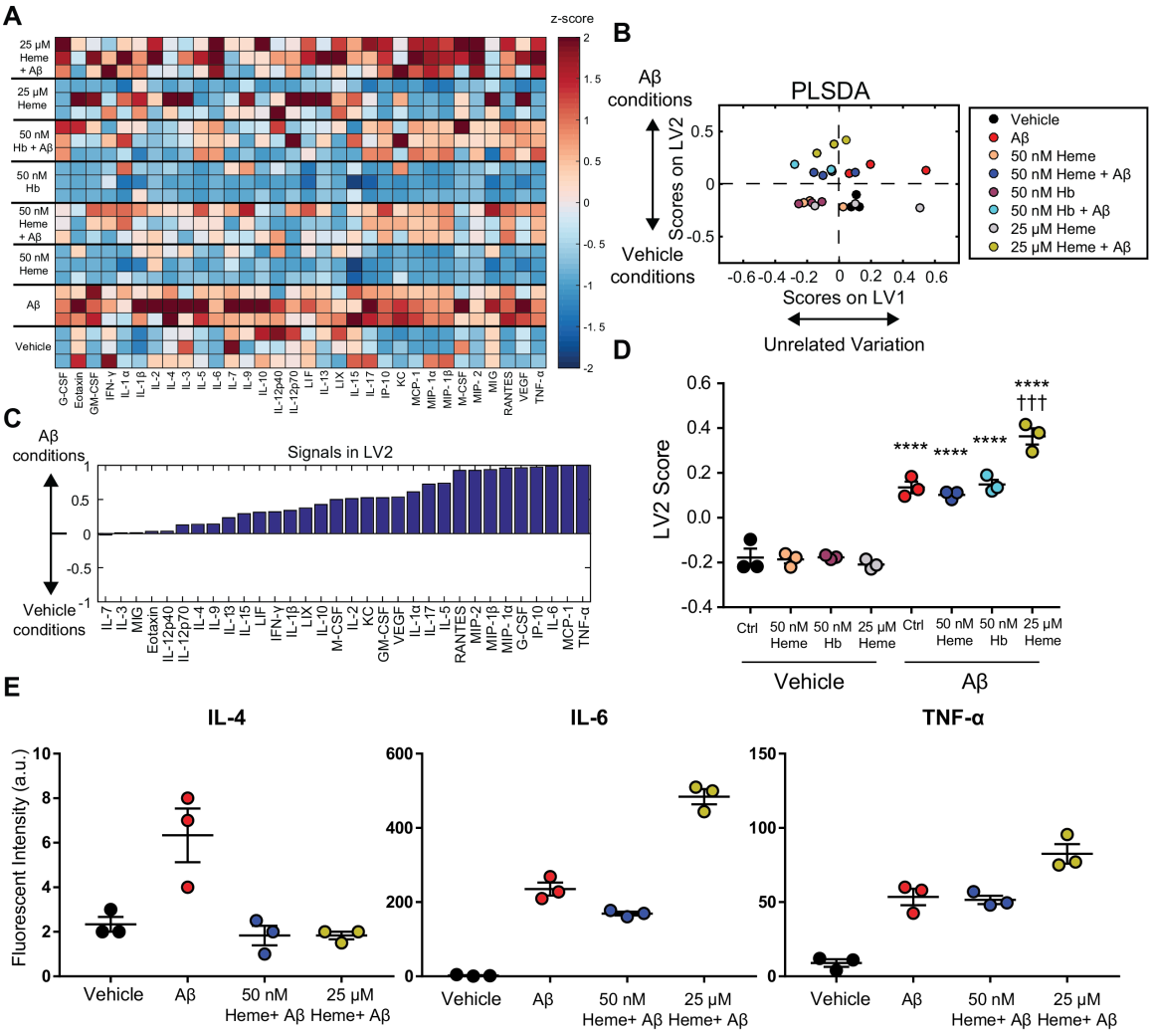

Figure 2-9. Heme and Hb modulate Aβ1-42 induced cytokine expression in SIM-A9 microglia. A. Quantification of 32 cytokines expressed into the medium of SIM-A9 microglia cultures via Luminex analysis. Each column is z-scored. Compared to vehicle control, cytokine expression is increased in response to 50 nM $A\beta_{1\text{-}42}$. Co-conditioning of $A\beta_{1\text{-}42}$ with either 50 nM heme or 50 nM Hb suppressed expression of some cytokines, while 25 μM heme increased expression of some cytokines. B. A PLSDA generated from the cytokine expression dataset, identified a latent variable (LV2), based on cytokine expression, which separates $A\beta_{1\text{-}42}$-only treated SIM-A9 microglia from all other conditions along the vertical axis. C. LV2 depicts a linear combination of cytokines that correlate with the $A\beta_{1\text{-}42}$-only condition, and identifies TNF-α as the top correlate with $A\beta_{1\text{-}42}$ treatment. D. Plotting LV2 scores for each group shows that the LV2 profile segregates Aβ1-42 treated astrocytes from all other conditions and further segregates the 25 μM heme + $A\beta_{1\text{-}42}$ from the $A\beta_{1\text{-}42}$-only condition. E. Plotting cytokine expression for 3 consistently measured cytokines reveals that heme suppresses expression of some cytokines and increases expression of others. Data are presented as mean ± SEM. ****I<0.0001 (vs.

vehicle control); ††† p<0.001 (vs $A\beta_{1-42}$); ordinary one-way ANOVA with Dunnett's post-hoc test.

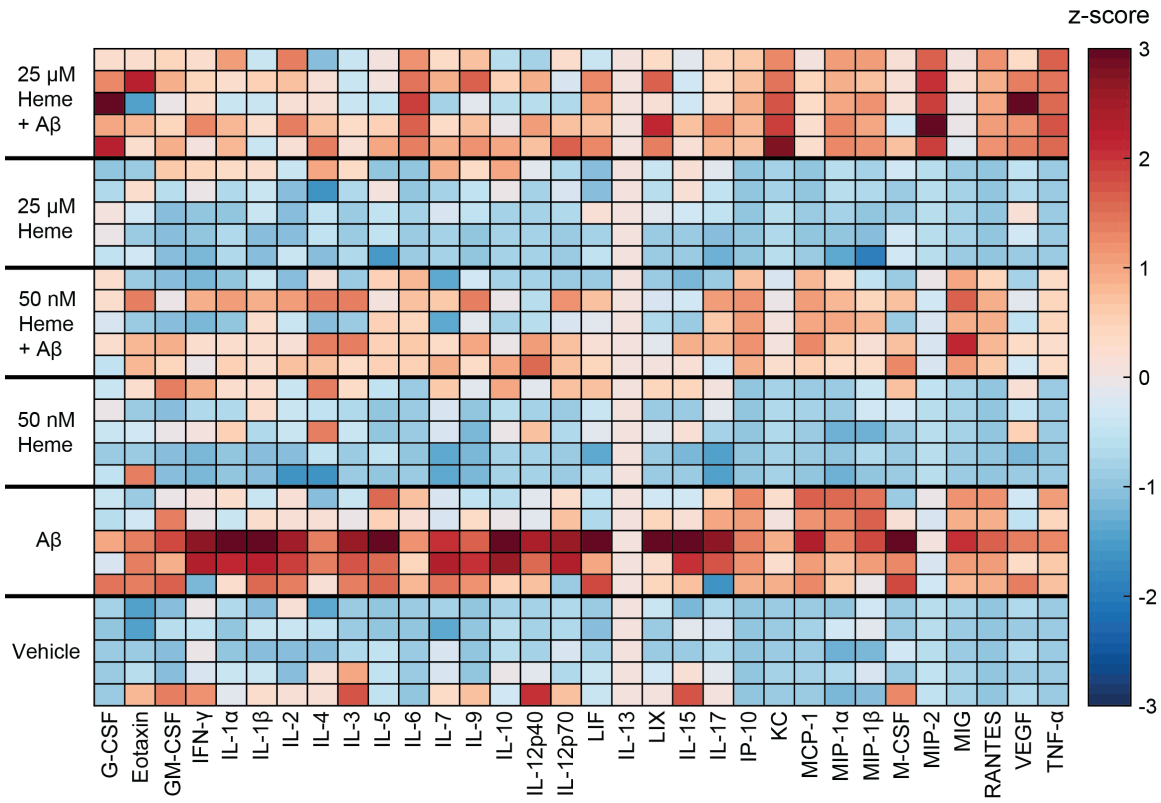

Figure 2-10. Heme modulates $A\beta_{1-42}$ induced cytokine expression in primary mouse microglia in a dose dependent manner. Quantification of 32 cytokines expressed into the medium of primary mouse microglia cultures via Luminex analysis. Each column is z-scored.

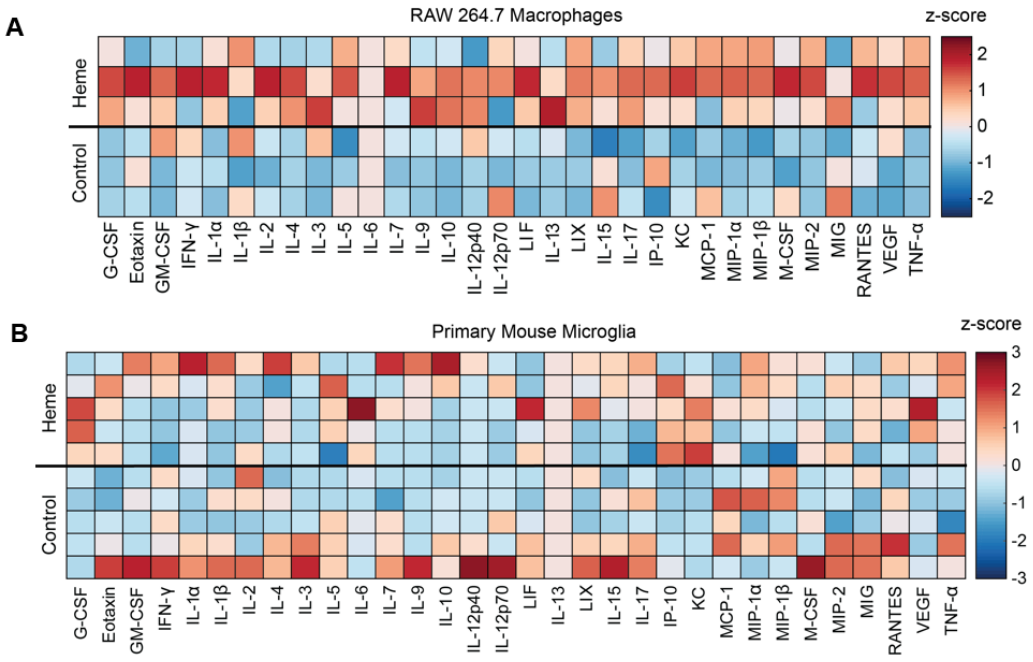

Figure 2-11. Cytokine expression by RAW 264.7 macrophages and primary mouse microglia in response to 25 µM heme. A. Quantification of 32 cytokines expressed into the medium of RAW 264.7 macrophage cultures via Luminex analysis. Each column is z-scored. Compared to vehicle control, cytokine expression is broadly increased in response to 25 µM heme. B. As in A for primary microglia. Compared to vehicle, cytokine expression of only a few cytokines is upregulated in response to 25 µM heme.

Since, in contrast to astrocytes, the effect of heme on $A\beta_{1\text{-}42}$-mediated cytokine expression was dose-dependent in SIM-A9 microglia, we sought to look at whether other immune functions has dose-dependent phenotypes as well. We again quantified SIM-A9 internalization of fluorescein-labeled, E. coli particles and found that both 50 nM and 25 µM heme suppressed bead uptake (**Figure 2-12A**). To determine if these effects were mirrored in phagocytic uptake specifically, we incubated SIM-A9 microglia with pH-sensitive pHrodo® Zymosan particles and found that indeed, both high and low doses of heme dramatically decreased phagocytosis (**Figure 2-12B-C**).

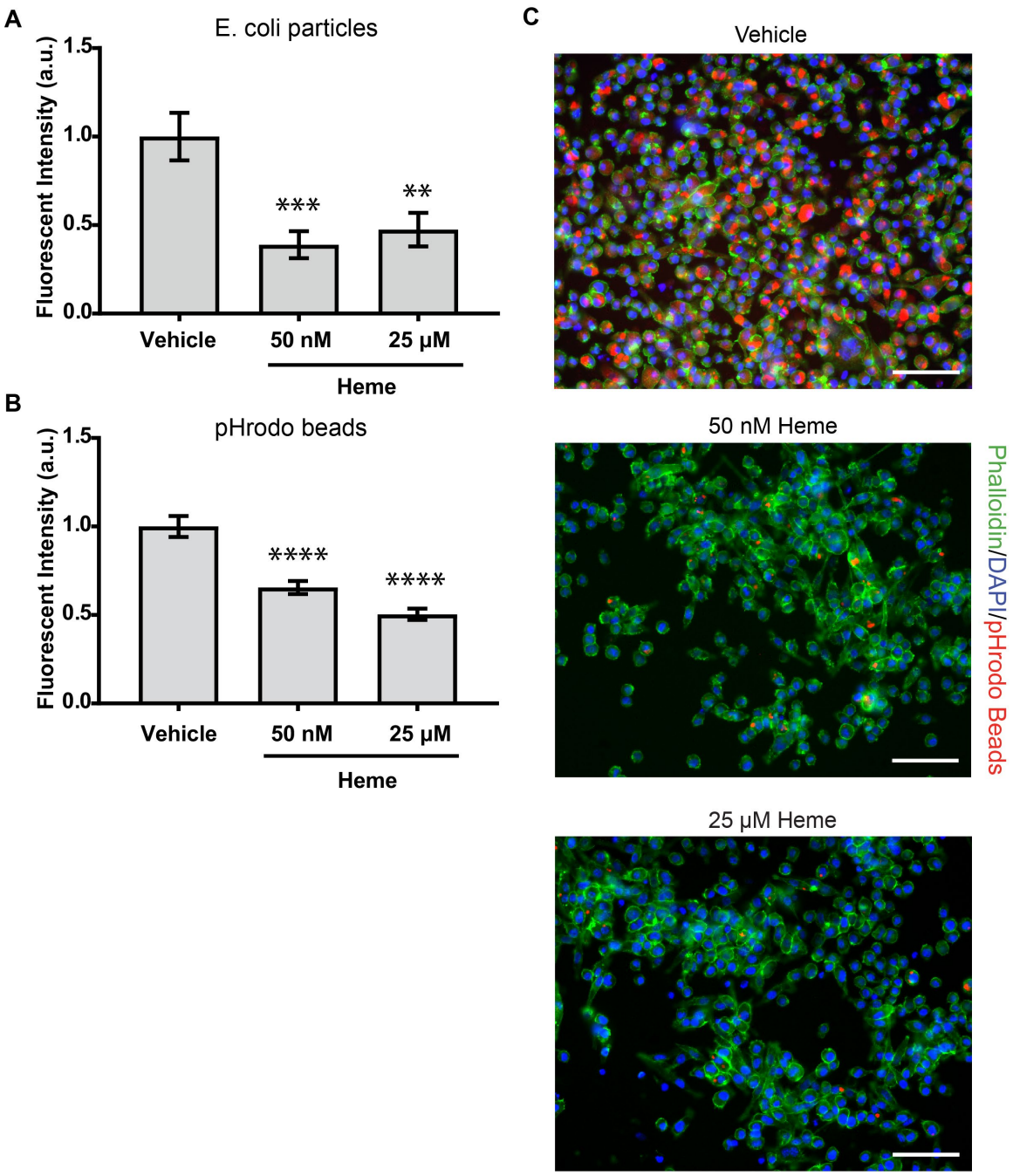

Figure 2-12. High and low doses of heme suppress SIM-A9 phagocytic capacity. A. SIM-A9 microglia, pre-incubated with 50 nM or 25 µM heme, were incubated with trypan-quenched, fluorescein labeled, killed E.coli particles. Particle internalization, measured by fluorescent intensity using a microplate reader, significantly decreased upon incubation with both heme concentrations (n=45-48 wells, p=0.002; vehicle vs. 50 nM heme, p=0.012; vehicle vs 25 µM heme). B. SIM-A9 microglia, pre-incubated with 50 nM or 25 µM heme, were incubated with pH sensitive pHrodo beads to assess phagocytic capacity. The percentage of total cells uptaking beads, quantified by fluorescence microscopy and

ImageJ, was significantly reduced upon treatment with Hb (n=32 images; $p<0.0001$; vehicle vs. 50 nM heme and vehicle vs. 25 μM heme). C. Representative fluorescent microscopy images of pHrodo bead (red) phagocytosis by control, 50 nM heme, and 25 μM heme treated SIM-A9 microglia co-stained for phalloidin (green) and DAPI (blue). Scale bars: 50 μm. *This figure was originally published in the Journal of Biological Chemistry. Sankar et al. Heme and hemoglobin suppress amyloid β–mediated inflammatory activation of mouse astrocytes. J. Biol. Chem. 2018; 293: 11358-11373. © the American Society for Biochemistry and Molecular Biology*

2.4 Discussion

Glial immune activity is recognized as a key component of AD pathology [162], but it remains debated whether glial activity is deleterious [128] or neuroprotective [129, 163]. In reality, it is likely that the consequences of neuroinflammation occupy a continuum between neuroprotective and neurodegenerative. In terms of protective effects in the context of AD, glial activation is essential for clearance of cytotoxic Aβ species [58, 59]. On the contrary, in terms of aggravating AD pathogenesis, excessive neuroinflammation contributes to a number of detrimental effects, including "fatigued" glia that are unable to clear Aβ, generation of toxic reactive oxygen species, and hyperactivated microglia that indiscriminately phagocytize neurons [56, 62, 64, 134]. Further complicating matters is the reality that different species of Aβ may affect neuroinflammation in very different ways, and the effects of each species may be modulated by other aspects of tissue pathology. In the work described in this chapter, we have identified heme and Hb as key AD-relevant immunomodulators and have probed mechanisms that mediate the inflammatory activation of astrocytes, both in $A\beta_{1–42}$ dependent and independent capacities. Moreover, we have identified key $A\beta_{1-42}$ species that are responsible for astrocyte activation and the effects of heme and Hb on the inflammatory potential of these species. Overall, our data indicate that heme and Hb suppress the $A\beta_{1–42}$-mediated inflammatory activation of astrocytes,

suggesting that these factors contribute to AD pathogenesis by impairing Aβ clearance mechanisms.

Simultaneous analysis of the relative expression of 32 cytokines into culture media provided a broad view of astrocyte inflammatory response to $A\beta_{1–42}$, heme, Hb, and heme or Hb-bound species of $A\beta_{1–42}$. First, we applied a HFIP pretreated $A\beta_{1–42}$ alone and in combination with either heme or Hb to astrocyte cultures (**Figure 2-3A**). PLSDA identified a latent variable, which is a composite variable including all analytes measured (**Figure 2-3B-C**). Scoring each sample on this latent variable demonstrated that both heme and Hb reduced cytokine expression which was highly upregulated by $A\beta_{1–42}$ (**Figure 2-3E**). From this analysis, $A\beta_{1–42}$ conditioning strongly correlates with RANTES, GM-CSF, and IL-1β, which were all downregulated in cultures co-treated with heme or Hb (**Figure 2-3F**). Of these, RANTES is a pro-inflammatory chemokine and involved in microglial recruitment [164, 165], GM-CSF promotes microglial proliferation [166], and IL-1β is a highly pro-inflammatory cytokine up-regulated early in AD [167] that has been shown to promote Aβ clearance in a mouse model [168]. Interestingly, application of heme or Hb at low concentration (50 nM) did not strongly suppress expression of other cytokines, including IP-10, KC, and MCP-1, which are all involved in immune cell recruitment [152, 153, 169]. However, application of a high dose of heme (25 μM) reduced these cytokines as well, suggesting that dose-dependent effects are associated with heme/Hb suppression of $A\beta_{1-42}$-induced inflammatory response. Since few changes in cytokine expression were observed in response to Hb or either dose of heme alone, it is likely that these dose-dependent changes are indicative of dose-dependent modifications to Aβ. Notably, the cytokines

modulated by heme and Hb are well-established to modulate immune activity, but have not generally been found to be neurotoxic.

Performing similar analysis on SIM-A9 microglia produced markedly different results. Similarly to astrocytes, $A\beta_{1-42}$ broadly upregulated cytokines and neither Hb nor high or low doses of heme produced robust cytokine effects on their own (**Figure 2-9A-D**). However, in stark contrast to the astrocytes, modulation of $A\beta_{1-42}$-induced cytokine expression by heme was highly dichotomous with respect to dosage. In the case of 50 nM heme or Hb, many cytokines were downregulated compared to the $A\beta_{1-42}$ only condition (**Figure 2-9A**). Several cytokines, including IL-4, IL-9, and KC were suppressed upon co-treatment of $A\beta_{1-42}$ with either 50 nM and 25 μM doses of heme. However, as identified by PLSDA (**Figure 2-9B-D**), many cytokines which were either suppressed or unchanged in response to 50 nM heme were in fact upregulated in response to co-treatment with 25 μM heme, including TNF-α, IL-6, and MCP-1. Notably, these results were very consistent between primary mouse microglia and the SIM-A9 microglia (**Figure 2-10**), suggesting that the SIM-A9 cell line is highly representative of the behavior of primary cells.

Interestingly, in contrast to the astrocytes, heme shifted $A\beta_{1-42}$-induced cytokine expression towards a more neurotoxic profile, particularly when considering the dose-dependent effects. Cytokines such as IL-4 and IL-9, which were suppressed by both low and high doses of heme are known to be involved in neuroprotection [55, 170]. Conversely, TNF-α and IL-6, which were upregulated by co-treatment with high heme are known to contribute to neurotoxicity in the context of AD [171, 172]. Taken together, heme could promote Aβ-induced neurotoxicity by microglia, by both downregulating secretion of neuroprotective factors and upregulating secretion of neurotoxic factors.

Concerning differences in modulation of cytokine expression between astrocytes and microglia, one possible explanation is that heme imparts dose-dependent modifications to Aβ, which results in distinct Aβ species/aggregation states between 50 nM and 25 μM heme. It is possible that the cellular targets of these species are distinct between astrocytes and microglia, which are known to present different extracellular receptors [62, 173], resulting in very different downstream effects. A similar argument can be made regarding the differences in cytokine expression in response to 25 μM heme alone between RAW 264.7 macrophages and microglia. Although peripheral macrophages and microglia share a common myeloid origin, environmental factors ultimately cause difference in receptor expression, ultimately leading to differing responses to external stimuli such as heme [174].

As previously postulated, mechanisms of heme and Hb immunomodulatory activity produced by binding or physically modifying $A\beta_{1–42}$ represent one possible explanation for dose-dependent effects on cytokine expression. Evidence for heme and Hb downregulating astrocyte inflammatory activity through physically modifying $A\beta_{1–42}$ stems from our finding that heme and Hb bind to a particularly inflammatory species of $A\beta_{1–42}$ [127]. Indeed, our analysis revealed that a soluble HMW oligomeric species of $A\beta_{1–42}$ (>75 kDa) produced the principal inflammatory response compared with other fractions (**Figure 2-4**, **Figure 2-5**, **Figure 2-6**). Moreover, the $A\beta_{1–42}$ HMW soluble oligomer was found to be the only species that was verified to be associated with heme or Hb [127] and strongly suppressed cytokine expression compared with the unbound oligomer. Further, this result is particularly important because it provides a physiological context to previously described Aβ–heme and Aβ–Hb interactions, as soluble Aβ oligomers are abundant in human AD brain tissue and have high binding affinities and neurotoxic properties [155, 175].

Altogether, the isolation of distinct $A\beta_{1–42}$ species and the effect of heme or Hb on their distribution and inflammatory activation of astrocytes highlight the complex and nuanced nature of Aβ-mediated immune signaling. Indeed, the observation of changes in neuroinflammation over the course of AD may reflect the competing effects of multiple Aβ, Aβ–heme, and/or Aβ–Hb species that have differing immunomodulatory activities. Additionally, the peroxidase activity of heme–Aβ complexes may further act to modulate the inflammatory response [82].

A second mechanism of heme/Hb control of inflammatory activity is via direct action on astrocyte signaling, which is supported by our observations that heme and Hb suppressed killed *E. coli* particle internalization, phagocytosis, and CD36 expression (**Figure 2-7**, **Figure 2-8**) in experiments free of $A\beta_{1–42}$. Our results in astrocytes generally point toward heme as having anti-inflammatory effects at both low and high heme concentrations. Moreover, we found that scavenger activity of astrocytes was inhibited by low (50 nM) heme concentrations and that both low and high (25 μM) heme concentrations inhibited scavenger activity of SIM-A9 microglia (**Figure 2-12**). Nevertheless, the canonical role of heme in immune signaling, primarily delineated in macrophages and endothelial cells, is that it stimulates inflammation via receptors such as TLR4 [97]. As such, it is clear that the immunomodulatory roles of heme and Hb are distinct in the context of the brain.

Altogether, our data indicate that Hb and heme are potent modulators of astrocyte and microglial immune activity by both Aβ-independent and Aβ-dependent mechanisms. Given reports of increased Hb in late-stage AD and in transgenic mouse models, Hb and heme signaling and physical activity represent possible mechanisms responsible for

astrocyte fatigue in AD tissues, thereby permitting amyloid pathogenesis. Additionally, recent findings of BBB leakage early in AD suggest that Hb concentration may be locally increased at the vascular wall [176]. By extension, Hb and heme activity may be responsible for a high prevalence of cerebral amyloid angiopathy in AD patients [176]. Taken together, this work suggests that intervening in Hb/heme signaling may represent a novel therapeutic strategy for AD. Furthermore, this approach establishes a rigorous methodology to analyze the immunomodulatory effects of diverse proteins and other molecules that co-localize or associate with Aβ.

CHAPTER 3. DETERMINING THE EFFECTS OF HEME ON ASTROCYTE IMMUNE SIGNALING MECHANISMS *IN VITRO*

3.1 Introduction

While Hb and heme have been traditionally known for their oxygen-carrying properties [73, 74], recent work has implicated them as potent immunomodulatory signaling molecules, mediating both pro- and anti-inflammatory effects. In many pathological conditions, heme and Hb directly induce the expression of a wide array of pro- and anti-inflammatory cytokines [177, 178] and heme has also been shown to enhance chemokine expression and chemotaxis of immune cells [98]. Heme-mediated immunomodulatory signaling may occur through both extra- and intra-cellular mechanisms. With regards to extracellular mechanisms of action, heme has been characterized to activate TLR4 in multiple cell types, resulting in inflammatory cytokine expression and cell activation [95-97]. Exogenous heme has also been reported to promote cytokine expression via activating TLR2 [179]. Furthermore, Hb has been shown to modulate IL-10 expression via the scavenger receptor CD163 [177]. Heme further exerts pro-inflammatory effects intracellularly, through activating inflammatory transcription factors, including p53 [103, 104], and Rev-erbα [105-110]. Conversely, catabolism of heme via HO-1 also occurs intracellularly, producing anti-inflammatory by-products including, CO, biliverdin, and bilirubin, which suppress pro-inflammatory cytokine expression and upregulate anti-inflammatory cytokine expression, among many other anti-inflammatory activities [112-116].

Mechanistically, modulation of pro- and anti-inflammatory activation by heme and Hb can occur through kinase signaling pathways. In various contexts, heme has been reported to modulate phospho-signaling through the MAPK pathway [97, 99, 100, 180], protein tyrosine kinases [101, 102], the NF-κB pathway [97, 180], and the PI3K/Akt/mTOR pathway [180]. Heme degradation products, specifically bilirubin, have also been shown to modulate phospho-signaling in multiple contexts [181-183]. Moreover, independently of heme, Hb has been shown to modulate the NF-κB pathway [111].

Phospho-signaling pathways are heavily involved in neuroinflammatory processes linked to AD. The MAPK and NF-κB pathways are both strong inflammatory regulators, due to their direction transduction of cytokines and their downstream regulation of transcription factors that promote expression of pro-inflammatory cytokines and other mediators of inflammation [184, 185]. Most relevant to AD is the PI3K/Akt/mTOR pathway, which is involved in both early and late pathological stages of the disease. With regards to modulating neuroinflammation in AD, this pathway is well established to modulate glial activation and cytokine expression [186, 187] and is a critical regulator of autophagy in astrocytes [188].

Having previously observed numerous changes in astrocyte immune function in response to heme (**CHAPTER 2**) [127], herein, we elucidate the immunomodulatory signaling mechanisms driven by heme in astrocytes. Our data reveal that both exogenous and intra-cellular heme robustly modulate phosphorylation of the Akt/mTOR signaling pathway. Interestingly, we found that extracellularly, heme activates Akt/mTOR signaling through activating Insulin-like growth factor 1 receptor (IGF1R). Finally, we found that dysregulation of the Akt/mTOR pathway by heme was directly linked to expression of

CD36 and HO-1, suggesting that astrocyte immune mechanisms disrupted by heme are at least partially regulated by the Akt/mTOR pathway.

3.2 Materials and Methods

3.2.1 Primary mouse astrocyte cultures

Primary mouse astrocyte cultures were derived and maintained as described in Chapter 2.2.2. Briefly, astrocytes were derived from postnatal day 0–1 CD1 mice (Charles River Laboratories) under a protocol approved by the Georgia Institute of Technology Institutional Animal Care and Use Committee. Astrocytes were cultured in astrocyte medium (ScienCell) with 2% fetal bovine serum (FBS) (ScienCell), 1% penicillin/streptomycin solution (ScienCell), and 1% astrocyte growth serum (ScienCell), for up to four passages for experiments.

3.2.2 Cell conditioning and lysis

For phospho-protein signaling experiments, primary mouse astrocytes were plated in 6-well plates. At 80% confluency, cells were serum starved for 1 hour in serum free astrocyte media. For receptor or phospho-signaling inhibition experiments, cells were serum starved in combination with either BMS536924 (100 nM; Selleck Chemicals, Houston, TX), or rapamycin (10 nM; Selleck Chemicals). Cells were conditioned for indicated time points between 5 min and 24 h with combinations of hemin chloride (25 μM; EMD Millipore), ALA (800 μM, Sigma Aldrich), BMS536924 (100 nM; Selleck Chemicals), and rapamycin (10 nM; Selleck Chemicals). Cell lysates were collected using the Bio-Plex cell lysis kit, with the addition of one cOmplete mini protease inhibitor tablet

and 20 µl of PMSF per 5 ml of lysis buffer. Lysates were placed in microcentrifuge tubes and inverted at 4 °C for 10 min, then centrifuged at 4 °C for 10 min at 13,000 rpm. Supernatant was collected and stored at -80 °C.

3.2.3 Multiplexed phospho-protein signaling analysis

Cell lysates were thawed on ice and centrifuged at 4 °C for 10 min at 13,000 rpm. Protein concentrations were determined using a Pierce BCA protein assay (Thermo Fisher Scientific) and normalized with Milliplex® MAP assay buffer (EMD Millipore) to 2 µg of protein/25 µl for Akt/mTor pathway analysis, 0.75 µg of protein/25 µl for MAPK pathway analysis, or 0.75 µg of protein/25 µl for NFκB pathway analysis. These protein concentrations were selected because they fell within the linear range of bead fluorescence intensity versus protein concentration for detectable analytes. Multiplexed phospho-protein quantification was conducted for the Akt/mTOR, MAPK, and NF-κB signaling pathways using the Milliplex® MAP Akt/mTOR 11-Plex (p-Akt, p-GSK3α/β, p-IGF1R,p-IR, p-IRS1, p-mTOR, p-p70S6K, p-PTEN, p-RPS6, and p-TSC2), MAPK/SAPK 10-Plex (p-ATF2, p-Erk1/2, p-HSP27, p-JNK, p-c-Jun, p-MEK1, p-MSK1, p-p38, p-p53), and NFκB 6-Plex (c-Myc, p-FADD, p-IκBα, p-IKKα/β, p-NF-κB, TNFR1) phospho-signaling magnetic bead kits (EMD Millipore). All kits were read on a MAGPIX® system (Luminex, Austin, TX).

3.2.4 Heme uptake quantification

Primary astrocytes were plated in T-75 flasks in complete astrocyte medium. At 70% confluency, cells were transfected with 10 µg of pcDNA3.1-HS1 [189] using Lipofectamine LTX with PLUS Reagent (Invitrogen), in astrocyte media containing 10%

heme depleted (HD) FBS and 0.5 mM succinylacetone (SA) (Sigma), to inhibit heme synthesis. After 24 hours, the media was replaced with fresh astrocyte media containing 10% HD FBS and 0.5 mM SA. Cells were then conditioned with either fresh 0.5 mM SA, 800 µM ALA, or 25 µM heme in astrocyte media with 10% HD FBS, for one of the following time points: 5 min, 15 min, 30 min, 1 h, 4 h, 8 h, 24 h. After conditioning, media was aspirated, cells were rinsed with Dulbecco's PBS (DPBS), and lifted with Trypsin-EDTA solution (Sigma). Cells were washed three times with DPBS to remove trypsin, resuspended in 500 µL DPBS, and pushed through a 35µm nylon mesh strainer prior to analysis. Cells were analyzed via flow cytometry on a BD LSRFortessa™ flow cytometer (BD, Franklin Lakes, NJ), equipped with a 488 nm argon laser and a 561 nm yellow-green laser. EGFP was excited via the 488 laser and emission filtered using a 530/30 nm bandpass filter while mKATE2 was excited via the 561 laser and emission filtered using a 610/20 nm bandpass filter. Data was analyzed using FlowJo v10.4.2 (BD, Franklin Lakes, NJ). Astrocyte were gated using forward and side scatter parameters and transfected cells were gated using negative gating on an untransfected control, ensuring that only transfected astrocytes were considered for analysis.

3.2.5 Immunofluorescent staining

Cells were fixed with 4% PFA, permeabilized for 10 min at RT with 0.1% Triton X-100, and blocked with a 5% BSA, 3% goat serum (Sigma) solution for 1 h. Primary antibody incubation was performed overnight at 4 °C, using the HO-1 antibody (1:200; Novus) in 0.5% BSA wash buffer. After washing with wash buffer, fixed cells were incubated with Alexa Fluor 555 goat anti-mouse secondary antibody (1:200; Thermo Fisher Scientific) for 2 h at RT. Cells were co-stained with DAPI (100 ng/ml; Thermo

Fisher Scientific) for nuclei. Cells were imaged using epifluorescent microscopy on a Zeiss Axio Observer Z.1 inverted microscope.

3.2.6 Western blot

Cell lysates, obtained as described above, were thawed on ice and then centrifuged for 10 min at 10,000 rpm and 4 °C. Protein concentration was determined using a Pierce BCA protein assay and equal amounts of protein were dissolved in reducing sample buffer, boiled, and loaded onto sodium dodecyl sulfate (SDS)-polyacrylamide gels. Following separation by electrophoresis, proteins were transferred to a Hybond P 0.45-µm polyvinylidene fluoride membrane (GE Healthcare). Membranes were blocked at room temperature (RT) for 1 h with 5% milk in Tris-buffered saline containing 0.01% Tween 20 (TBST). Membranes were probed at 4 °C overnight with rabbit anti-CD36 (1:500; Novus Biologicals, Littleton, CO) and mouse anti-α-tubulin (1:2000; Sigma). Membranes were then incubated with Alexa Fluor–conjugated secondary antibodies (1:2000; Thermo Fisher Scientific) for 2 h at RT. Imaging of blots was performed using an Odyssey CLx imager (LI-COR Biosciences, Lincoln, NE). Protein quantification was performed using Image Studio Lite version 5.2 (LI-COR Biosciences).

3.2.7 Partial least-squares discriminant analysis

As in Chapter 2.2.12, PLSDA was performed in MATLAB using the partial least squares algorithm by Cleiton Nunes available on the Mathworks File Exchange. All data were z-scored before inputting into the algorithm. For all analyses, an orthogonal rotation in the LV1-LV2 plane was performed to identify a new LV1 that better separated groups.

LV1 error bars were generated by iteratively excluding samples without replacement 1000 times and report the mean ± SD computed across all regenerated models.

3.2.8 Statistics

All statistical analyses were performed using GraphPad Prism version 8 (GraphPad Software, La Jolla, CA). Values are presented as mean ± SEM. Statistical significance was determined, as appropriate, using Student's t test or ordinary one-way ANOVA followed by either Sidak's or Holm-Sidak's post hoc test. Normality of data was tested using the Shapiro–Wilk test of normality. Levels of significance were set as follows: $*p < 0.05$, $**p < 0.01$, $***p < 0.001$, $****p < 0.0001$.

3.3 Results

3.3.1 Exogenous heme modulates the Akt/mTOR pathway in astrocytes in the presence of Aβ

Because phospho-protein signaling occurs on a much faster time scale (on the order of minutes) than other phenotypic responses [190], we analyzed phosphoproteins from astrocytes conditioned with combinations of $A\beta_{1–42}$, 50 nM heme, and 50 nM Hb at 5- and 15-min time points (**Figure 3-1**, **Figure 3-2**). To simultaneously account for data from both time points, we concatenated the time point data and used PLSDA to identify signaling differences between conditions. Analyzing the effects of heme alone identified two axes of interest with respect to heme and $A\beta_{1–42}$ (**Figure 3-1**A). First, LV1 separated heme + $A\beta_{1–42}$ to the right with all other conditions to the left. Among other signals in the pathway, LV1 consisted of phospho-Akt, phospho-PTEN, and phospho-TCS2 at the 5-min time point as

top correlates with the heme + $A\beta_{1–42}$ condition (**Figure 3-1**B). The PLSDA also determined that both heme and heme + $A\beta_{1–42}$ were increased along LV2 (**Figure 3-1**A), which consisted of phospho-mTOR at 15 min, and phospho-IRS1 at both 5- and 15-min time points as top correlates with heme or heme + $A\beta_{1–42}$ (**Figure 3-1**C). Plotting all condition groups along LV1 revealed that heme + $A\beta_{1–42}$ was significantly different from heme alone (**Figure 3-1**D), whereas plotting along LV2 revealed that treatment either with heme alone or with heme + $A\beta_{1–42}$ was significantly different from vehicle controls (**Figure 3-1**E). Thus, these data indicate that heme can significantly shift signaling within the Akt/mTOR signaling pathway, which is modulated by $A\beta_{1–42}$. Applying the same analysis to Hb revealed that Hb did not significantly modulate signaling within the pathway compared with either control or $A\beta_{1–42}$ alone (**Figure 3-2**).

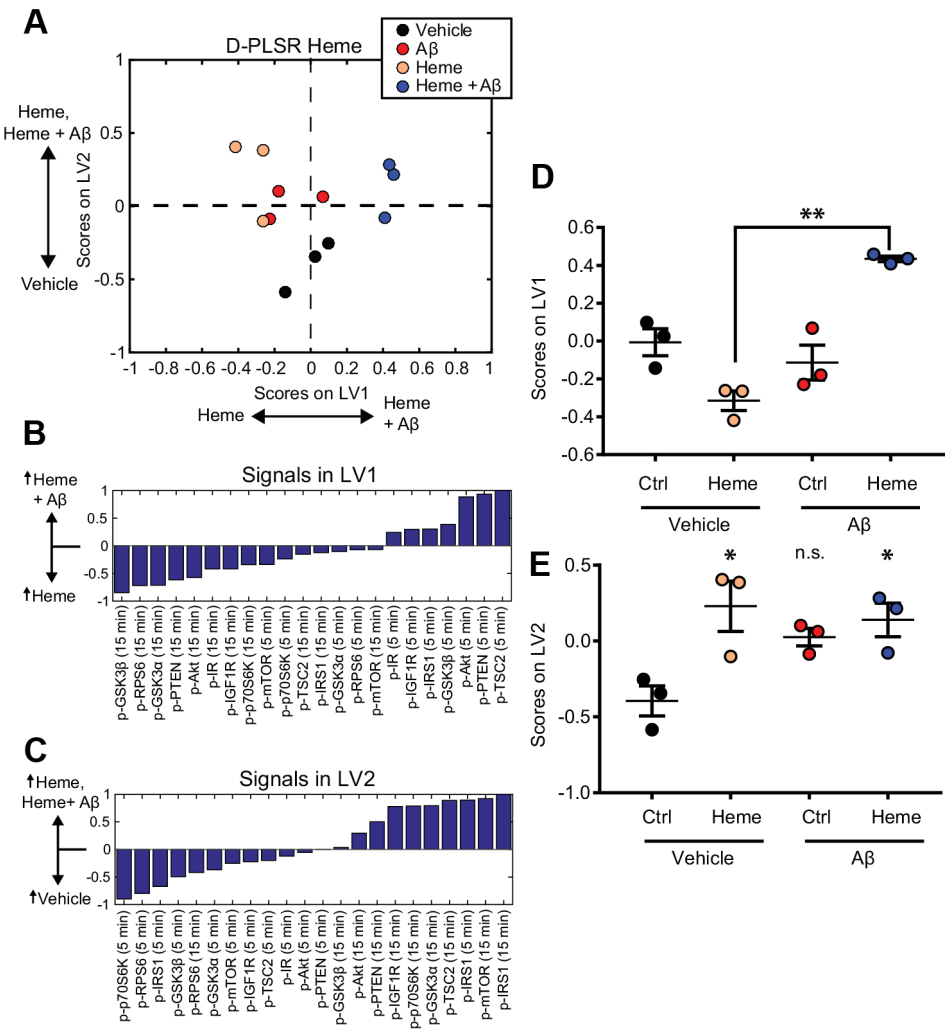

Figure 3-1. Akt/mTOR pathway signaling is modulated by heme and Aβ at 5 and 15 minutes. A. PLSDA of astrocyte Akt/mTOR phospho-protein signaling identifies a latent variable (LV1) that separates the heme + $A\beta_{1\text{-}42}$ condition from the heme-only condition along the horizontal axis and, second, a latent variable (LV2) that separates all heme conditions from the vehicle condition along the vertical axis. B. LV1 depicts a linear combination of phosphoproteins at the 5- and 15-min time points that correlate with the heme + $A\beta_{1\text{–}42}$ or heme-only conditions. LV1 identifies upstream elements of the pathway, including p-PTEN, p-Akt, and p-TSC2, at 5 min as top correlates with the heme + $A\beta_{1\text{–}42}$ condition. C. LV2 depicts a linear combination of phosphoproteins at the 5- and 15-min time points that correlate with the heme and heme + $A\beta_{1\text{–}42}$ conditions or the vehicle control. LV2 identifies p-mTOR at 15 min and p-IRS at 15 and 5 min as top correlates with both heme conditions. D. Plotting LV1 scores for each group shows that the LV1 profile significantly segregates the heme + $A\beta_{1\text{–}42}$ signaling effects from heme-only signaling effects (**p<0.01, Kruskal-Wallis test with Dunn's multiple comparisons test). E. Plotting LV2 scores for each group shows that the LV2 profile significantly segregates all heme conditions from the vehicle control (*p<0.05, ordinary one-way ANOVA with Sidak's multiple comparisons test, compared to vehicle control). This figure was modified from its

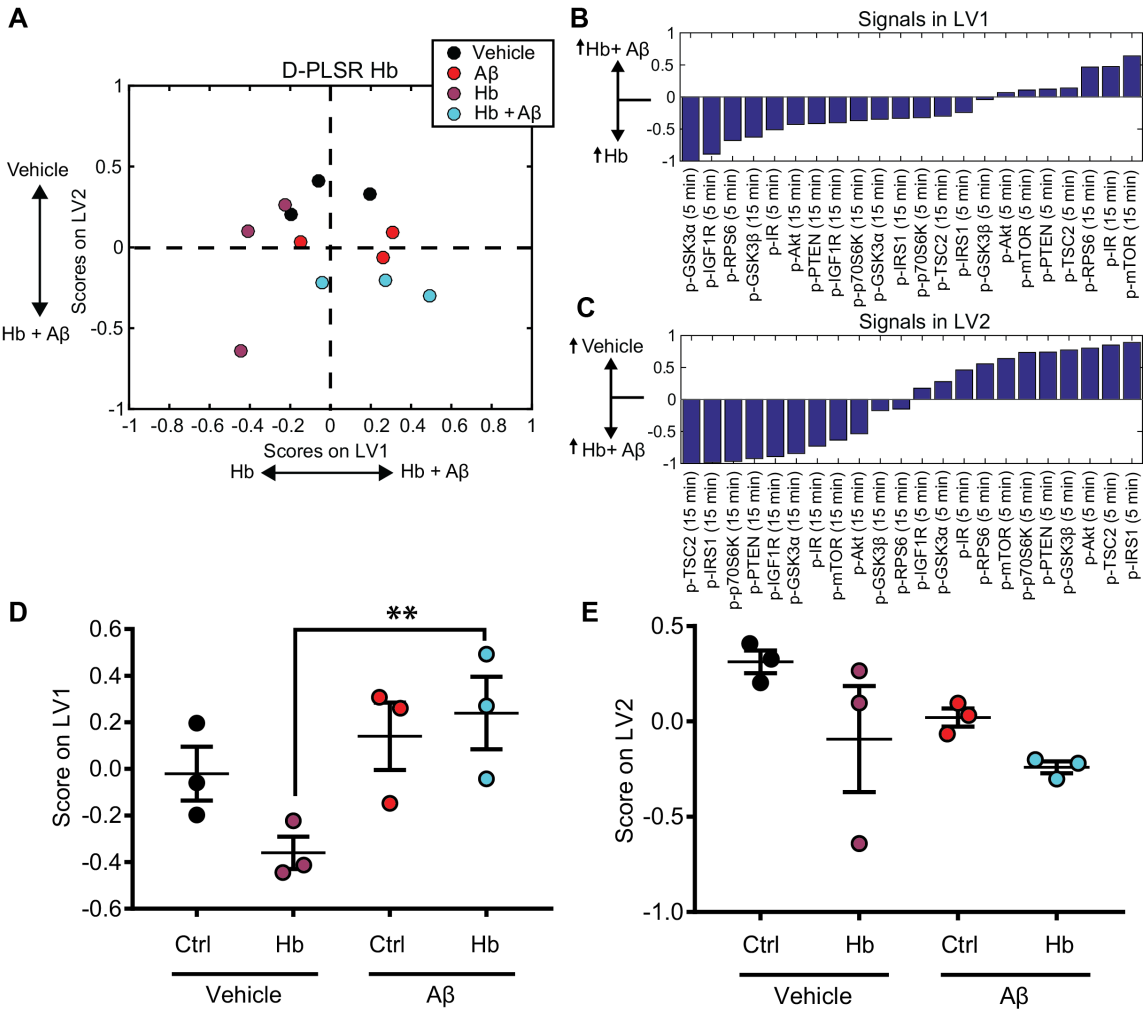

Figure 3-2. Akt/mTOR pathway signaling is not significantly modulated by Hb and Aβ at 5 and 15 minutes. A. PLSDA analysis of astrocyte Akt/mTOR phospho-protein signaling identifies a latent variable (LV1) which separates the Hb+Aβ condition from the Hb-only condition along the horizontal axis, and second a latent variable (LV2) which separates, to a lesser extent, the Hb+Aβ condition from the vehicle condition along the vertical axis. B. LV1 depicts a linear combination of phospho-proteins at the 5 and 15 min time points that correlate with the Hb+$A\beta_{1\text{-}42}$ or Hb-only conditions. LV1 identifies p-mTOR at the 15 min time point as the top correlated with Hb+$A\beta_{1\text{-}42}$. C. LV2 depicts a linear combination of phospho-proteins at the 5 and 15 min time points that correlate with the Hb+$A\beta_{1\text{-}42}$ or vehicle conditions. D. Plotting LV1 scores for each group shows that the LV1 profile significantly segregates the Hb+$A\beta_{1\text{-}42}$ signaling effects from Hb-only signaling effects (n=3, p=0.0097; Hb vs. Hb+$A\beta_{1\text{-}42}$). E. Plotting LV2 scores does not show any significant differences between groups on this axis. Data represented as mean ± SEM. **p<0.01; ordinary one-way ANOVA with Sidak's post hoc test.This figure was modified from its original publication in the Journal of Biological Chemistry. Sankar et al. Heme and hemoglobin suppress amyloid β–mediated inflammatory activation of mouse

astrocytes. J. Biol. Chem. 2018; 293: 11358-11373. © the American Society for Biochemistry and Molecular Biology

3.3.2 Exogenous heme upregulates the Akt/mTOR, NF-κB, and MAPK phospho-protein signaling pathways in astrocytes

In order to more robustly examine the effects of heme on phospho-signaling outside of the context of Aβ, we conducted more thorough analyses of heme-driven phospho-signaling using a higher concentration of heme (25 μM), which is within a concentration range characteristic of hemolytic disorders [145, 191]. Since peak Akt/mTOR activation has been previously reported to occur on the order of 30 min in many cell types [192-194], we quantified astrocyte Akt/mTOR pathway phosphorylation in response to 30 min of 25 μM heme treatment (**Figure 3-3**A). PLSDA revealed that a profile of phospho-proteins in the Akt/mTOR pathway was robustly upregulated in response the heme treatment (**Figure 3-3**B-C). Individually plotting top analytes from this analysis, including p-mTOR, p-TSC2, p-PTEN, p-GSK3β, p-GSK3α, and p-Akt revealed that these changes were also significant on an individual protein level (**Figure 3-3**D). Similar analysis of the NF-κB signaling pathway revealed modest upregulation of a panel of phospho-proteins in this pathway, with top correlates with heme treatment including p-IκBα and p-NF-κB (**Figure 3-4**).

Since the MAPK pathway has been reported to be upregulated more quickly than the Akt pathway in astrocytes, we conducted a similar analysis of MAPK signaling using a 15 min time point [195]. Again, PLSDA analysis revealed modest upregulation of a profile of phospho-proteins in response to heme, with top correlates including p-Erk1/2 and p-Atf2 (**Figure 3-5**).

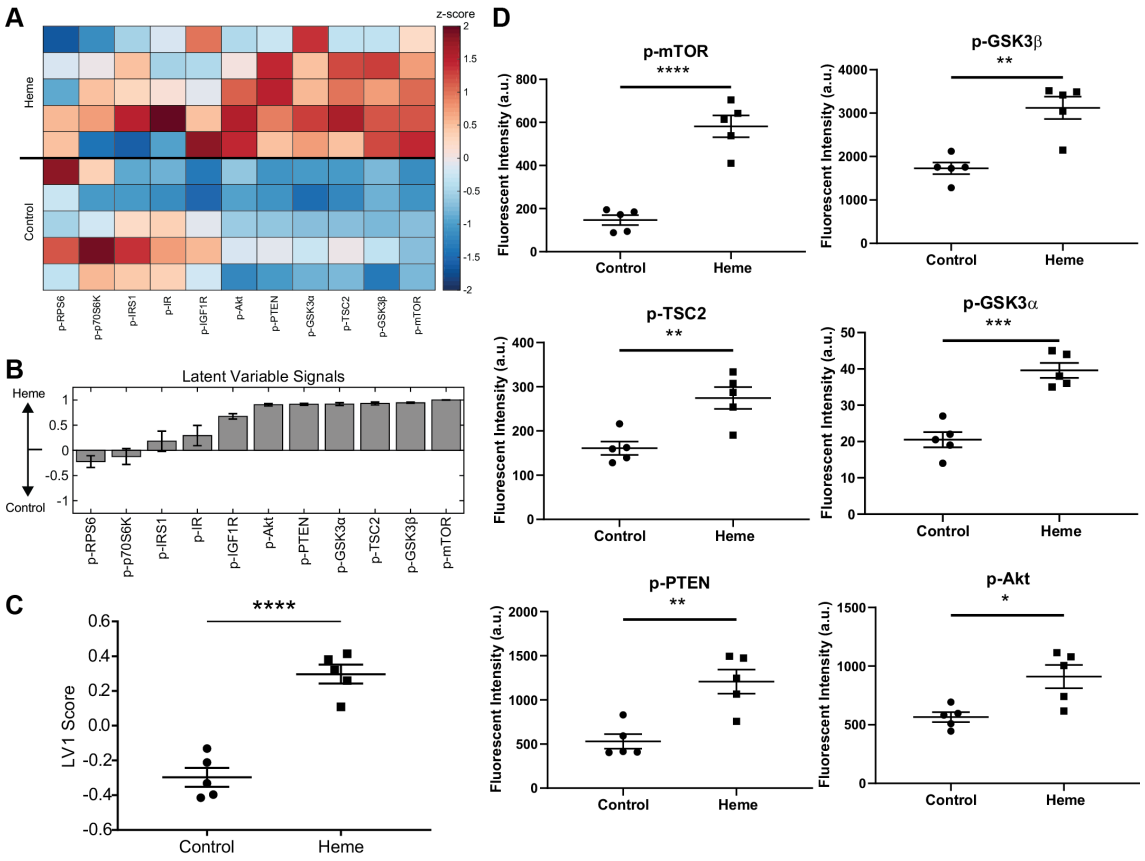

Figure 3-3. Heme upregulates the Akt/mTOR pathway in astrocytes after 30 minutes. A. Quantification of phosphorylation of 11 Akt/mTOR pathway phospho-proteins in primary astrocytes via Luminex analysis. Each column is z-scored and each row represents an individual sample. B. PLSDA identified a latent variable, which consisted of a weighted combination of phospho-proteins which best separated groups. Error bars are generated using a LOOCV (mean ± SD). C. Scoring each sample on this latent variable (LV1) revealed that heme treated samples were significantly upregulated on LV1 (error bars, mean ± SEM; ****p<.0.0001, Student's t-test). D. Individually plotting top analytes from LV1 reveals significant upregulation of p-mTOR, p-GSK3β, p-TSC2, p-GSK3α, p-PTEN, and p-Akt (error bars, mean ± SEM; ****p<.0.0001, ***p<.0.001, **p<.0.01, *p<.0.05, Student's t-test).

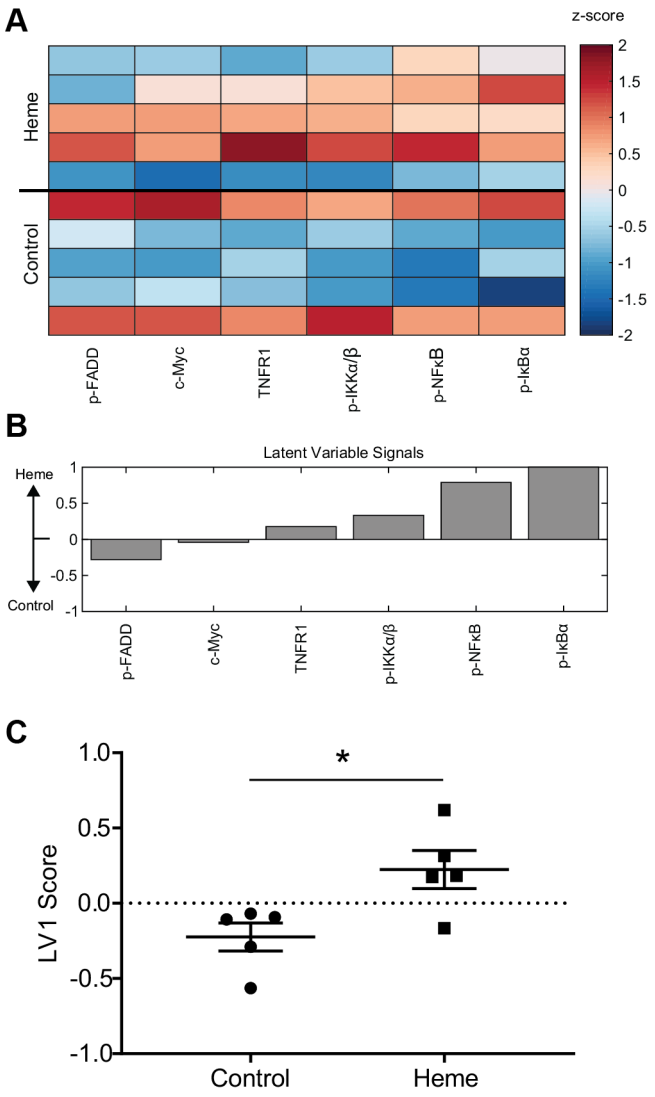

Figure 3-4. Heme upregulates the NF-κB pathway in astrocytes after 30 min. A. Quantification of phosphorylation of 6 NF-κB pathway phospho-proteins in primary astrocytes via Luminex analysis. Each column is z-scored and each row represents an individual sample. B. PLSDA identified a latent variable, which consisted of a weighted combination of phospho-proteins which best separated groups. C. Scoring each sample on this latent variable (LV1) revealed that heme treated samples were significantly upregulated on LV1 (error bars, mean ± SEM; *p<.0.05, Student's t-test).

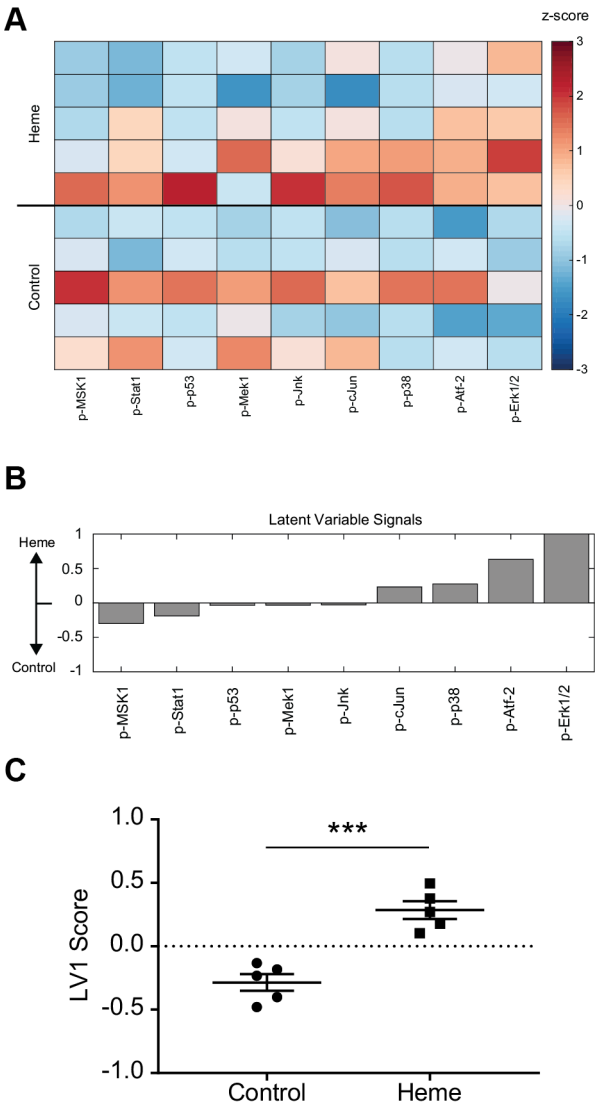

Figure 3-5. Heme upregulates the MAPK pathway in astrocytes after 15 min. A. Quantification of phosphorylation of 10 MAPK pathway phospho-proteins in primary astrocytes via Luminex analysis. Each column is z-scored and each row represents an individual sample. B. PLSDA identified a latent variable, which consisted of a weighted combination of phospho-proteins which best separated groups. C. Scoring each sample on this latent variable (LV1) revealed that heme treated samples were significantly upregulated on LV1 (error bars, mean ± SEM; ***p<.0.001, Student's t-test).

3.3.3 Heme uptake by astrocytes is rapid

To begin to elucidate the extracellular vs. intracellular contributions of heme on modulating Akt/mTOR phospho-signaling, we utilized a novel, genetically encoded ratiometric heme sensor, HS1 [189], to monitor heme uptake dynamics in astrocytes. HS1 is composed of an internal fluorescent standard, mKATE2, and the heme reporter, eGFP, whose fluorescence is quenched upon binding the heme-binding domain. Thus, labile heme can be quantified in terms of the eGFP:mKATE2 fluorescence ratio, with a lower eGFP:mKATE2 ratio indicating a relatively higher intracellular labile heme pool. Performing fluorescence microscopy determined successful expression of both mKATE2 and eGFP by primary mouse astrocytes after transfection with HS1 (**Error! Reference source not found.**).

In order to obtain information on an individual cell basis for a large volume of cells, we used flow cytometry to analyze heme uptake dynamics in astrocytes using HS1. HS1 transfected astrocytes were conditioned with either succinylacetone (SA) as a heme depleted control or 25 μM heme for either 5 min, 15 min, 30 min, 1 h, 4 h, or 24 h time points. Plotting histograms of eGFP to mKATE2 ratio and calculating mean eGFP to mKATE2 ratio for each time point revealed that exogenous heme uptake was rapid, with ~50% saturation of HS1 occurring within the first 30 minutes and HS1 saturation occurring within 4 h (**Figure 3-7A-B)**.

To determine how Akt/mTOR signaling dynamics corresponded with heme uptake dynamics, phosphorylation of critical nodes of the pathway, namely Akt and mTOR, was conducted over a similar time course. Interestingly, this analysis identified that peak Akt

and mTOR phosphorylation upregulation occurs early, from 15-30 min, when HS1 is ~50% saturated (**Figure 3-7B-D**). Moreover, from 4 - 24 h when HS1 is fully saturated, Akt and mTOR phosphorylation is decreased compared to control conditions (**Figure 3-7B-D**). Together, these findings suggest that early phospho-signaling upregulation may be due to extracellular effects of heme while later downregulation of signaling may be due to intracellular effects.

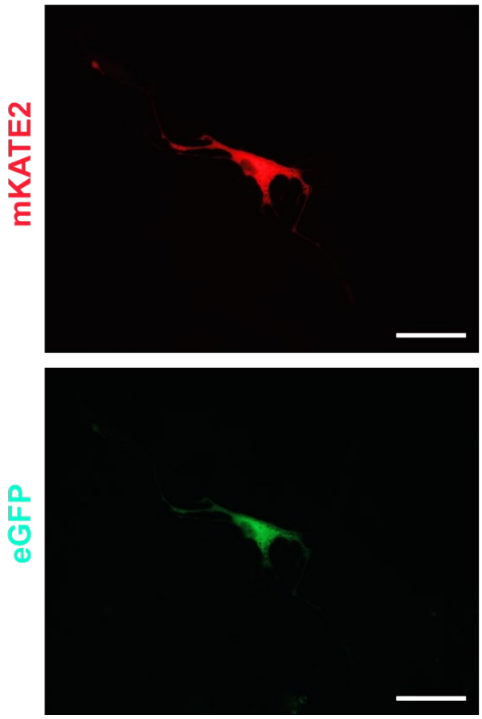

Figure 3-6. HS1 is expressed by primary mouse astrocytes. Red indicates expression of the mKATE2 internal standard and green indicates expression of eGFP. Scale bars: 20 µM

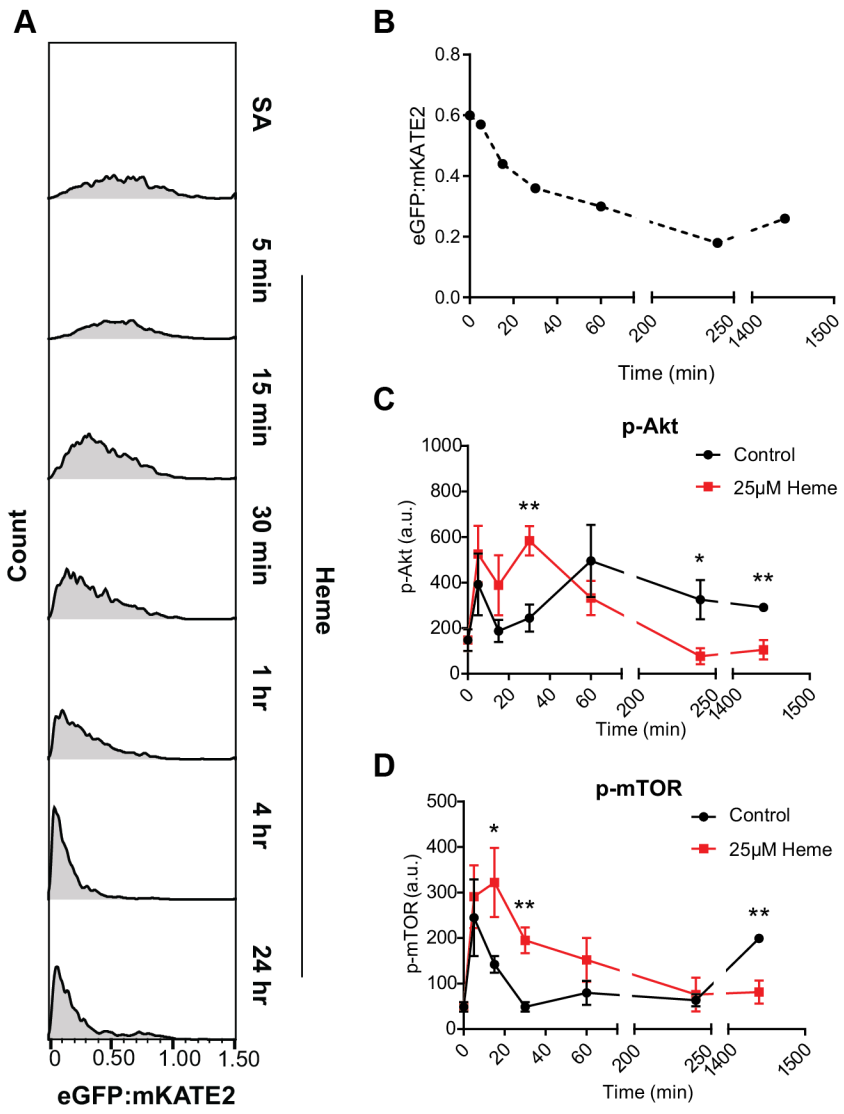

Figure 3-7. Heme uptake dynamics in astrocytes. A. Histograms depicting eGFP:mKATE2 ratio of astrocytes transfected with HS1 and treated with either SA for 24 hours or 25 μM heme for 5 min, 15 min, 30 min, 1 h, 4 h, or 24 h. B. Mean eGFP:mKATE2 ratio plotted over time. C. Time course of Akt phosphorylation in response to 25 μM heme or control conditions, quantified via Luminex analysis. (error bars, mean ± SEM; *p<0.05,**p<.0.01, Student's t-test) D. As in C for mTOR phosphorylation.

3.3.4 Upregulation of intracellular labile heme downregulates the Akt/mTOR pathway

To further elucidate the specific Akt/mTOR pathway signaling effects of intracellular heme, we sought to upregulate intracellular labile heme independently of

applying extracellular heme. To do so, we treated astrocytes with 800 µM δ-aminolevulinic acid (ALA), which is the first compound in the heme biosynthesis pathway (**Figure 3-8**). As a result, ALA is uptaken by cells and intracellular heme synthesis is increased. In order to determine the time required for ALA to upregulate labile heme in astrocytes, we used HS1 to compare labile heme levels for time points between 4 and 24 hours after ALA treatment (**Figure 3-9**). This revealed that HS1 saturation, and therefore labile heme upregulation, occurred between 4 and 8 hours after ALA treatment (**Figure 3-9**).

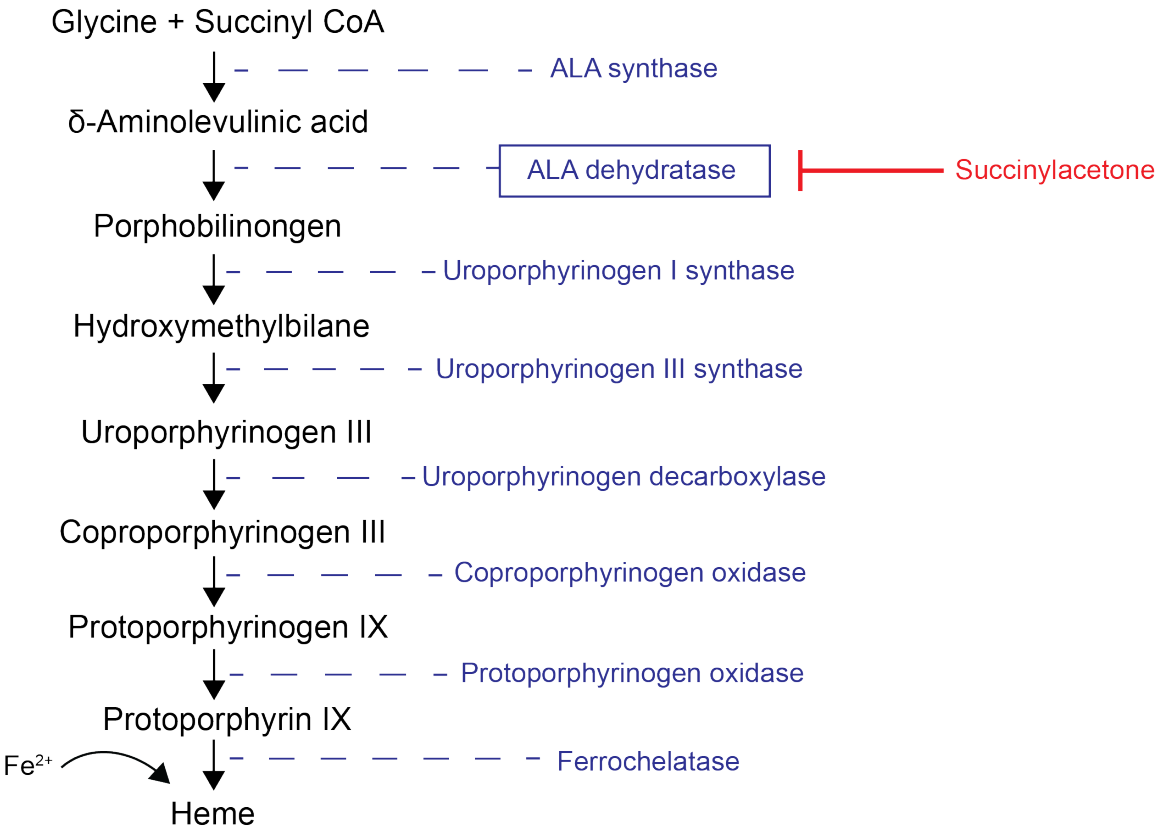

Figure 3-8. Heme biosynthesis pathway. Heme synthesis consists of a series of enzymatic steps, initiated by the synthesis of δ-aminolevulinic acid (ALA) from glycine and succinyl CoA. Succinylacetone inhibits the second step of heme synthesis by inhibiting the enzymatic activity of ALA dehydratase.

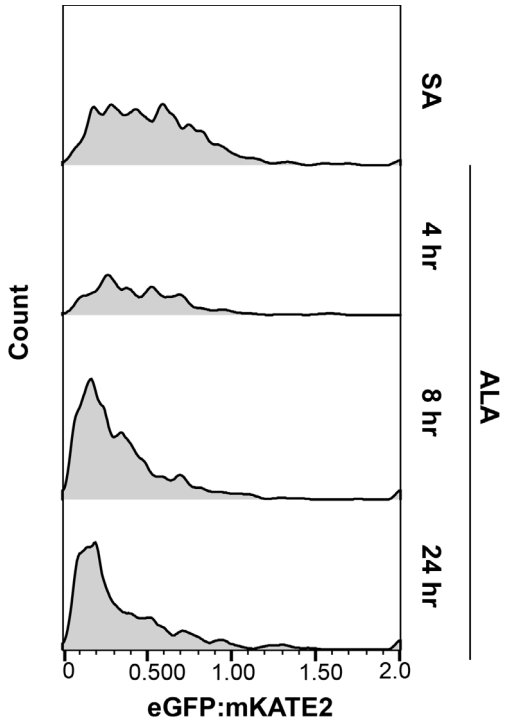

Figure 3-9. ALA upregulates intracellular labile heme in astrocytes. Histograms depicting eGFP:mKATE2 ratio of astrocytes transfected with HS1 and treated with either SA for 24 hours or 800 μM ALA for 4, 8, or 24 h.

To determine how labile heme upregulation affected Akt/mTOR signaling, we quantified Akt/mTOR pathway phospho-signaling at 6 and 8 hours after ALA treatment, which were within the window of labile heme upregulation as indicated by HS1. Interestingly, performing a PLSDA for both 6 hours (**Figure 3-10**A-C) and 8 hours (**Figure 3-10**D-F) revealed that upregulation of labile heme by ALA significantly suppressed expression of panels of phospho-proteins in the Akt/mTOR pathway at both time points. This is in stark contrast to the significant upregulation of the pathway observed 30 min after treatment with exogenous heme (**Figure 3-3**).

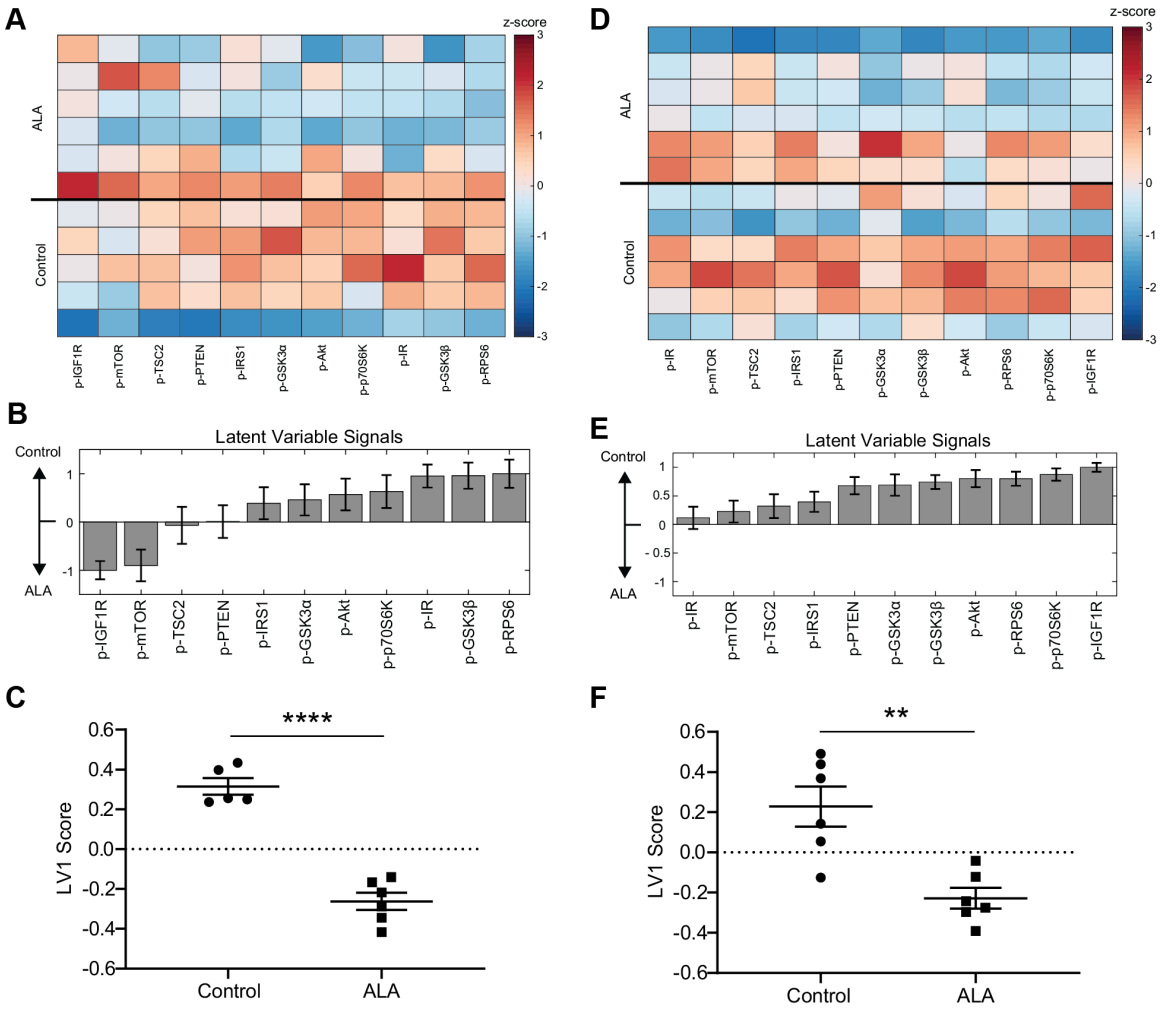

Figure 3-10. Upregulating intracellular heme using ALA suppresses Akt/mTOR pathway phosphorylation. A. Quantification of phosphorylation of 11 Akt/mTOR pathway phospho-proteins in primary astrocytes via Luminex analysis, after 6 hour ALA treatment. Each column is z-scored and each row represents an individual sample. B. PLSDA identified a latent variable, which consisted of a weighted combination of phospho-proteins which best separated groups. C. Scoring each sample on this latent variable (LV1) revealed that ALA treated samples were significantly downregulated on LV1 (error bars, mean ± SEM; ****p<.0.001, Student's t-test). D. As in A, for 8 hour after ALA treatment. E. As in B, for 8 hour ALA treatment. F. As in F, for 8 hour ALA treatment (error bars, mean ± SEM; **p<.0.01, Student's t-test)

3.3.5 Exogenous heme activates the Akt/mTOR pathway through activation of IGF1R

Due to rapid upregulation of Akt/mTOR signaling in response to exogenous heme (**Figure 3-7**) and distinctly different signaling effects in response to upregulation of intracellular heme (**Figure 3-10**), we hypothesized that heme may activate the Akt/mTOR pathway through activating cell surface receptors. Since IGF1R and insulin receptor (IR) are well characterized as receptors upstream of Akt and mTOR (**Figure 3-11**), we used BMS536924, a competitive inhibitor for IGF1R and IR, to block ligand-induced phosphorylation of these receptors [196]. Excitingly, we found that blocking IGF1R/IR attenuated Akt/mTOR pathway upregulation by heme, as determined by PLSDA (**Figure 3-12**). Since PLSDA identified IGF1R, and not IR, as a top correlate with heme treatment (**Figure 3-12B**), it is likely that IGF1R may be predominantly involved in this response. This suggests a novel role for heme as an agonist of IGF1R.

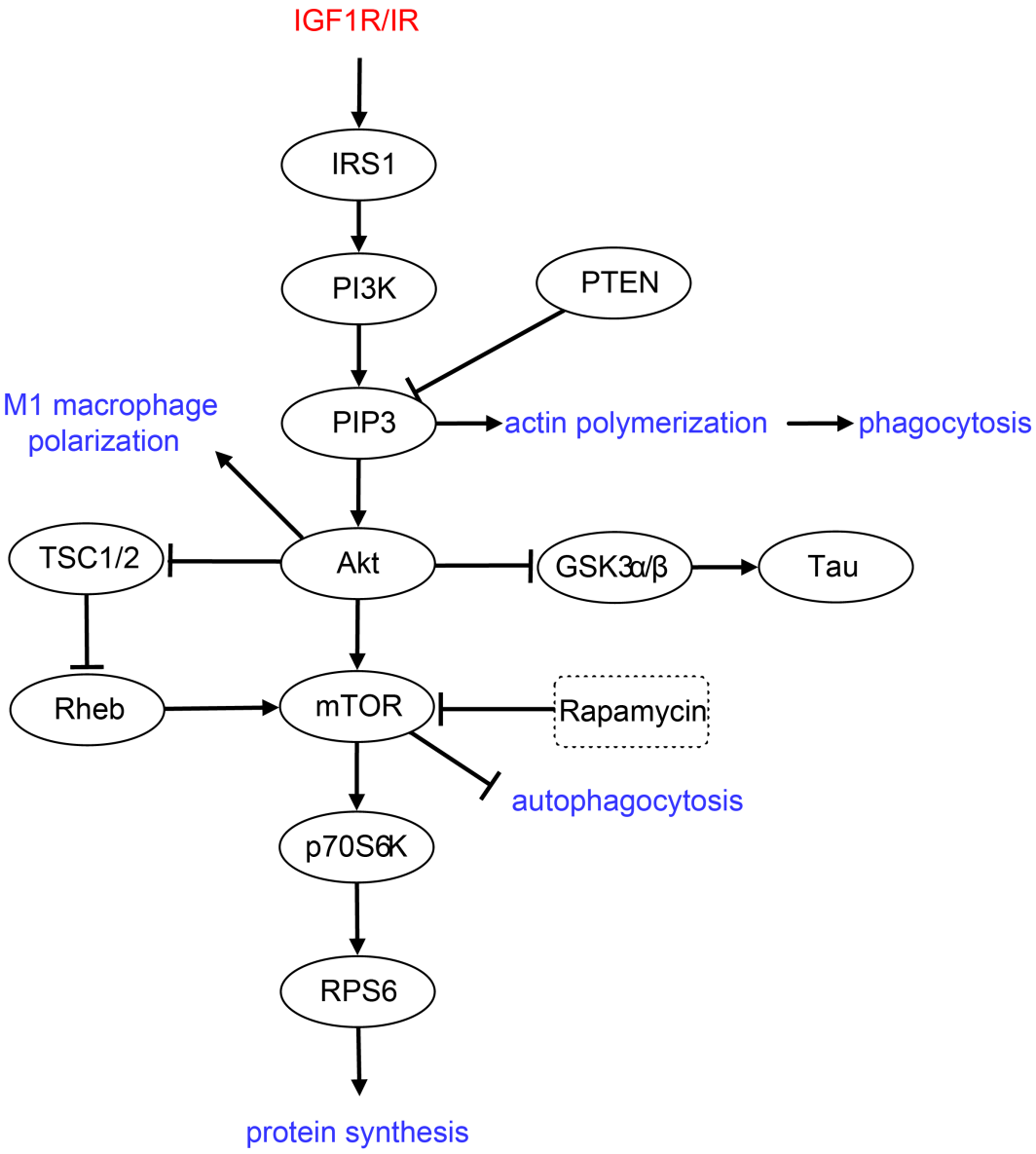

Figure 3-11. Illustration of the PI3K/Akt/mTOR signaling network, depicting nodes involved in mediating immunomodulatory and phagocytic functions. This figure was modified from its original publication in the Journal of Biological Chemistry. Sankar et al. Heme and hemoglobin suppress amyloid β–mediated inflammatory activation of mouse astrocytes. J. Biol. Chem. 2018; 293: 11358-11373. © the American Society for Biochemistry and Molecular Biology.

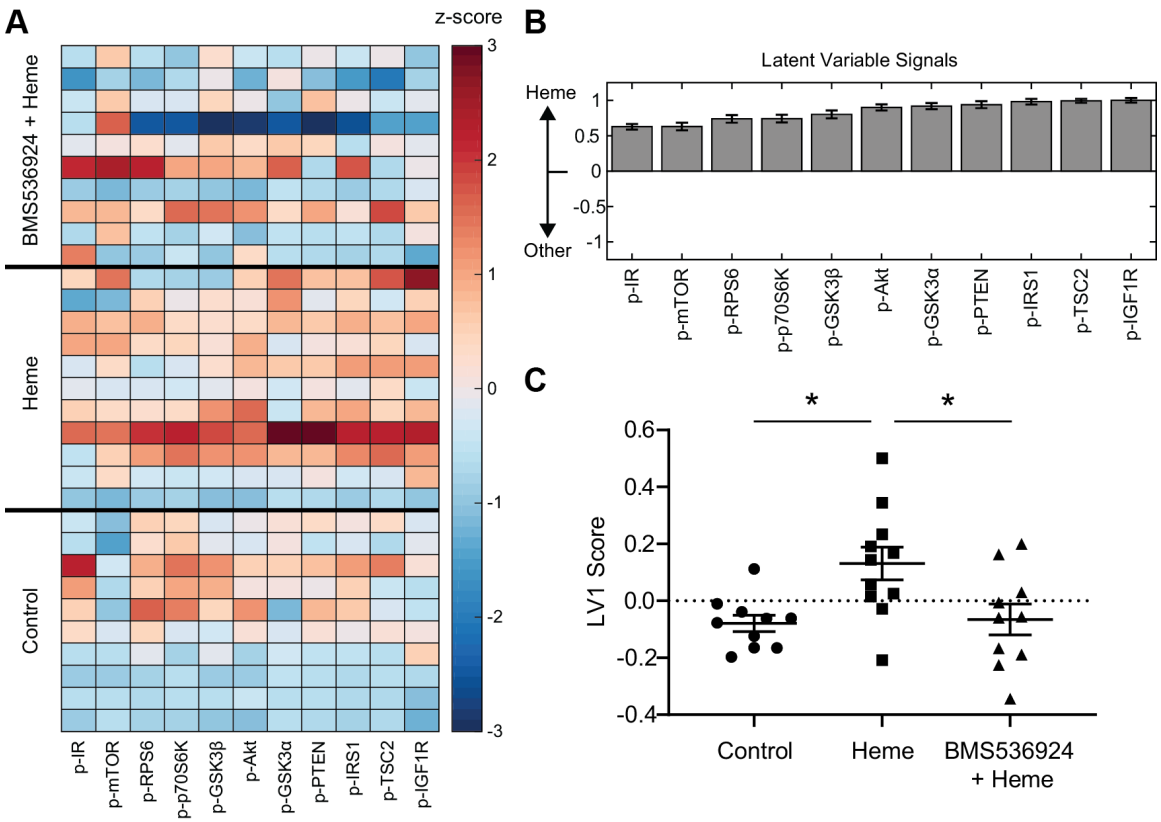

Figure 3-12. Inhibition of IGFIR/IR suppresses Akt/mTOR pathway activation in response to heme. A. Quantification of phosphorylation of 11 Akt/mTOR pathway phospho-proteins in primary astrocytes via Luminex analysis, after 30 minutes of heme treatment. B. PLDSA identified LV1, which separates heme treated astrocytes from all other groups. Error bars are generated using a LOOCV (mean ± SD). C. Scoring each sample on LV1 reveals that 25 μM heme significantly upregulates LV1 while inhibition of IGFIR/IR with BMS536924 attenuates this effect. (mean ± SEM, **p*<0.05, ordinary one-way ANOVA, with Holm-Sidak's post-hoc test.)

3.3.6 The Akt/mTOR pathway is linked to immune function in astrocytes

Given the robust modulation of the PI3K/Akt/mTOR signaling pathway in response to heme and the strong link between this pathway and regulation of immune expression, we next investigated whether perturbing Akt/mTOR signaling would restore immune phenotypes dysregulated by heme. We began by looking at CD36 expression, which we previously found to be strongly suppressed in response to heme (**Figure 2-7**). We

hypothesized that inhibition of the pathway would restore astrocyte scavenger receptor expression. To test this, we used rapamycin, which inhibits signaling through mTOR, a central node within the PI3K/Akt pathway (**Figure 3-11**). Indeed, co-treatment of heme + $A\beta_{1\text{-}42}$ with 10 nM rapamycin yielded partial recovery of CD36 expression.

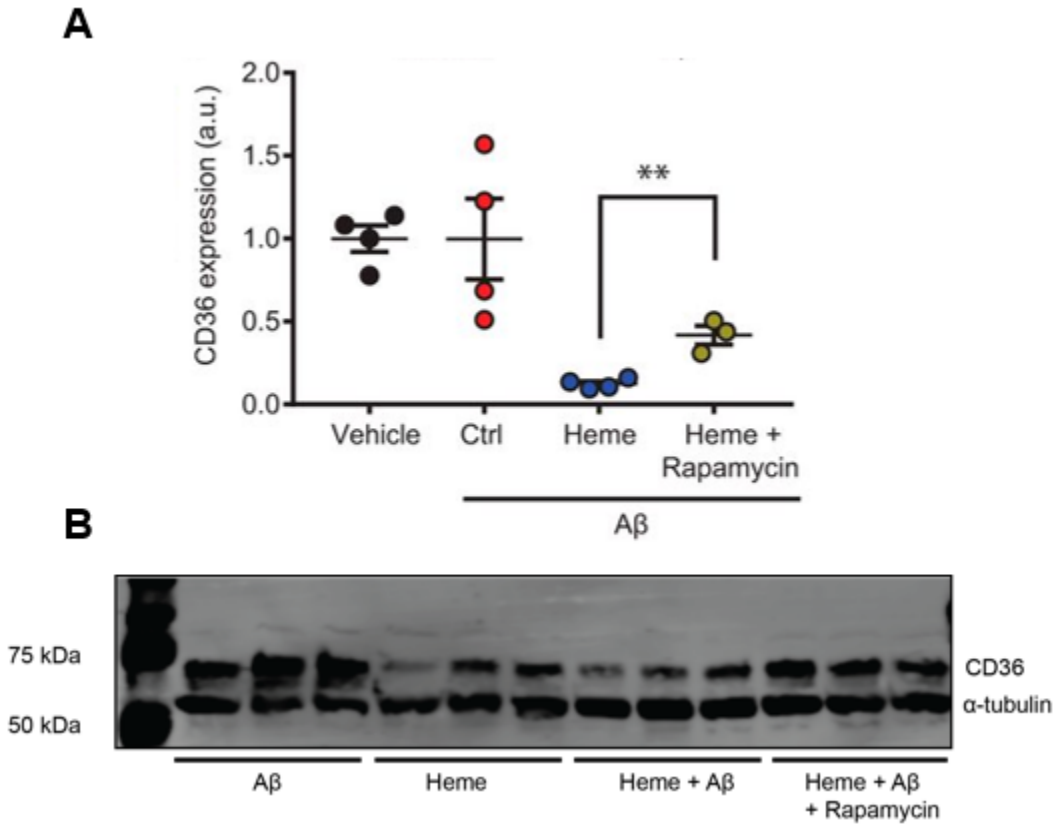

Figure 3-13. CD36 expression by astrocytes is partially recovered in response to rapamycin treatment. A. Co-treatment of astrocytes with heme + rapamycin increases CD36 expression compared with heme treatment alone. B. Western blot depicting CD36 expression (mean ± SEM, $^{**}p<0.01$, Student's t-test). This figure was modified from its original publication in the Journal of Biological Chemistry. Sankar et al. Heme and hemoglobin suppress amyloid β–mediated inflammatory activation of mouse astrocytes. J. Biol. Chem. 2018; 293: 11358-11373. © the American Society for Biochemistry and Molecular Biology

Since we observed numerous anti-inflammatory phenotypes in response to heme in astrocytes, we hypothesized that HO-1 activity may be involved in mediating these

processes, since it heme-inducible and is known to have anti-inflammatory roles [112-116]. Given the involvement of the Akt/mTOR pathway in regulating immune activity the link between HO-1 and kinase signaling [117, 119], we further hypothesized that the Akt/mTOR pathway may regulate HO-1 expression in astrocytes. Indeed, we found that HO-1 expression was significantly upregulated after 24 hours of heme treatment, suggesting that it could be downstream of Akt/mTOR pathway activation and responsible for anti-inflammatory phenotypes in astrocytes (**Figure 3-14A**). Moreover, we found that inhibiting mTOR with rapamycin significantly decreased HO-1 expression in response to heme **(Figure 3-14B-C**), suggesting that HO-1 expression is partially regulated by the Akt/mTOR pathway.

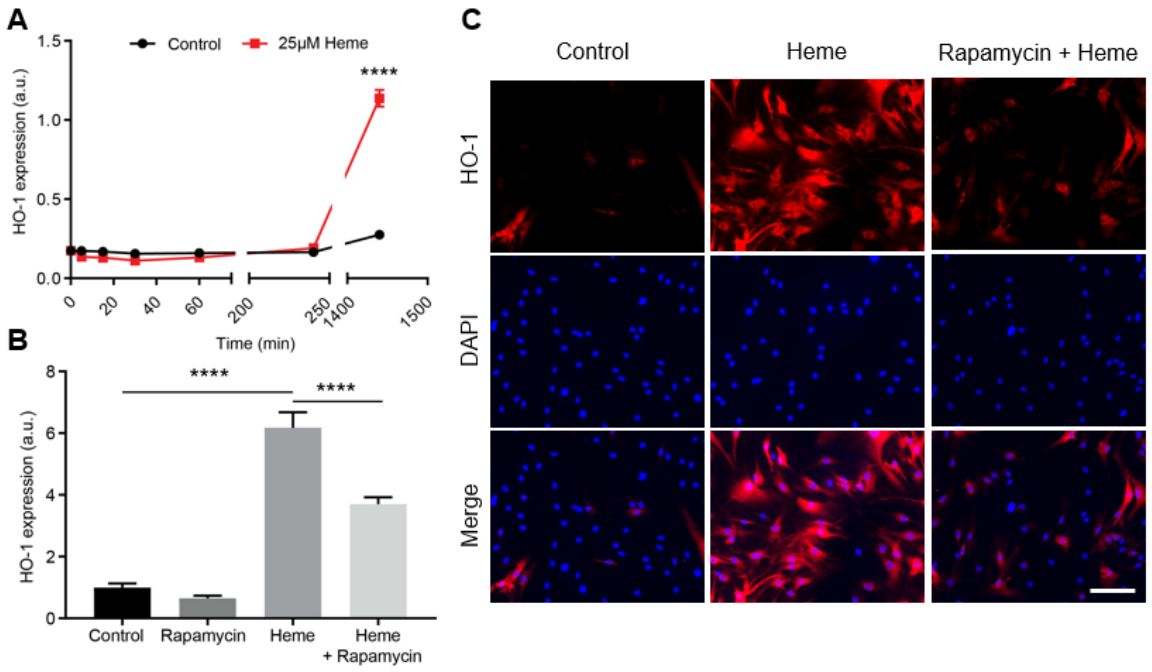

Figure 3-14. Upregulation of HO-1 in astrocytes by exogenous heme is mTOR dependent. A. Time course of HO-1 expression by astrocytes in response to exogenous heme (mean ± SEM, ****p<0.0001, Student's t-test). B. HO-1 expression after 24 hours of heme treatment is suppressed upon co-treatment with rapamycin (mean ± SEM, ****p<0.0001, ordinary one-way ANOVA with Sidak's post-hoc test) C. Representative images of astrocyte HO-1 expression after 24 hours for control, heme and rapamycin + heme conditions.

3.4 Discussion

Heme is increasingly recognized for its role as a modulator of immune signaling, but to date this role has not been well-studied in the context of the brain. Excess heme in the brain is associated with a number of pathological conditions including, but not limited to, AD, ischemic stroke, and traumatic brain injury [78, 141, 197]. Thus, unraveling the signaling mechanisms of heme in the brain can provide broad insight into heme-mediated neuroinflammatory dysfunction, which is applicable to a variety of conditions. Elevated levels of heme in AD and related conditions could be due to a number of factors, including extravasation and lysis of red blood cells through a leaky brain vasculature and hyper-

production of heme by glia and neurons under pathological conditions [75, 84]. Thus, both intracellular and extracellular heme may contribute to modulation of the neuro-immune environment in AD.

To begin to elucidate the signaling roles heme may exert on astrocytes, we began by broadly quantifying how heme alters phospho-signaling in the PI3K/Akt/mTOR, MAPK, and NF-κB pathways. These pathways were selected due to their importance in modulating immune phenotypes including cytokine expression and scavenger activity [184-186]. Furthermore, these pathways have been reported to be modulated by heme in a variety of other cell types, including peripheral immune cells [97, 99, 100, 180]. Performing multiplex Luminex assays and PLSDA, we found that heme modestly upregulated the MAPK and NF- κB pathways, and robustly upregulated the Akt/mTOR pathway (**Figure 3-5**, **Figure 3-4**, **Figure 3-3**). Interestingly, modulation of the Akt/mTOR pathway occurred in both Aβ-dependent and Aβ-independent manners (**Figure 3-1**, **Figure 3-3**), and changes were exclusive to free heme, not Hb (**Figure 3-2**).

Findings of robust upregulation of the Akt/mTOR pathway in astrocytes are particularly interesting given the numerous immune functions in astrocytes it regulates which are relevant to AD. The Akt/mTOR pathway regulates expression of cytokines [198], scavenger activity [199], and autophagy [188, 200], and is also involved in regulating migration [198] and glial scar formation [201]. These findings are particularly consistent with our earlier findings of suppressed phagocytic capacity and scavenger activity in response to heme in astrocytes (**Figure 2-7**). In addition, this pathway regulates numerous homeostatic functions in astrocytes, including viability [202], growth [203], and glutamate transport [204].

Since both extra- and intra-cellular heme are pathologically relevant to AD, we further sought to elucidate the distinct signaling contributions of extra- vs. intra- cellular heme. To do this, we began by characterizing exogenous heme uptake dynamics using a genetically encoded, ratiometric, fluorescent heme sensor, HS1. Quantification of eGFP:mKATE2 ratio over a time course indicated that HS1 was ~50% saturated within 30 min of exogenous heme treatment and was fully saturated between 4 and 24 h (**Figure 3-7A-B**). Compared with heme uptake dynamics, time courses of Akt and mTOR phosphorylation revealed significant increases in phosphorylation within 30 min, and decreases at 24 hours when compared to controls (**Figure 3-7C-D)**. Taken together with the heme uptake dynamics data, this suggests that rapid Akt/mTOR signaling within the first 30 min may be driven by extracellular heme, while intracellular heme may be responsible for suppression of the pathway at longer time points. Further supporting these data were our findings that upregulating intracellular heme synthesis with ALA downregulated Akt/mTOR pathway signaling compared to controls (**Figure 3-9**, **Figure 3-10**), consistent with findings of Akt and mTOR downregulation 24 h after exogenous heme treatment (**Figure 3-7C-D)**. Taken together, these data indicate diverse signaling capabilities for intracellular vs. extracellular heme. One plausible explanation for this dichotomy is that extracellular heme triggers phospho-signaling through binding extracellular cell surface receptors and intracellular heme may elicit anti-inflammatory responses through activating HO-1.

Given that heme has been shown to bind and activate cell surface receptors in other contexts [95-97], we sought to identify whether similar mechanism could be responsible for the extracellular signaling effects produced by heme. Since IGF1R and IR are canonical

receptors upstream of Akt and mTOR (**Figure 3-11**) and are implicated in AD pathology, we used a pan inhibitor of IGF1R and IR to block these receptors in the presence of heme. Excitingly, we found that blocking IGF1R/IR attenuated Akt/mTOR pathway upregulation in response to heme at 30 min (**Figure 3-12**). Since PLSDA identified IGF1R to be the top correlate with heme upregulation and IR to correlate poorly, it is likely that IGF1R is responsible for producing this effect (**Figure 3-12B**). Thus, these data suggest a novel mechanism for heme as an agonist of IGF1R in astrocytes. This finding is highly relevant given that dysfunctional IGF1R and IR signaling are characteristic of AD [205]and other pathologies comorbid with AD, such as diabetes. Moreover, IGF1R has shown to modulate Aβ clearance [206], suggesting that heme may inhibit astrocytic Aβ uptake through IGF1R/Akt/mTOR signaling.

Finally, our data suggest a mechanistic link between dysregulation of Akt/mTOR pathway signaling and immune phenotypes in astrocytes. Specifically, we found that CD36 and HO-1 expression, which are decreased and increased by heme, respectively, are partially restored to control-like conditions in response to inhibition of mTOR by rapamycin. Beyond neuroinflammation, kinase signaling can potentiate AD pathology through driving other pathological events. For example, both the MAPK and Akt/mTOR pathways are involved in modulating tau pathology [207, 208]. Thus, the findings of dysregulated phospho-signaling in response to heme could have implications to AD beyond modulating neuroinflammation.

CHAPTER 4. DETERMINING THE EFFECTS OF HEME ON NEUROINFLAMMATION *IN VIVO*

4.1 Introduction

Neuroinflammation is emerging as an important aspect of AD pathology, yet whether its contributions to AD pathogenesis are harmful or beneficial remains debated [128, 129, 162]. Among the beneficial contributions of neuroinflammation, activated astrocytes and microglia in AD migrate toward Aβ plaques and uptake and degrade Aβ [56, 63, 135-137]. Moreover, both astrocytes and microglia secrete chemokines, which function in further recruiting immune cells to Aβ plaque sites [138, 139]. However, glia can also become "fatigued" at later stages of AD, ultimately losing phagocytic capacity and increasing Aβ burden [61, 62]. In reality, it is likely that the consequences of neuroinflammation span a range from positive to negative effects, yet the factors that contribute to mediating this balance are not well established.

Elevated levels of Hb and heme are characteristic of AD [76-79] and physically bind Aβ, thereby modifying Aβ aggregation state and imparting unique peroxidase activity [78, 79, 82]. With relevance to inflammation, heme and Hb have been shown to demonstrate immunomodulatory signaling capabilities in peripheral macrophages and endothelial cells [95-97]. However, the immunomodulatory roles they may take on in the brain, specifically in an AD environment, remain unknown.

Herein, we elucidate the effects of heme on Aβ-dependent and Aβ-independent neuroinflammation *in vivo,* to expand upon our *in vitro* findings from Chapter 2.

Interestingly, our *in vivo* data show that many similarities to our *in vitro* results, suggesting that heme suppresses Aβ-induced cytokine expression and Aβ clearance. Additionally, our data show that depletion of heme synthesis *in vivo* robustly upregulates cytokines and chemokines in the cortex. Taken together, these data show for the first time *in vivo* that heme alters the neuro-immune environment, both in an out of the context of Aβ.

4.2 Materials and Methods

4.2.1 Recombinant $A\beta_{1-42}$ preparation

Unlabeled $A\beta_{1\text{-}42}$ was prepared as in Chapter 2.2.1. Briefly, HFIP-pretreated $A\beta_{1\text{-}42}$ (rPeptide) was diluted from a stock of 500 μM Aβ in 1% NH_4OH that was stored at −80 °C. Before reconstitution, $A\beta_{1\text{-}42}$ was retreated with 500 μl HFIP per milligram of $A\beta_{1\text{-}42}$ overnight to prevent pre-aggregation. HFIP was evaporated before dilution in 1% NH_4OH. HiLyte™ Fluor 555 labeled $A\beta_{1\text{-}42}$ (Anaspec, Fremont, CA) was also reconstituted to a 500 μM stock but received no HFIP pre-treatment.

4.2.2 Stereotactic injections and tissue collection

Eight to ten week old female CD-1® IGS mice from Charles River Laboratory (Strain code 022) were used. All procedures were approved by the Georgia Institute of Technology Institutional Animal Care and Use Committee. Mice were housed in a pathogen free facility with a twelve-hour light/dark cycle for a minimum of three days after arrival. Food and water were provided ad libitum. Mice were anesthetized with 5% inhaled isoflurane (0.8 L/min) in a small induction chamber and maintained at 1% to 3% isoflurane. After induction, 0.8 mg/kg sustained release buprenorphine was delivered via

intraperitoneal (IP) injection and 7 mg/kg 2% lidocaine was injected subcutaneously to the scalp. Mice were then mounted onto a stereotaxic instrument (David Kopf Instruments, Tujunga, CA) and secured with a head holder and non-rupture ear bars. Two symmetrical 0.25mm craniotomies were made in the skull with a micromotor high-speed drill (Stoelting Co., Chicago, IL) at coordinates roughly 3 mm caudal at 2 mm lateral from bregma according to stereotactic measurements. Either 0.002% NH_4OH, 1 μM hemin chloride, 1 μM unlabeled $A\beta_{1-42}$, or 1 μM HiLyte™ Fluor 555 labeled $A\beta_{1-42}$ was loaded into a Hamilton Neuros syringe with a point style 4 needle (Hamilton Company, Reno, NV). Using a 10 μm resolution stereotaxic arm (David Kopf Instruments), the syringe was descended into the tissue at a depth of 800 μm. Each animal was injected twice, each time with 100 nL of the appropriate solution at a rate of 25 nL/min, using a Quintessential Stereotaxic Injector (Stoelting). After the injection, the syringe remained in place for an additional 2.5 minutes before being removed from the brain. Craniotomies were left to heal naturally. The skull was sealed using 5-0 vicryl sutures (Ethicon Inc, Somerville, NJ). Antibiotic ointment was applied on top of the sutures. All surgical procedures were performed using sterile surgical technique in a positive pressure operating room. After surgery, mice were recovered under a heat lamp and housed in cages with post-operative bedding. Either 4 or 7 days after surgery, mice were sacrificed via cervical dislocation under anesthesia and the brain removed. For amyloid burden quantification experiments, brains were fixed in 4% PFA. For cytokine quantification experiments, injection regions were microdissected and lysed using the Bio-Plex cell lysis kit, with the addition of one cOmplete mini protease inhibitor tablet and 20 μl of PMSF per 5 ml of lysis buffer. Lysates

were placed in microcentrifuge tubes and inverted at 4 °C for 10 min, then centrifuged at 4 °C for 10 min at 13,000 rpm. Supernatant was collected and stored at -80 °C.

4.2.3 SA treatment and tissue collection

Eight week old male C57BL/6 mice from Jackson Laboratory (stock no. 000664) were used. All procedures were approved by the Georgia Institute of Technology Institutional Animal Care and Use Committee. Mice were housed in a pathogen free facility with a 12 h/12 h light/dark cycle for a minimum of three days after arrival. Food and water were provided ad libitum. For IP injection experiments, mice were subjected to IP injection of 40 mg/kg SA diluted in physiologic saline, daily for 14 days. Control mice were injected daily with physiologic saline. For delivery of SA via drinking water, SA was diluted to a final concentration of 0.3 mg/mL in drinking water, which was replaced once weekly for 14 days. For tissue collection, mice were sacrificed via cervical dislocation under anesthesia and the brain (frontal cortex) and liver tissues collected and flash frozen with liquid nitrogen. Tissues were lysed using the Bio-Plex cell lysis kit, with the addition of one cOmplete mini protease inhibitor tablet and 20 µl of PMSF per 5 ml of lysis buffer. Lysates were placed in microcentrifuge tubes and inverted at 4 °C for 10 min, then centrifuged at 4 °C for 10 min at 13,000 rpm. Supernatant was collected and stored at -80 °C.

4.2.4 Multiplexed phospho-protein and cytokine signaling analysis

Cell lysates were thawed on ice and centrifuged at 4 °C for 10 min at 13,000 rpm. Protein concentrations were determined using a Pierce BCA protein assay (Thermo Fisher Scientific) and normalized with Milliplex® MAP assay buffer (EMD Millipore) to 4 µg of

protein/25 µl for Akt/mTor pathway analysis and 6 µg of protein/25 µl for cytokine analysis because these dilutions fell within the linear range of bead fluorescence intensity versus protein concentration for detectable analytes. Multiplex Akt/mTOR pathway phospho-signaling analysis was conducted by adapting the protocol provided for the Milliplex® MAP Akt/mTOR 11-Plex with beads for p-Akt, p-GSK3α/β, p-IGF1R,p-IR, p-IRS1, p-mTOR, p-p70S6K, p-PTEN, p-RPS6, and p-TSC2. Multiplex cytokine analysis was conducted by adapting the protocol provided for the Milliplex® MAP mouse cytokine/chemokine 32-Plex kit, with beads for Eotaxin, G-CSF, GM-CSF, interferon-γ, IL-1α, IL-1β, IL-2, IL-3, IL-4, IL-5, IL-6, IL-7, IL-9, IL-10, IL-12p40, IL-12p70, IL-13, IL-15, IL-17, IP-10, KC, LIF, LIX, MCP-1, M-CSF, MIG, MIP-1α, MIP-1β, MIP-2, RANTES, TNF-α, and VEGF. Cytokine and phospho-protein signaling kits were read on a MAGPIX® system.

4.2.5 Immunohistochemistry and imaging

Brains were fixed in 4% PFA, paraffin processed, and embedded. Tissue slices were cut into 7 µm thick coronal or sagittal sections using a rotary microtome (Thermo Fisher) and affixed onto glass microscope slides (Electron Microscopy Sciences, Hatfield, PA). Tissue slices were deparaffinized in xylenes and rehydrated by washing with 100% ethanol, 95% ethanol, and deionized water. Antigen retrieval was performed in a microwave by boiling slides in 10 mM sodium citrate buffer at pH 6.0. Slides were rinsed in TBST. A hydrophobic ring was drawn around each individual tissue slice using an immunohistochemistry PAP pen (Enzo Life Sciences, Farmingdale, NY), after which samples were blocked for 1 h in Odyssey blocking buffer (OBB). Samples were incubated at 4 °C overnight with primary antibodies diluted in OBB: either with anti-GFAP (1:1000,

Novus) or anti-Iba1 (Invitrogen, 1:200), as appropriate. Slides were rinsed again in TBST and incubated with the Alexa Fluor 647 secondary antibody, diluted 1:200 in OBB. Slides were counterstained with 1 μg/uL DAPI, rinsed, and mounted with VECTASHIELD Antifade Mounting Medium (Vector Laboratories, Burlingame, CA). Samples were imaged using epifluorescent microscopy on a Zeiss Axio Observer Z.1 inverted microscope.

4.2.6 Quantification of Aβ burden

Aβ burden was quantified using Fiji [209]. Briefly, for each brain, the full region containing the injection site was coronally sectioned. Aβ burden for each slice and injection site was quantified in terms of integrated density. Total Aβ burden for each animal and injection site was quantified by summing integrated density for each tissue slice containing Aβ.

4.2.7 Partial least-squares discriminant analysis

As in Chapters 2.2.12 and 3.2.7, PLSDA was performed in MATLAB using the partial least squares algorithm by Cleiton Nunes available on the Mathworks File Exchange. All data were z-scored before inputting into the algorithm. For all analyses, an orthogonal rotation in the LV1-LV2 plane was performed to identify a new LV1 that better separated groups.

4.2.8 Statistics

All statistical analyses were performed using GraphPad Prism version 8 (GraphPad Software, La Jolla, CA). Values are presented as mean ± SEM. Statistical significance was

determined using Student's T-test. Normality of data was tested using the Shapiro–Wilk test of normality. Levels of significance were set as follows: *$p < 0.05$, **$p < 0.01$, ***$p < 0.001$, ****$p < 0.0001$.

4.3 Results

4.3.1 Intracranial injection of Aβ and heme modulates local cytokine expression in WT mice

In order to isolate the specific neuroinflammatory effects of heme and $A\beta_{1-42}$ *in vivo*, we stereotactically injected combinations of heme and $A\beta_{1-42}$ into the cortex and quantified cytokine expression in the cortical tissue 4 days after injection (**Figure 4-1**). To account for surgical variabilities from animal to animal, two injections were made in each animal, one in each hemisphere of the brain, with each injection corresponding to a different experimental group. This allowed for direct comparison of two conditions in a single animal. The experimental design and groups are delineated in **Figure 4-1** and **Table 4-1**.

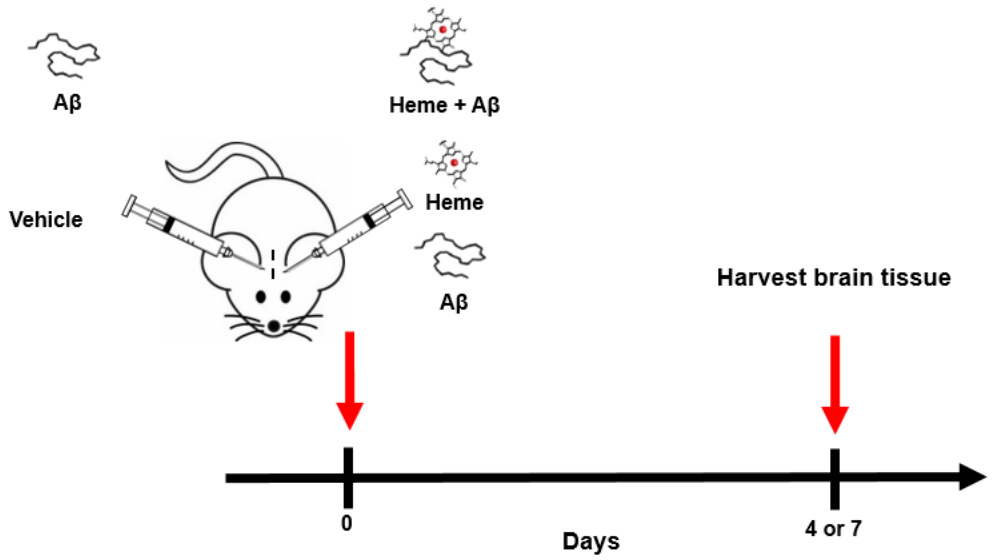

Figure 4-1. Experimental timeline for intracranial injection experiments. On day 0, mice were injected once in each hemisphere with combinations of vehicle, heme, $A\beta_{1-42}$, and heme + $A\beta_{1-42}$. On either day 4 or day 7, brains were harvested for analysis.

Table 4-1. Experiment groups for quantification of cytokines after intracranial injection of $A\beta_{1-42}$ and heme

Strain	Left Hemisphere	Right Hemisphere	Days
CD-1	1 μM $A\beta_{1-42}$	0.002% NH_4OH (Vehicle)	4
CD-1	1 μM Heme + 0.002% NH_4OH (Vehicle)	0.002% NH_4OH (Vehicle)	4
CD-1	1 μM $A\beta_{1-42}$	1 μM $A\beta_{1-42}$ + 1 μM Heme	4

We first examined the *in vivo* inflammatory effects of $A\beta_{1-42}$ by itself, as compared to a vehicle control injection. In order to do so, we used a Luminex assay to quantify expression of a panel of 32 cytokines into the tissue surrounding the injection site 4 days after 100 nL of 1 μM $A\beta_{1-42}$ or vehicle was stereotactically injected (**Figure 4-2A)**. Using PLSDA, we found identified a profile of cytokines (LV1) that separated the vehicle injection samples from the $A\beta_{1-42}$ injection samples. Plotting each sample in terms of its score on LV1 revealed that $A\beta_{1-42}$ upregulated expression of this profile of cytokines (**Figure 4-2B-C**). Interestingly, several of the top cytokines upregulated by $A\beta_{1-42}$ from this analysis (ie. IL-9, IL-4, IL-1α, IL-1β) were previously identified to be robustly upregulated in response to $A\beta_{1-42}$ by microglia and astrocytes in our *in vitro* experiments (**Figure 2-3, Figure 2-9, Figure 2-10**).

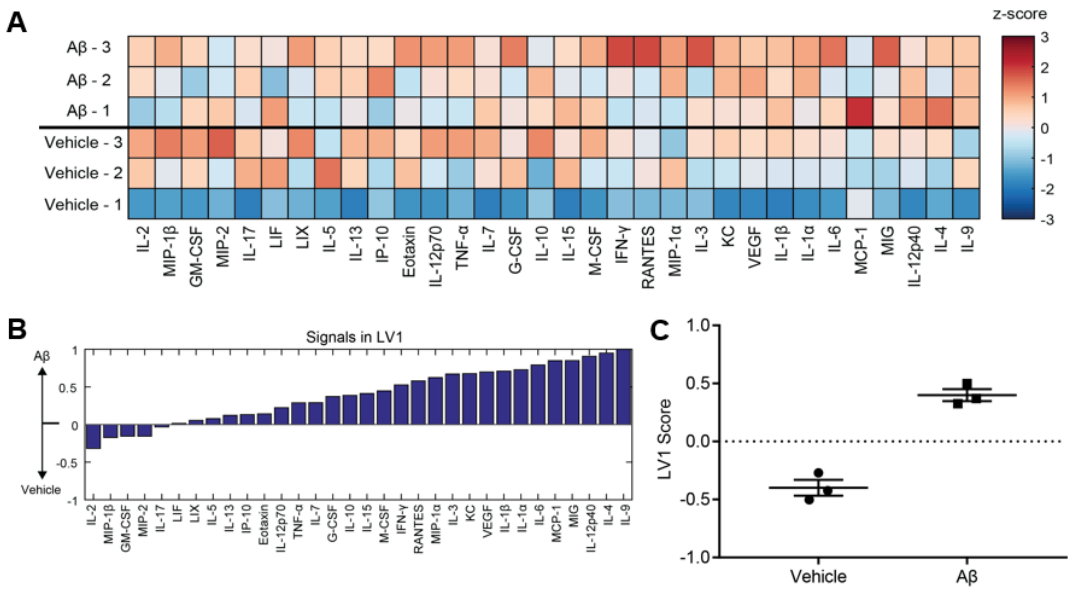

Figure 4-2. Intracranial injection of Aβ$_{1-42}$ broadly upregulates expression of cytokines in surrounding tissue. A. Quantification of 32 cytokines expressed into the cortex via Luminex analysis. Each column is z-scored and each row represents an individual sample. Each individual animal is identified by numbers 1-3. B. PLSDA identified a latent variable (LV1), which consisted of a weighted combination of cytokines which best separated groups. C. Scoring each sample on LV1 revealed that Aβ injection upregulated this profile compared to vehicle injection.

Since our *in vitro* studies found that heme modulates Aβ$_{1-42}$-induced cytokine expression in both astrocytes and microglia, we next sought to investigate whether these findings were mirrored *in vivo*. Thus, we again used a multiplex Luminex assay, this time to compare cytokine expression in the tissue surrounding the injection site between injection of 1 μM Aβ$_{1-42}$ and injection of 1 μM Aβ$_{1-42}$ + 1 μM heme (**Figure 4-3A**). Again performing PLSDA, we identified LV1 which best separated the Aβ$_{1-42}$ group from the Aβ$_{1-42}$ + heme group (**Figure 4-3B**). Plotting each sample in terms of its score on LV1 revealed that Aβ$_{1-42}$ + heme downregulated expression of this profile of cytokines with respect to Aβ$_{1-42}$ alone (**Figure 4-3C**). This analysis identified that top cytokines downregulated in response to co-treatment of heme and Aβ$_{1-42}$ included M-CSF, IL-7, and IL-9, again very consistent with cytokines that were downregulated by heme in earlier *in vitro* experiments

(**Figure 2-3, Figure 2-9, Figure 2-10**). While LV1 revealed that most cytokines were downregulated in response to heme, it also showed that a few cytokines, most notably the IP-10, were downregulated (**Figure 4-3B**).

Performing a similar analysis comparing cytokine expression in response to vehicle vs. heme injection revealed that heme on its own modestly upregulated a panel of cytokines, the top of which included IL-10, Macrophage Inflammatory Protein (MIP)-2, and Interferon gamma (IFNγ) (**Figure 4-4A-C**). However, these changes were much more variable and less robust that the $A\beta_{1-42}$ injection experiments. The lack of strong changes in cytokine expression in response heme is in line with our *in vitro* findings which indicated that heme on its own did not stimulate cytokine expression changes in astrocytes or microglia (**Figure 2-3, Figure 2-9, Figure 2-10, Figure 2-11**).

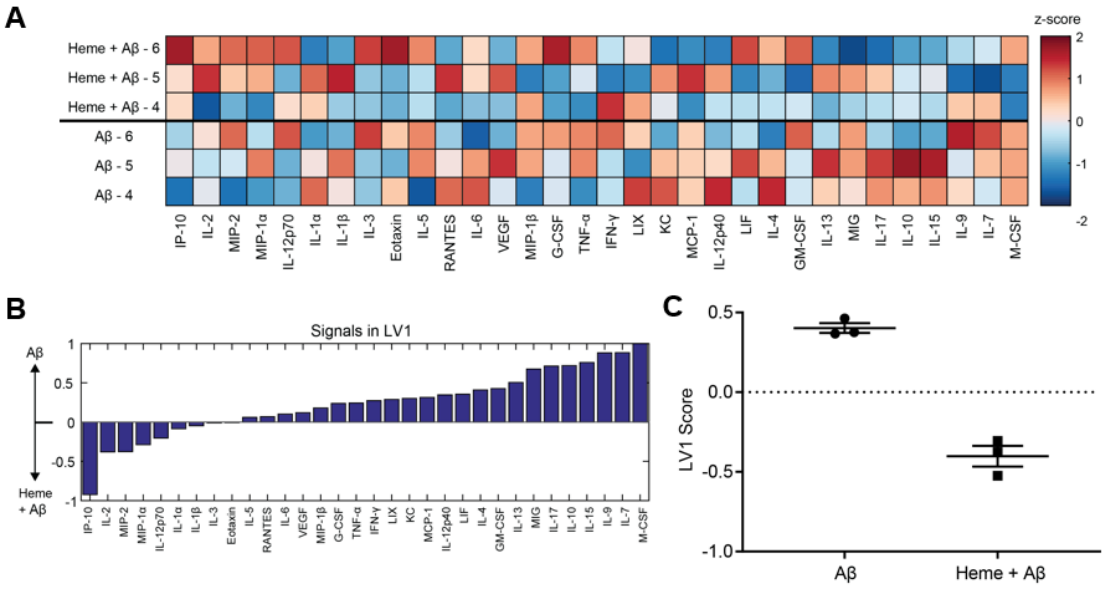

Figure 4-3. Intracranial injection of equimolar heme with Aβ$_{1-42}$ suppresses expression of some cytokines in surrounding tissue. A. Quantification of 32 cytokines expressed into the cortex via Luminex analysis. Each column is z-scored and each row represents an individual sample. Each individual animal is identified by numbers 4-6. B. PLSDA identified a latent variable (LV1), which consisted of a weighted combination of cytokines which best separated groups. C. Scoring each sample on LV1 revealed that heme + Aβ injection downregulated this profile compared to Aβ injection.

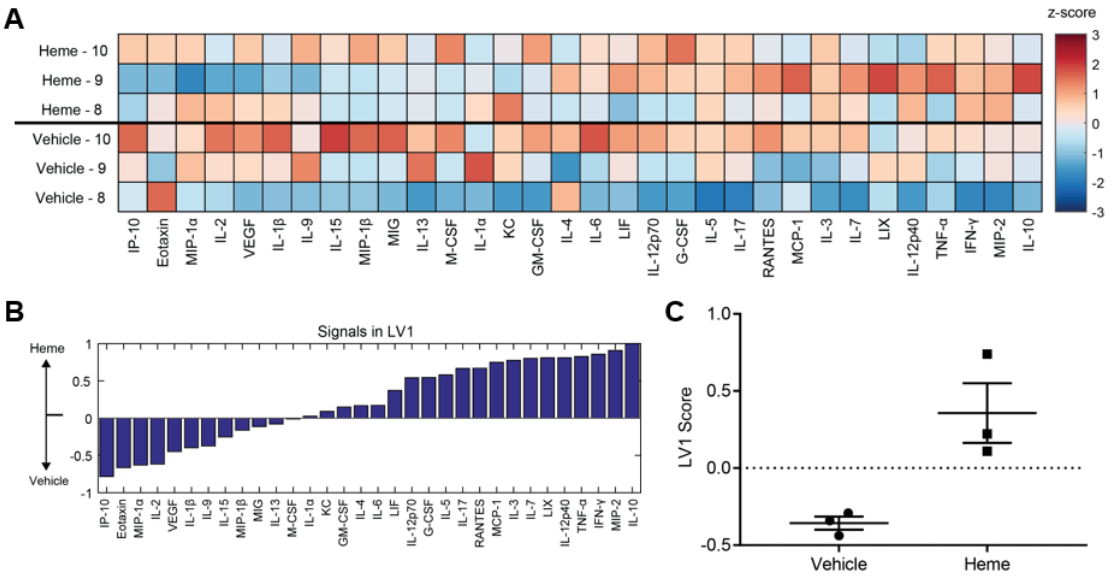

Figure 4-4. Intracranial injection of heme upregulates expression of some cytokines in surrounding tissue. A. Quantification of 32 cytokines expressed into the cortex via Luminex analysis. Each column is z-scored and each row represents an individual sample. Each individual animal is identified by numbers 8-10. B. PLSDA identified a latent variable (LV1), which consisted of a weighted combination of cytokines which best separated groups. C. Scoring each sample on LV1 revealed that heme injection upregulated this profile compared to vehicle injection.

4.3.2 Activated astrocytes are recruited to Aβ injection sites

In order to determine which cell types could be responsible for producing cytokine responses in the area surrounding the injection site, immunohistochemistry was performed to identify microglia and astrocytes in the vicinity of the injection site. Staining for activated astrocytes using GFAP as a marker revealed that at both the 4 day and 7 day time points, injection of Aβ produced a robust local astrocytic response. Specifically, activated astrocytes were recruited to the injection site and could be seen to engulf Aβ plaques (**Figure 4-5, Figure 4-6).** Conversely, Iba1 staining revealed minimal microglial activation in the area surrounding the injection site at day 7 and no activated microglia were seen to surround Aβ plaques (**Figure 4-7**).

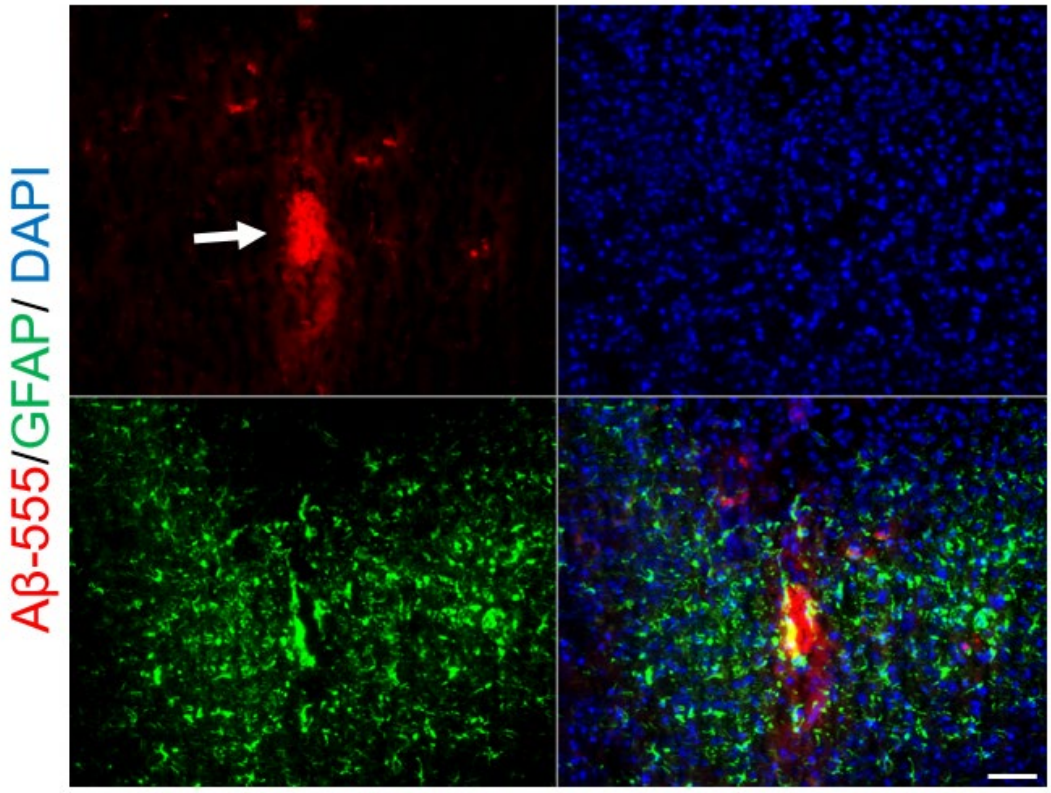

Figure 4-5. Activated astrocytes expressing GFAP are recruited to $A\beta_{1-42}$ injection site 4 days after injection. Arrow indicates $A\beta_{1-42}$ aggregate. Scale bar, 50 μM.

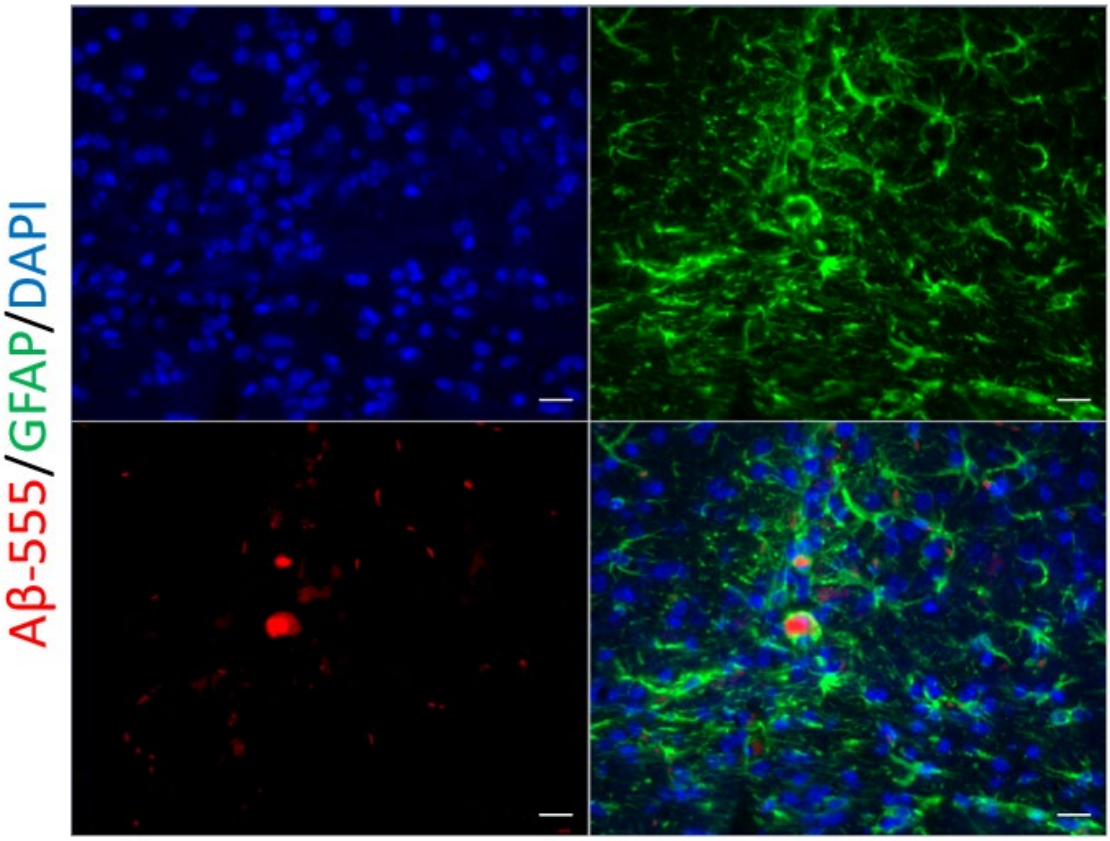

Figure 4-6. Activated astrocytes expressing GFAP are recruited to $A\beta_{1-42}$ injection site 7 days after injection. Scale bar, 20 μM

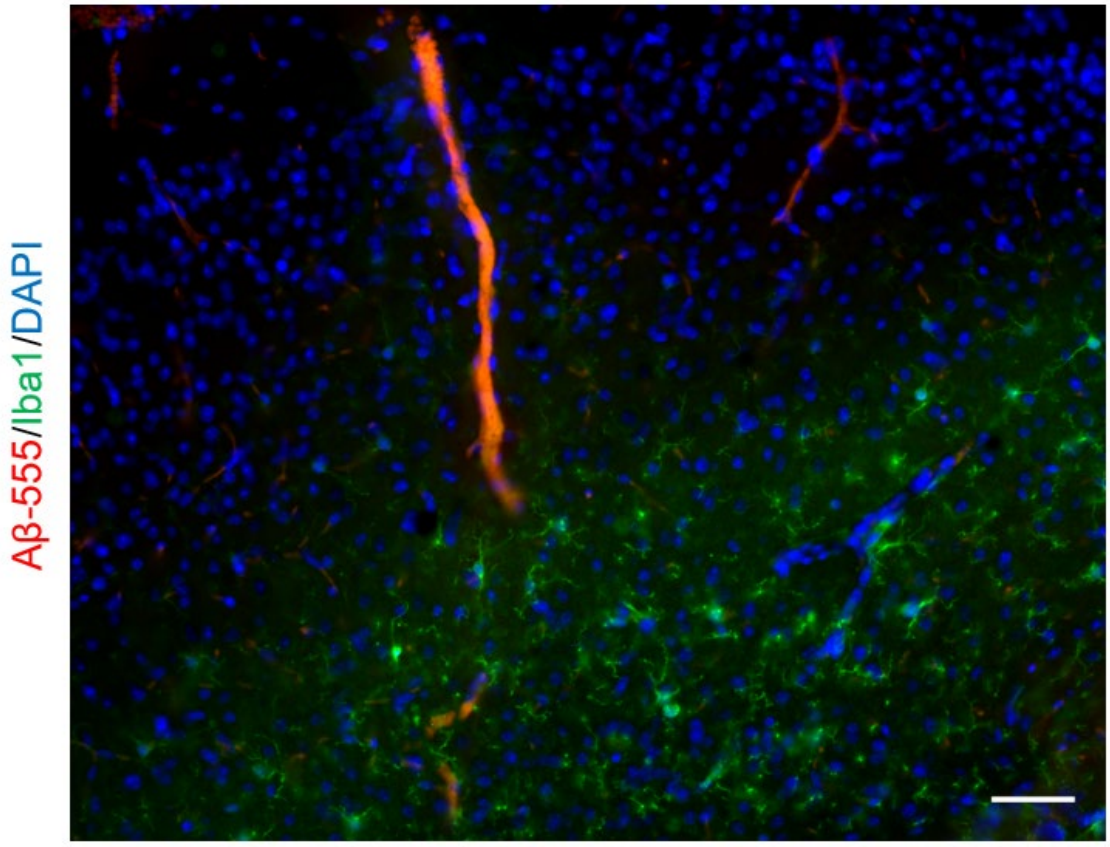

Figure 4-7. Iba-1 positive microglia are present in the vicinity of the $A\beta_{1-42}$ injection site 7-days after injection but do not engulf $A\beta_{1-42}$. Scale bar, 50 μM.

4.3.3 Intracranial injection of Aβ and heme suppresses Aβ clearance in WT mice

Having observed that heme modulated $A\beta_{1-42}$-induced cytokine changes *in vivo*, we were next interested in assessing whether heme would also affect clearance of Aβ, particularly since our *in vitro* studies found that scavenger activity was suppressed in both astrocytes and microglia in response to heme (**Figure 2-7, Figure 2-12**). Again, we used stereotactic injection of $A\beta_{1-42}$ into WT mice as our model to investigate this, this time using HiLyte Fluor 555, fluorescently labeled $A\beta_{1-42}$. As before, animals each received two intracranial injections, one of 1 μM $A\beta_{1-42}$ in the left hemisphere and the other with 1 μM $A\beta_{1-42}$ + 1 μM heme in the right hemisphere (**Table 4-2**). Aβ burden was quantified at either

4 days or 7 days after injection (**Figure 4-1**). Quantification revealed that at 4 days after injection, there was a trend towards higher Aβ burden in the presence of heme (**Figure 4-8, Figure 4-10A**). At the 7 day time-point, Aβ burden in the presence of heme was significantly increased compared to injection without heme (**Figure 4-9**, **Figure 4-10B**).

Table 4-2. Experiment groups for quantification of Aβ burden after intracranial injection of $A\beta_{1-42}$ (HiLyte Fluor 555) and heme

Strain	**Left Hemisphere**	**Right Hemisphere**	**Days**
CD-1	1 μM $A\beta_{1-42}$ (HiLyte Fluor 555)	1 μM $A\beta_{1-42}$ (HiLyte Fluor 555) + 1 μM Heme	4
CD-1	1 μM $A\beta_{1-42}$ (HiLyte Fluor 555)	1 μM $A\beta_{1-42}$ (HiLyte Fluor 555) + 1 μM Heme	7

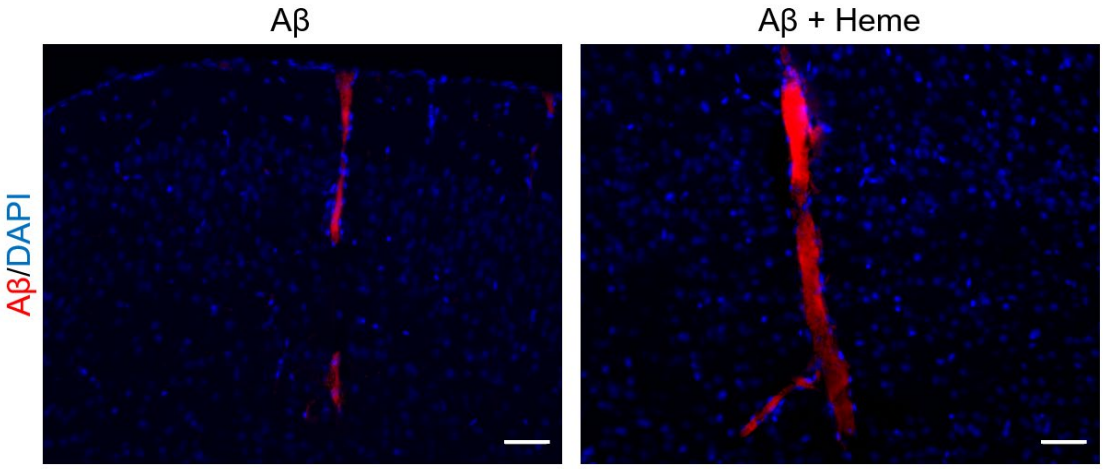

Figure 4-8. Representative images of $A\beta_{1-42}$ injections 4 days after injection into the cortex. $A\beta_{1-42}$ burden is higher when injected in combination with heme (right) compared to on its own (left). Scale bar, 50 μM.

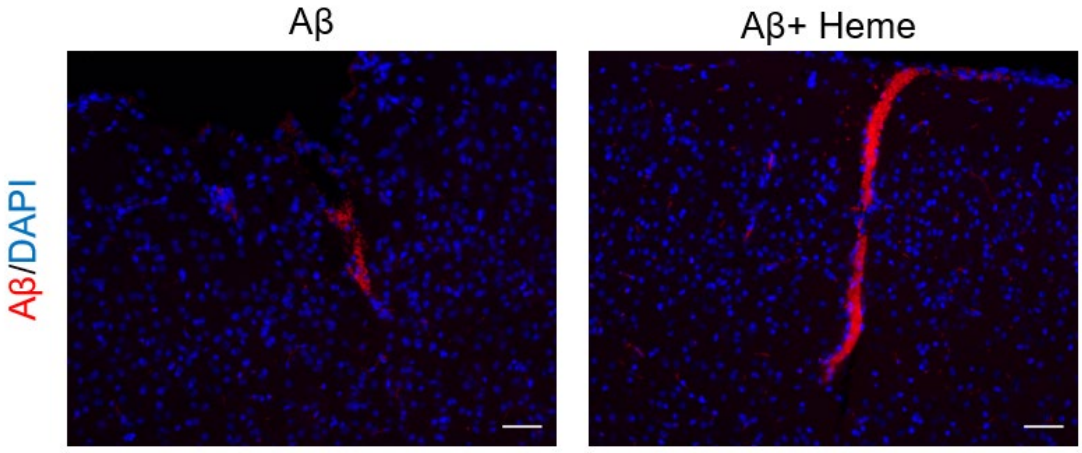

Figure 4-9. Representative images of $A\beta_{1-42}$ injections 7 days after injection into the cortex. $A\beta_{1-42}$ burden is higher when injected in combination with heme (right) compared to on its own (left). Scale bar, 50 μM.

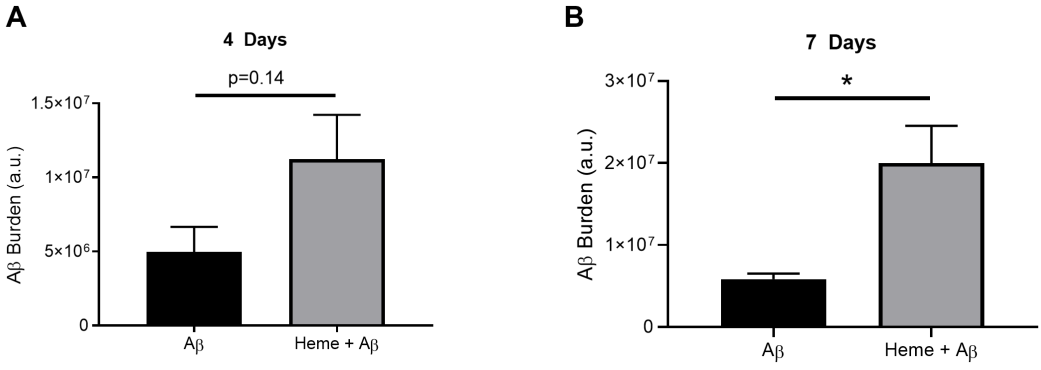

Figure 4-10. Intracranial injection of $A\beta_{1-42}$ with heme into WT mice suppresses $A\beta_{1-42}$ clearance. A. Quantification of Aβ 4 days after injection into the cortex. Aβ burden trends towards increased when $A\beta_{1-42}$ is injected in combination with heme. B. As in A for 7 days after injection (n=3; mean ± SEM, **p*<0.05; Student's t-test).

4.3.4 Suppression of heme synthesis with succinylacetone upregulates cytokine expression and suppresses Akt/mTOR signaling in WT mice

Since upregulation of intracellular heme synthesis is suspected to contribute to elevated heme levels in AD [84] and upregulating heme synthesis in primary astrocytes suppressed $A\beta_{1-42}$-induced cytokine expression much like extracellular heme, we next sought to examine whether suppressing heme synthesis *in vivo* could promote neuroinflammatory activation. To do this, we delivered 40 mg/kg SA daily to WT C57BL/6 mice via IP injection daily for 2 weeks. Quantifying total heme in the liver and the brain cortex after these two weeks revealed that heme was indeed significantly reduced in these tissues in response to daily SA injection (**Figure 4-11**). In order to determine the neuroinflammatory effects of heme depletion in the brain, we again performed multiplexed quantification of a panel of 32 cytokines from cortical tissue using a Luminex immunoassay and analysed this data using PLSDA (**Figure 4-12**). Our analysis identified pro-inflammatory cytokine profile, LV1, which separated SA-injected mice from saline-

injected mice (**Figure 4-12B**). Plotting each animal in terms of its score on this profile revealed that SA-injected mice were significantly upregulated on this profile compared to saline-injected mice (**Figure 4-12C**). Top correlates with SA-injection included IL-6, MCP-1, M-CSF, and MIP-1β, all of which are known to have strong chemotactic properties [210-214]. Interestingly, similar findings, although less robust, were observed with SA delivery in drinking water for 14 days (**Figure 4-13**Figure 4-13). Again, top correlates with SA possessed highly chemotactic functions, this time including G-CSF [215] and GM-CSF [216] in addition to MCP-1, M-CSF, and IL-6.

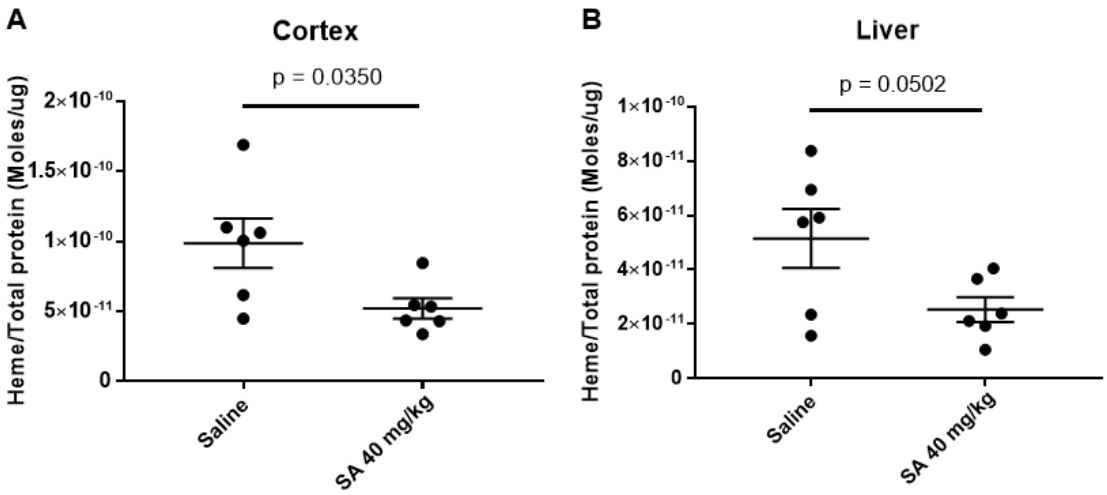

Figure 4-11. Total heme in cortex and liver is reduced after 14-day daily SA injection. A. Total heme in the cortex of WT mice, as quantified by a porphyrin fluorescence assay, is significantly reduced after 14-day daily IP injection of 40 mg/kg SA (mean ± SEM, Student's t-test). B. As in A for liver. Porphyrin fluorescence assay courtesy of Dr. Rebecca Donegan.

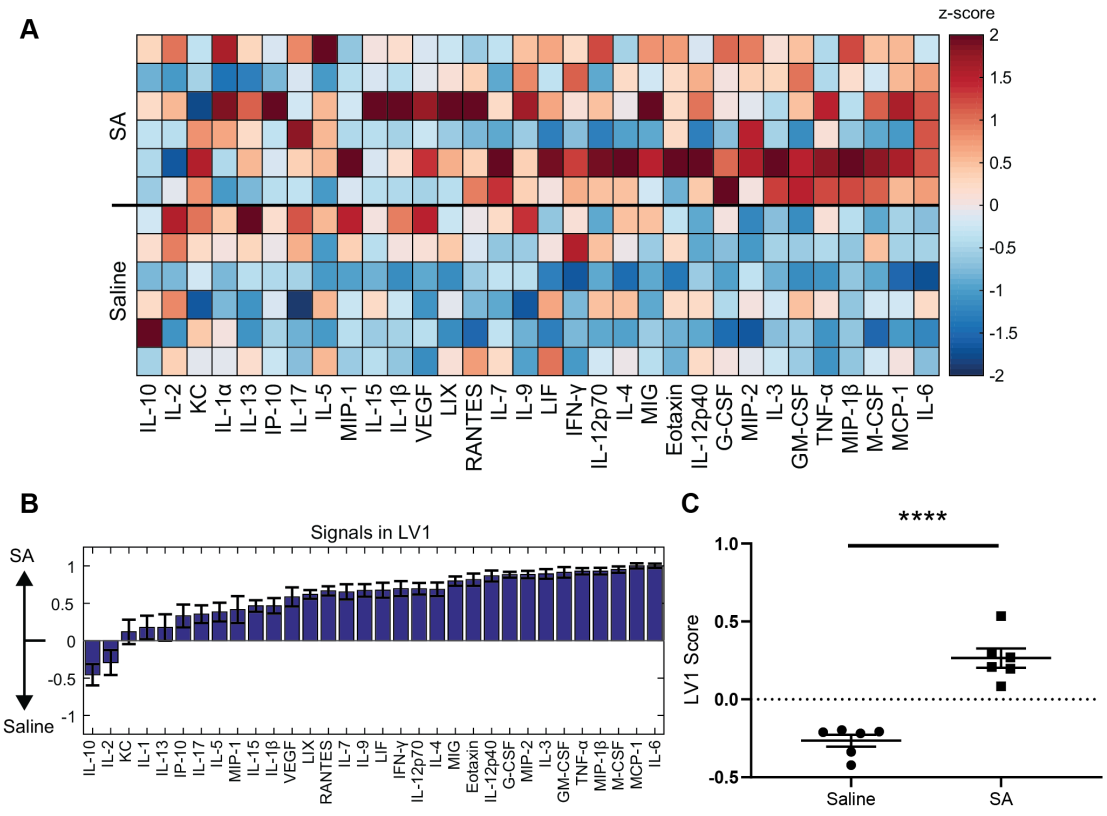

Figure 4-12. Cortical cytokine expression is upregulated in WT mice after 14-day daily SA injection. A. Quantification of expression of 32 cytokines in WT mouse cortices, via Luminex analysis. Each column is z-scored and each row represents an individual animal. B. PLSDA identified a latent variable (LV1), which consisted of a weighted combination of cytokines which best separated groups. Error bars are generated using a LOOCV (mean ± SD). C. Scoring each sample on LV1 revealed that SA treated samples were significantly upregulated on LV1 (error bars, mean ± SEM; ****p<.0.0001, Student's t-test).

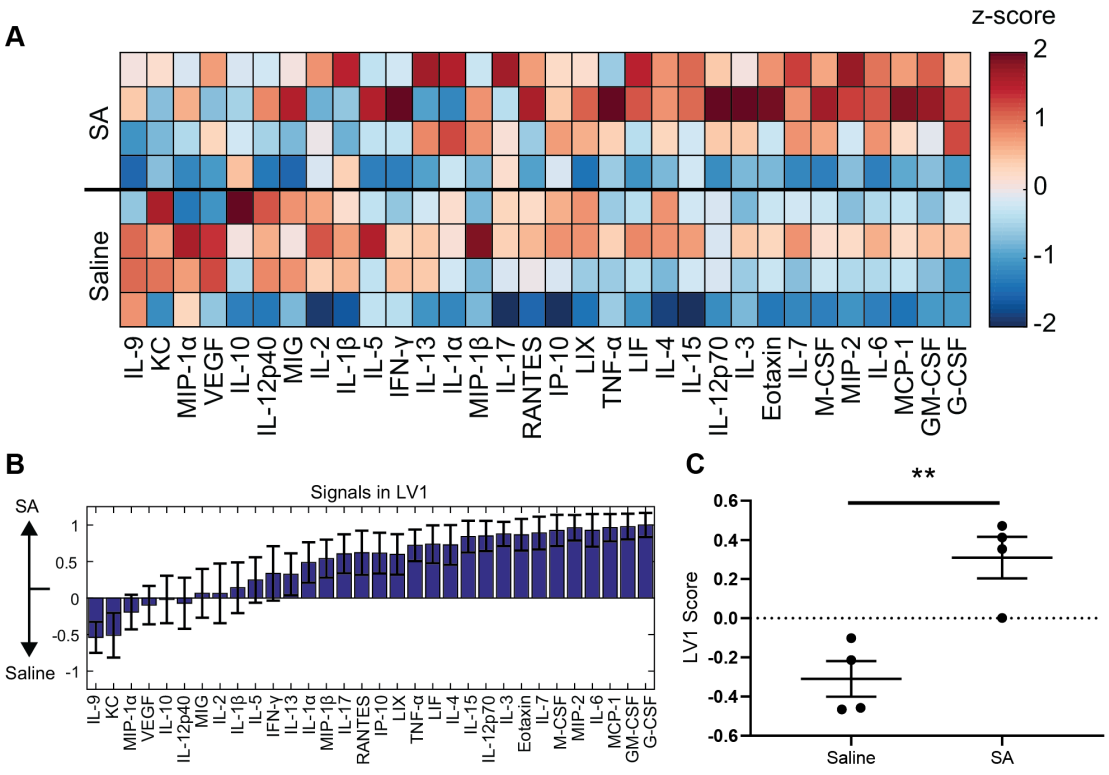

Figure 4-13. Cortical cytokine expression is upregulated in WT mice after 14-day SA treatment via drinking water. A. Quantification of expression of 32 cytokines in WT mouse cortices, via Luminex analysis. Each column is z-scored and each row represents an individual animal. B. PLSDA identified a latent variable (LV1), which consisted of a weighted combination of cytokines which best separated groups. Error bars are generated using a LOOCV (mean ± SD). C. Scoring each sample on LV1 revealed that SA treated samples were significantly upregulated on LV1 (error bars, mean ± SEM; $^{**}p<.0.0001$, Student's t-test).

Given the intra- and extra-cellular effects heme exerted on the Akt/mTOR pathway *in vitro* (**CHAPTER 3**). A multiplexed Luminex immunoassay was used to quantify 11 phospho-proteins from the Akt/mTOR pathway in cortical tissue from mice injected daily with SA for 14-days (**Figure 4-14**A). Again, PLSDA identified a profile of phospho-proteins, LV1, which best separated groups (**Figure 4-14**B). Scoring each sample in terms of this profile revealed that mice receiving daily SA injections had significantly reduced LV1 scores (**Figure 4-14C**).

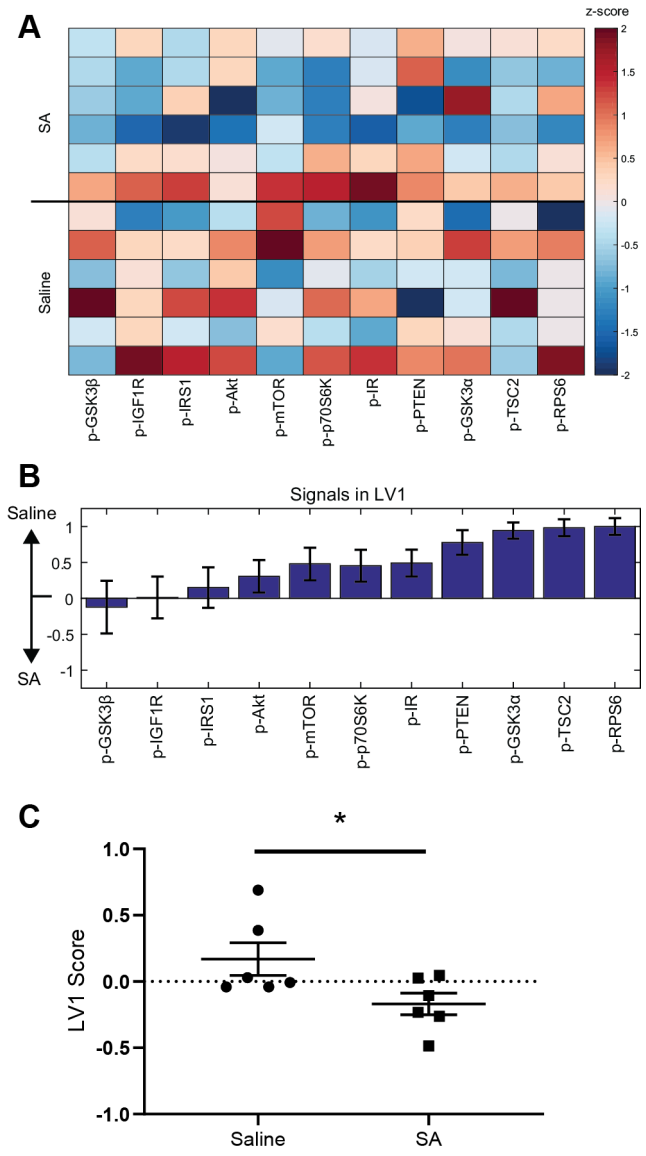

Figure 4-14. Cortical Akt/mTOR pathway phospho-signaling in suppressed in WT mice after 14-day daily SA injection. A. Quantification of phosphorylation of 11 Akt/mTOR pathway phospho-proteins in WT mouse cortices, via Luminex analysis. Each column is z-scored and each row represents an individual animal. B. PLSDA identified a latent variable (LV1), which consisted of a weighted combination of phospho-proteins which best separated groups. Error bars are generated using a LOOCV (mean ± SD). C. Scoring each sample on LV1 revealed that SA treated samples were significantly downregulated on LV1 (error bars, mean ± SEM; *p<.0.05, Student's t-test).

4.4 Discussion

Hb and its cofactor heme, are gaining attention for their implications in AD. Notably, both Hb and heme have been shown to be upregulated in the brains of AD patients as well as in Aβ mouse models [76, 78, 79]. Numerous factors likely contribute to this upregulation. Since vascular dysfunction is a prominent feature of AD, red blood cells can extravasate into the brain parenchyma and lyse, resulting in accumulation of Hb and Hb-derived free heme in the brain [75]. Further evidence suggests that heme and Hb synthesis by neurons and glia may be upregulated in AD environments [76, 79, 84]. Further increasing their relevance to AD pathogenesis, these factors have been shown to physically bind the AD hallmark protein, Aβ [78, 79]. Moreover, heme has potent immunomodulatory capabilities [95-97], suggesting its involvement in neuroinflammation in AD. However to date, the role heme plays in modulating neuroinflammation in *in vivo* AD environments remains unknown.

Although there are transgenic mouse models available that exhibit Aβ pathology as well as Aβ co-localization with Hb, [76, 79] such models have many limitations. Specifically, commonly used models such as the 5XFAD and APP/PS1 lines develop multiple pathologies in addition to Aβ plaques [217, 218], making it difficult to interrogate the specific effects of one pathology alone. Since we were specifically interested in isolating the effects of heme and Aβ on neuroinflammation, we began by using WT CD-1 mice intracranially injected with different combinations of heme and Aβ as our model. Similar approaches have been previously used to study isolated effects of Aβ *in vivo* [219-221].

In order to broadly assess local changes to the neuroinflammatory environment in response to $A\beta_{1\text{-}42}$, we began by isolating cortical tissue surrounding the injection site 4 days after injection and quantifying expression of 32 cytokines using a multiplexed immunoassay (**Figure 4-2A**). Using PLSDA, we found that expression of a highly pro-inflammatory profile of cytokines (LV1) was robustly upregulated in response to injection of $A\beta_{1\text{-}42,}$ as compared to contralateral injection of a vehicle control in the same animal (**Figure 4-2B-C**). This analysis identified IL-9, IL-4, and IL-12p40 upregulation to most strongly correlate with $A\beta_{1–42}$ injection. This finding is highly consistent with our *in vitro* experiments, which revealed that primary mouse astrocytes, primary mouse microglia, and SIM-A9 microglia all upregulated production of IL-9 and IL-4 in response to $A\beta_{1–42}$ treatment (**Figure 2-3, Figure 2-9, Figure 2-10**). While our *in vitro* experiments did not demonstrate robust changes in IL-12p40 in response to $A\beta_{1–42}$ treatment, IL-12p40 has been shown to correlate with Aβ burden in APP/PS1 mouse models and be elevated in humans with AD [37, 222]. Among other cytokines highly upregulated by $A\beta_{1–42}$ injection are those with highly pro-inflammatory and chemotactic properties, including MIG, IL-6, IL-1α, and IL-1β. Again, these cytokines are highly upregulated by astrocytes and microglia in response to $A\beta_{1\text{-}42}$ *in vitro* (**Figure 2-3, Figure 2-9, Figure 2-10**), in transgenic AD mouse models [37, 223], and in humans with AD [224-226]. Thus, taken together, these data suggest that intracranial $A\beta_{1–42}$ injection produces a localized, yet highly physiologically relevant model of neuroinflammation in AD and can be utilized to interrogate the Aβ-dependent immunomodulatory effects of molecules that co-localize or associate with Aβ.

Having established that intracranial injection of $A\beta_{1\text{-}42}$ produces a neuroinflammatory response both consistent with our *in vitro* models and relevant to AD; we next sought to examine how heme modulated this response. As such, we again used multiplexed cytokine quantification and PLSDA to compare the cytokine expression profiles in response to injection of $A\beta_{1–42}$ on its own and in combination with equimolar heme (**Figure 4-4**). Notably, this analysis revealed that several cytokines were downregulated in response to co-injection of heme with $A\beta_{1–42}$ when compared with injection of $A\beta_{1–42}$ on its own. Among the top downregulated cytokines identified by the analysis were M-CSF, IL-7, and IL-9 (**Figure 4-3B**), all of which were also robustly suppressed by heme in *in vitro* astrocyte and microglia experiments (**Figure 2-3, Figure 2-9, Figure 2-10).** Given that M-CSF is known to contribute to microglial activation, recruitment, and phagocytosis of Aβ [210, 211, 227], IL-7 is expressed by reactive microglia and astrocytes [228, 229], and IL-9 can promote immune cell recruitment [230], suppression of these factors by heme *in vivo* further suggests a role for heme in suppressing glial activation and Aβ clearance. Furthermore, minimal *in vivo* modulation these cytokines in response to heme outside of the context of Aβ (**Figure 4-4**) suggests that these effects are Aβ-dependent. While most cytokines that were modulated in the presence of heme were downregulated, LV1 identified that IP-10 on its own was inversely correlated with the heme + $A\beta_{1\text{-}42}$ condition. Since IP-10 was not strongly up- or down-regulated in response to heme + $A\beta_{1\text{-}42}$ *in vitro* (**Figure 2-3, Figure 2-9, Figure 2-10**), it is possible that there are feedback mechanisms apparent exclusively *in vivo* that are responsible for this effect.

Taken together, the cytokine expression profiles produced in response to heme, $A\beta_{1\text{-}42}$, and heme + $A\beta_{1\text{-}42}$ injections were largely consistent with, although less robust than,

in vitro microglia and astrocyte experiments performed in Chapter 2. Both astrocytes and microglia demonstrated robust upregulation of cytokine expression in response to $A\beta_{1-42}$ and suppression of many cytokines in response to co-treatment with equimolar heme *in vitro* (**Figure 2-3, Figure 2-9, Figure 2-10)**. Differences present between *in vitro* and *in vivo* cytokine responses to heme and Aβ may be explained by the presence of multiple cell types *in vivo*. While individual cell types can produce distinct responses in monoculture, cross talk between cell types *in vivo* can dramatically alter responses. For example, astrocytic calcium signaling can be modulated by Aβ [231] and cytokines [232, 233], and can affect microglia responses [234, 235]. Furthermore, microglia can activate astrocytes astrocytes can inhibit microglia via secretion of cytokines and other molecular factors [235, 236]. Finally, neurons can produce cytokines in response to certain pathological conditions, further contributing to complex signaling mechanisms distinct from *in vitro* conditions [227, 237-239].

Interestingly, immunohistochemistry revealed that *in vivo*, activated astrocytes are more strongly recruited to $A\beta_{1-42}$ injection sites at 4 day and 7 day time points than microglia (**Figure 4-5, Figure 4-6, Figure 4-7**), suggesting that the cytokine responses observed may be predominantly secreted by astrocytes. This finding is surprising, since microglia are widely acknowledged as the primary immune cells of the brain [240]. However, since microglia typically respond more rapidly to injury and astrocytes at later recovery stages [235, 241, 242], it is plausible that microglial activity is robust immediately after injection (ie. within 24 hours), and that astrocytic responses dominate after several days. These findings further support the role for astrocytes in mediating neuroinflammation in AD.

Having earlier determined that heme suppresses scavenger activity of astrocytes and microglia *in vitro* (**Figure 2-7, Figure 2-12**), we hypothesized that Aβ clearance would be suppressed *in vivo* in the presence of heme. Indeed, we found that injecting Aβ into the cortex with equimolar heme significantly increased Aβ burden 7 days after injection, compared to injection of Aβ alone (**Figure 4-9, Figure 4-10**). This suggests that *in vivo* inhibition of Aβ clearance mechanisms in the presence of heme, likely by astrocytes given their recruitment to the injection site and engulfment of injected Aβ (**Figure 4-5, Figure 4-6**). As discovered in our earlier *in vitro* experiments, suppression of scavenger receptor expression, specifically CD36, in response to heme could contribute to this reduction in Aβ uptake by astrocytes (**Figure 2-7**). Taken together, these findings suggest that heme may contribute to the glial fatigue that is observed in AD [61, 64].

Although heme is well established to be upregulated in AD tissues [78], the mechanisms through which this occurs are still unclear. While leakage of brain vasculature is likely a strong contributor, upregulation of intracellular heme synthesis is also suspected to contribute to elevated heme levels in AD [84]. Thus, to determine specifically how elevated heme synthesis can alter neuroinflammatory conditions, we depleted heme using the heme synthesis inhibitor, SA. Daily injection of SA for 14 days significantly reduced heme in the cortex of the brain as well as in the liver (**Figure 4-11**), which is one of the primary heme synthesis organs [243]. Remarkably, PLSDA analysis revealed that heme depletion via SA treatment robustly upregulated expression of a profile of cytokines (**Figure 4-12**). Moreover, cytokines were similarly upregulated when SA was delivered via drinking water for 14 days (**Figure 4-13**). Top correlates with SA treatment using both delivery methods include IL-6, MCP-1, M-CSF, MIP-1β, G-CSF, and GM-CSF and are

well known for their highly chemotactic properties [210-216]. This strong upregulation of chemotactic factors, which function in recruiting immune cells, suggests that suppressing heme synthesis could upregulate activation and recruitment of astrocytes and microglia, ultimately contributing to increased clearance of Aβ in an AD environment.

The Akt/mTOR pathway is known to be involved in regulating a number of critical immune functions, including cytokine expression, and was found to be robustly modulated by intra- and extra-cellular heme in Chapter 3. Therefore, we sought to extend this analysis *in vivo* and quantified Akt/mTOR pathway signaling in response to 14-day daily SA injection. PLSDA revealed significant suppression of Akt/mTOR pathway signaling with SA treatment (**Figure 4-14**). Interestingly, these findings were in contrast to *in vitro* astrocyte signaling experiments, which conversely showed that *increasing* intracellular labile heme using ALA suppressed Akt/mTOR signaling (**Figure 3-10**). However, our *in vitro* studies clearly identified that heme-driven Akt/mTOR signaling is rapid and highly dynamic (**Figure 3-7**). Since *in vivo* Akt/mTOR signaling was quantified after a period of 14 days, it is conceivable that feedback mechanisms led to long-term suppression of Akt/mTOR signaling, but that upregulation may have occurred at earlier time points, triggering a cascade of signaling events that led to cytokine upregulation. Additionally, mTOR was previously found to regulate HO-1 expression in astrocytes (**Figure 3-14**), which typically has anti-inflammatory functions, Suppression of Akt/mTOR signaling by SA could downregulate HO-1 expression, thereby contributing to increased cytokine expression indirectly. Alternatively, cytokine upregulatation may have occurred through mechanisms independent of the Akt/mTOR pathway.

Moreover, since phospho-protein signals were quantified from bulk tissue, they are representative of the combined responses of multiple cell types in the brain. Various cell types can have distinct signaling responses to the same stimuli, as evident by differences in astrocytic and neuronal Akt/mTOR signaling dynamics in response to exogenous heme (**Figure 3-1, Figure A-**).

Altogether, our data indicate that heme is a potent modulator of neuroinflammation *in vivo,* both via by both Aβ-independent and Aβ-dependent mechanisms. Heme-driven neuroinflammatory signaling could contribute to glial fatigue and suppression of glial activation, thereby exacerbating amyloid pathogenesis. Due to vascular leakage in AD, implications of heme signaling are particularly pertinent to the build-up of Aβ on vascular walls [176]. Lack of clearance of Aβ on vascular walls could contribute to aggravated BBB breakdown, ultimately creating a cycle where heme pathology and Aβ pathology exacerbate each other and worsen AD pathogenesis.

CHAPTER 5. CONCLUSION

The prevalence of AD is rapidly increasing, yet we still lack effective means by which to halt or slow disease progression. Repeated failures of clinical trials targeting Aβ have brought to light that AD pathogenesis is complex and multifaceted, involving the contribution of many pathological events. Thus, successful therapeutic strategies will likely involve simultaneously targeting multiple pathologies that manifest during the course of the disease. Along these lines, neuroinflammation is emerging as a prominent aspect of AD, yet whether it is beneficial or deleterious remains a matter of debate. Furthermore, the molecular factors which could be involved in modulating that balance remain poorly understood.

Hb and its cofactor heme are gaining importance for their roles in modulating AD pathology. These factors have both been shown to be elevated in AD, likely due to a combination of extravasation of red blood cells through leaky brain vasculature [75] and excess production of these factors by neurons and glial cells [76, 79, 84]. In addition to their oxygen-carrying roles, heme and Hb have potent immunomodulatory and cell signaling functions [95-97]. However, to date, these roles have not been characterized in the context of the brain. Given that heme and Hb also physically binds the inflammatory AD hallmark protein Aβ, they may play significant roles in modulating the neuroinflammatory environment in AD. The work described in this dissertation sought to address this gap and improve the current understanding of the neuroinflammatory signaling roles of these factors in the context of AD.

5.1 Major contributions

This work identified unique roles of heme and Hb in modulating the neuroimmune environment in the context of AD, using both *in vitro* and *in vivo* models. We began by broadly characterizing the effects of heme and Hb on astrocyte and microglial immune function *in vitro.* Notably, we identified that heme and Hb suppress astrocyte and microglial activation in both Aβ-dependent and Aβ-independent manners. With regards to Aβ-dependent effects, we found that heme and Hb suppress Aβ-induced cytokine protein expression in cultured primary astrocytes and microglia. Moreover, we found that both heme and Hb bind a highly inflammatory HMW Aβ oligomer, which reverses Aβ- induced inflammation. Independently of Aβ, we found that exogenous heme and Hb suppress astrocyte and microglia phagocytosis and astrocytic expression of scavenger receptor CD36.

Given our findings that heme has diverse immunomodulatory effects in astrocytes, this work further identified intracellular signaling pathways heme acts through to exert these effects. We uniquely identified that the PI3K/Akt/mTOR phospho-signaling pathway is robustly modulated by both exogenous heme and intracellular labile heme in astrocytes. Interestingly, using the HS1 heme sensor to monitor heme uptake, we found that exogenous heme and intracellular heme have distinct signaling capabilities, specifically, that exogenous heme upregulates the PI3K/Akt/mTOR pathway while intracellular heme downregulates it. This work is also the first to utilize the HS1 heme sensor [189] as a tool to study heme signaling in the context of the brain. Furthermore, our work demonstrated a link between heme-induced PI3K/Akt/mTOR pathway dysregulation and immune dysfunction in astrocytes. Specifically, we found that mTOR partially regulates CD36 and

HO-1 expression in astrocytes, which are down- and up-regulated upon heme treatment, respectively.

Finally, our work validated the effects of heme on neuroinflammation using *in vivo* mouse models. Paralleling our *in vitro* findings, our data revealed that intracranial injection of heme with Aβ into the cortex suppressed Aβ-induced cytokine protein expression. Moreover, we found that co-injection of heme with Aβ suppresses Aβ clearance *in vivo*, suggesting for the first time *in vivo* that heme may worsen Aβ pathology. Additionally, independently of Aβ, we found that depletion of heme synthesis by SA treatment upregulates cortical cytokine expression. This suggests for the first time the possibility to harness the neuro-immune system by targeting heme synthesis.

Taken together, the cumulative findings of this dissertation delineate numerous roles for heme in modulating neuroinflammation in AD environments. Overall, our data suggest that heme dysregulates inflammatory signaling mechanisms which suppress critical immune functions of both astrocytes and microglia. Most notably, our data indicate that heme may worsen Aβ clearance mechanisms, thus potentially contributing to exacerbated Aβ pathology and cognitive decline in AD. This work sets the stage for heme as a novel therapeutic target for AD and other acute and chronic neuroinflammatory conditions.

5.2 Future directions

This dissertation characterizes how heme and Hb modulated numerous Aβ-dependent and Aβ-independent neuroinflammatory processes *in vitro* and *in vivo*. This work sets the stage for future studies in several different directions both in and out of the

context of AD. With regards to AD, there is much to be learned regarding the effects of heme on neuronal function in AD environments. Hb, heme and HO activity have previously been shown to have important regulatory roles in neurons, particularly in response to stress [91, 244]. Thus, in addition to dysregulating neuroinflammatory processes in AD, heme may be involved in modulating neuronal function and viability in AD, which are ultimately linked to cognitive function. Along these lines, preliminary experiments (Appendix A) have shown that heme can alter neuronal phospho-protein signaling and post-synaptic density expression, suggesting that elevated levels of heme could promote AD pathogenesis through neurodegenerative mechanisms in addition to the neuroinflammatory mechanisms, which are relevant to astrocytes and microglia. Future directions may also interrogate how crosstalk between astrocytes, microglia, and neurons may be disrupted in the presence of heme.

Our work for first time utilizes the HS1 heme sensor to study heme signaling in the context of the brain. The present work demonstrates proof of concept for the utility of the HS1 sensor in studying heme signaling in the brain, using astrocytes as a model, setting the stage for diverse use of this sensor in various cell types and pathological environments. Future studies can utilize HS1 and its variants [189] to conduct elaborate studies regarding heme signaling in AD environments. For example, having demonstrated in Chapter 3 that HS1 can be used to study heme uptake dynamics, future work can employ similar methods to study how factors associated with AD pathology (ie. Aβ) can affect heme uptake and labile heme pools. Particularly of interest is the possibility to study organelle-specific heme signaling in AD environments using HS1 variants [189]. Finally, current work to develop protocols to apply HS1 to histological analysis of brain tissue sections will allow for

imaging of free heme in tissue slices for the first time. Applying this technology to human AD brain tissue sections can allow for powerful studies involving the localization of heme with respect to Aβ plaques, within specific cell types, and within subregions of the brain. Since physiologically relevant concentrations of heme in the brain are currently unknown, optimizing this sensor for this application can lead to profound, quantitative insights into how heme concentrations are altered in the brain in disease.

Further with regard to heme in AD, *in vivo* studies can be translated to transgenic AD mouse models, including the 5XFAD and APP/PS1 models which present both Aβ and neuroinflammatory pathology [217, 218]. The APP/PS1 model specifically has been shown to exhibit elevated levels of Hb, which co-localizes with neurons and glial cells [76, 79], making it a relevant model to these studies. Given that our findings in WT mice showed that heme depletion robustly upregulated cytokine and chemokine expression, it will be important to see whether these findings translate to AD mouse models. Furthermore, whether upregulation of chemotactic factors contributes to increased Aβ clearance in these models remains an open question. Ultimately, findings of decreased Aβ burden in response to heme depletion in AD model mice could define a new paradigm for the development of heme-based therapeutics for AD.

Although the focus of this dissertation was to elucidate the role of heme in AD environments, this work sets the stage for studies on the involvement of heme in brain-related pathologies beyond AD. Heme is implicated in numerous other neuropathological conditions, most notably traumatic brain injury and ischemic stroke which are characterized by blood leakage into the brain and therefore excess exogenous heme [245, 246]. Our findings of robust Akt/mTOR phospho-protein signaling dysregulation in

response to exogenous heme are largely translatable to these scenarios, since they were observed outside of the context of Aβ. Since this pathway is strongly linked to inflammation and immune function, it is possible that heme may have neuroinflammatory consequences in these acute neuropathological conditions as well. Furthermore, our findings that the Akt/mTOR pathway regulates HO-1 expression is particularly relevant to these conditions, in which HO-1 induction is observed [247, 248]. Lastly, our findings of the neuroinflammatory consequences of Aβ and heme physical association may be translatable to Parkinson's disease, which is characterized by the aggregation of α-synuclein protein [249]. Since these aggregates are also neuroinflammatory [250], association between α-synuclein and heme could modulate the neuroinflammatory environment in Parkinson's disease.

Taken together, the work reported in this dissertation paves the way for a myriad of future studies with respect to the neuroimmunomodulatory roles of heme in AD, and other neuropathologies. Given the vast neuroinflammatory and immunomodulatory signaling capabilities of heme reported in this work and others, targeting heme could ultimately be a therapeutic strategy for neurodegenerative conditions.

APPENDIX A. EFFECTS OF HEME ON PRIMARY NEURONS *IN VITRO*

A.1 Neuronal culture methods

Neuron cultures were derived from E14–15 CD1 embryos (Charles River), according to a protocol approved by the Georgia Institute of Technology Institutional Animal Care and Use Committee. Embryo cortices were isolated according to an existing protocol [251] and triturated in plating medium consisting of Neurobasal media (Invitrogen) with 10% FBS, 1% Glutamax (Gibco) and 1% antibiotic/antimycotic solution (Sigma). Cells were plated at a density of $6.5*10^5$ cells/well in poly-d-lysine (Sigma)-coated 6 well plates. Cells were left to attach overnight after which media was changed to Neurobasal media with 2% B-27 supplement (Gibco) and 1% antibiotic/antimycotic solution. After 3 more days in culture, 1 μM cytosine β-D-arabinofuranoside (Sigma) was added to prevent mitosis of non-neuronal cells. Neurons were used for experiments between days 10 and 14 in culture. For conditioning experiments, conditions were applied together with a change of one-half of the medium in each well.

A.2 Results

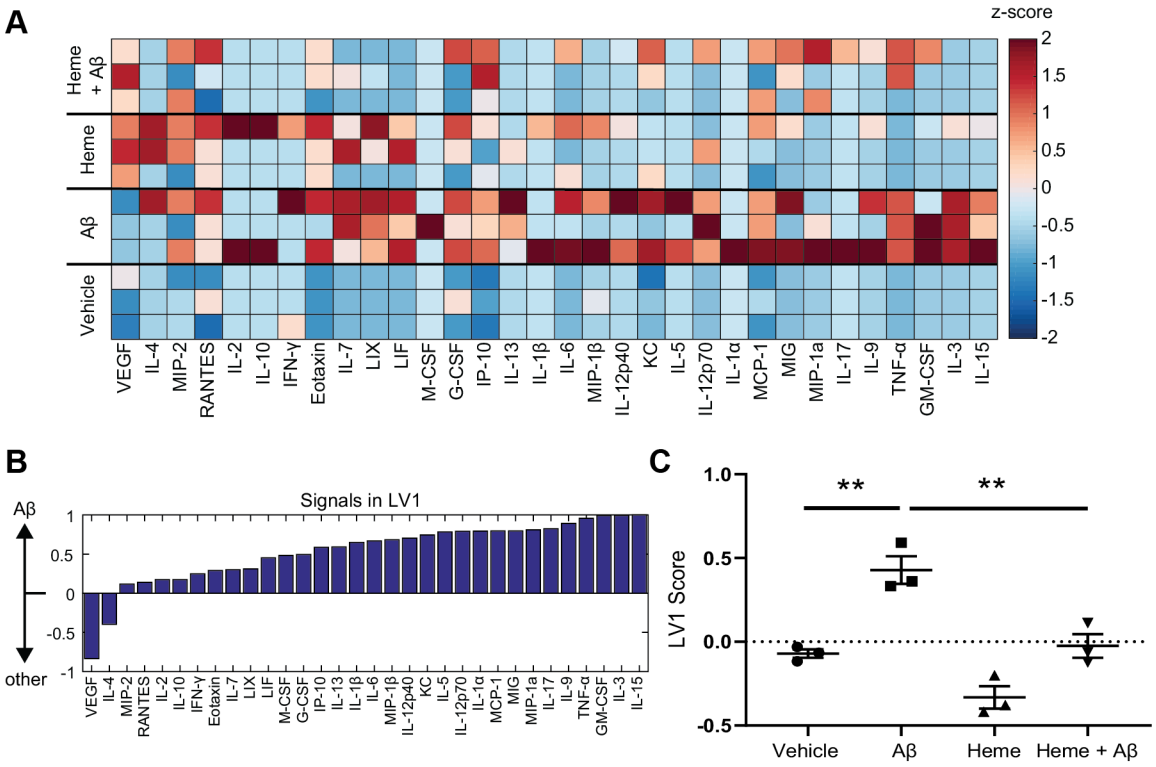

Figure A-1. Neuronal cytokine expression is stimulated by Aβ$_{1-42}$ and suppressed by heme. A. Quantification of 32 cytokines expressed into the medium of primary mouse neuron cultures via Luminex analysis. Each column is z-scored and each row represents an individual well. B. PLDSA identified LV1 which separates Aβ treated neurons from all other groups. C. Scoring each sample on LV1 reveals that Aβ (50 nM) treated neurons are significantly upregulated on LV1 while co-treatment with equimolar heme suppresses expression of this cytokine profile (mean ± SEM, $^{**}p<0.01$; ordinary one-way ANOVA with Sidak's test.)

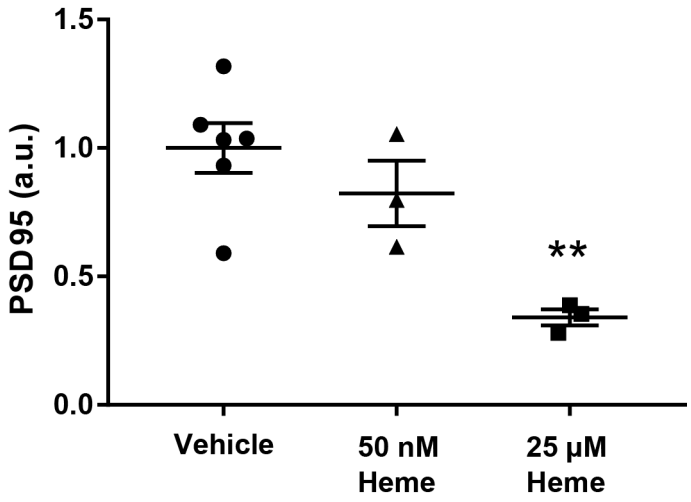

Figure A-2. Postsynaptic density 95 (PSD95) protein expression is significantly reduced in primary mouse neurons after treatment with 25 µM heme for 24 h, as quantified by western blot (mean ± SEM, ; ordinary one-way ANOVA with Dunnett's test).

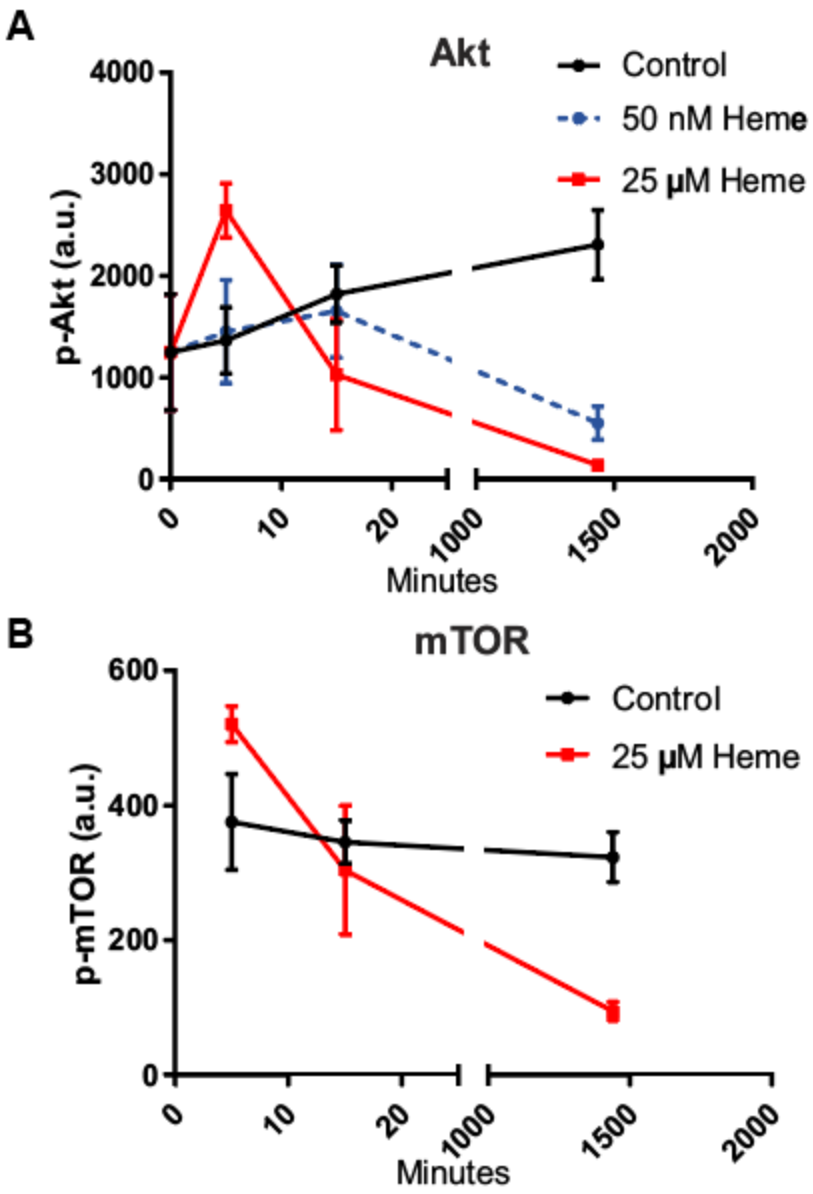

Figure A-3. Akt and mTOR phosphorylation time course in response to 25 µM heme. A. Heme upregulates Akt phosphorylation after 5 minutes but suppresses it after 24 h. B. As in A for mTOR.

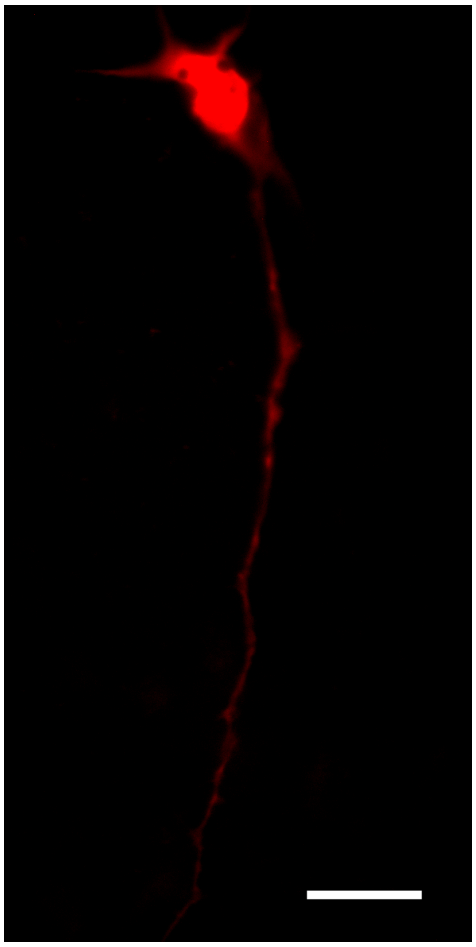

Figure A-4. Primary neuron transfected to express HS1. mKATE2 fluorescence is depicted in red. Scale bar, 20 μM.

APPENDIX B. HEME MODULATES ASTROCYTE LAMP-1 EXPRESSION

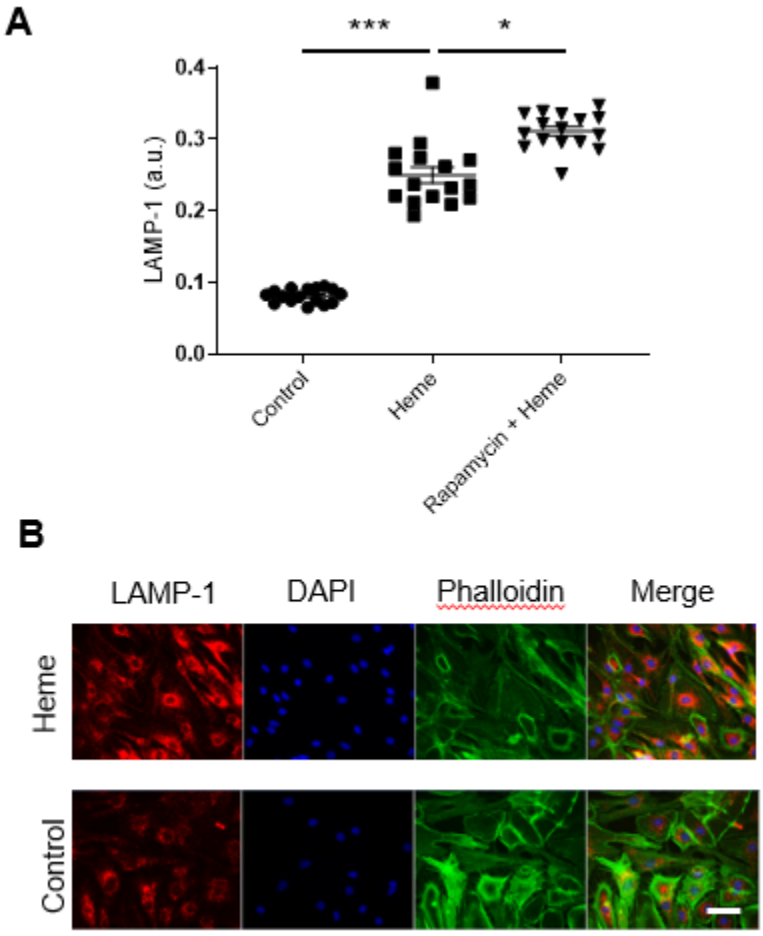

Figure B-1. Heme (25 µM) upregulates LAMP-1 expression in astrocytes. A. Heme upregulates LAMP-1 expression after 72 hours. Co-treatment with 10 nM rapamycin further upregulates LAMP-1 (mean ± SEM, ***p<0.001, *p<0.05, ordinary one-way ANOVA with Sidak's test). B. Representative images of LAMP-1 staining in control and heme treated conditions. Scale bar, 20 µm.

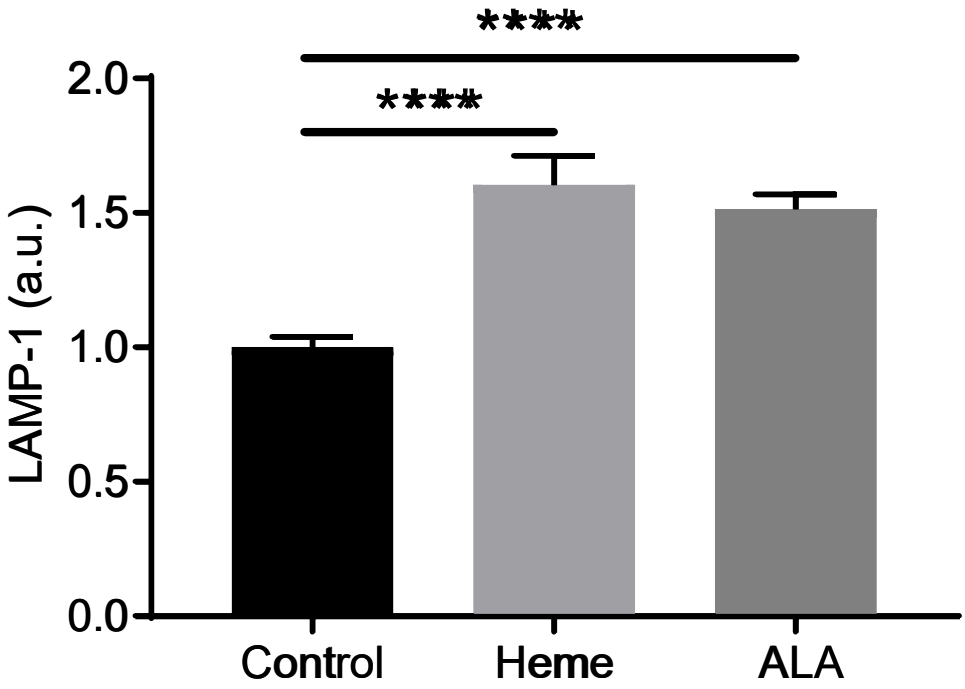

Figure B-2. Heme (25 µM) and ALA upregulate LAMP-1 expression in astrocytes after 72 hours (mean ± SEM, ****p<0.0001, ordinary one-way ANOVA with Dunnett's test).

APPENDIX C. INTRACELLULAR HEME UPREGULATION SUPPRESSES AMYLOID BETA- INDUCED ASTROCYTE CYTOKINE EXPRESSION

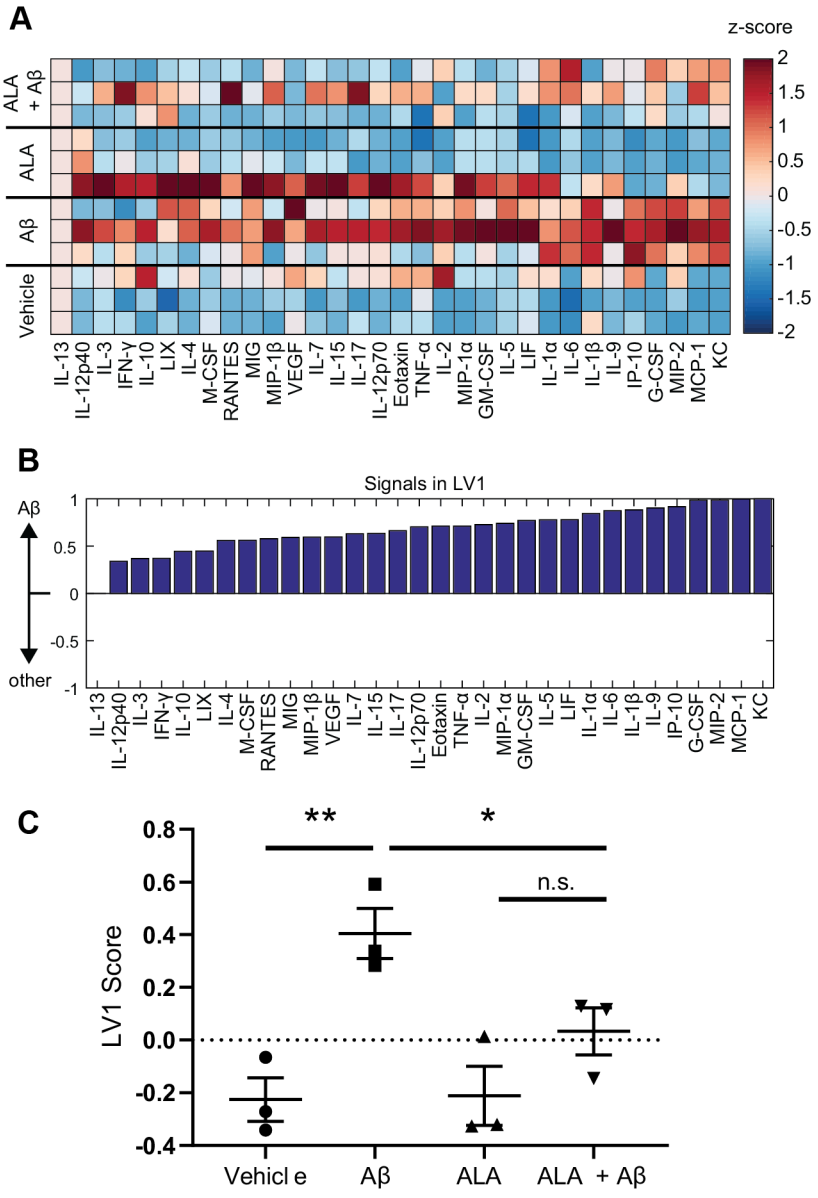

Figure C-1. ALA suppresses Aβ$_{1-42}$-induced cytokine expression in primary mouse astrocytes. A. Quantification of 32 cytokines expressed into the medium of primary mouse astrocyte cultures via Luminex analysis. Each column is z-scored and each row represents an individual sample. B. PLDSA identified LV1 which separates Aβ treated astrocytes

from all other groups. C. Scoring each sample on LV1 reveals that Aβ (50 nM) treated astrocytes are significantly upregulated on LV1 while co-treatment with 800 μM ALA suppresses expression of this cytokine profile (mean ± SEM, *p<0.05, **p<0.01; ordinary one-way ANOVA with Holm-Sidak's test.)

BIBLIOGRAPHY

1. Prince, M., et al., *World Alzheimer Report 2016*. 2016, Alzheimer's Disease International.

2. *2017 ALZHEIMER'S DISEASE FACTS AND FIGURES.* 2017, Alzheimer's Association.

3. Collaborators, G.B.D.D., *Global, regional, and national burden of Alzheimer's disease and other dementias, 1990-2016: a systematic analysis for the Global Burden of Disease Study 2016.* Lancet Neurol, 2019. **18**(1): p. 88-106.

4. Piaceri, I., B. Nacmias, and S. Sorbi, *Genetics of familial and sporadic Alzheimer's disease.* Front Biosci (Elite Ed), 2013. **5**: p. 167-77.

5. Gatz, J.L., et al., *Do depressive symptoms predict Alzheimer's disease and dementia?* J Gerontol A Biol Sci Med Sci, 2005. **60**(6): p. 744-7.

6. Faden, A.I. and D.J. Loane, *Chronic neurodegeneration after traumatic brain injury: Alzheimer disease, chronic traumatic encephalopathy, or persistent neuroinflammation?* Neurotherapeutics, 2015. **12**(1): p. 143-50.

7. Launer, L.J., et al., *Midlife blood pressure and dementia: the Honolulu-Asia aging study.* Neurobiol Aging, 2000. **21**(1): p. 49-55.

8. Jendroska, K., et al., *Ischemic stress induces deposition of amyloid beta immunoreactivity in human brain.* Acta Neuropathol, 1995. **90**(5): p. 461-6.

9. Leibson, C.L., et al., *Risk of dementia among persons with diabetes mellitus: a population-based cohort study.* Am J Epidemiol, 1997. **145**(4): p. 301-8.

10. Tysiewicz-Dudek, M., F. Pietraszkiewicz, and B. Drozdzowska, *Alzheimer's disease and osteoporosis: common risk factors or one condition predisposing to the other?* Ortop Traumatol Rehabil, 2008. **10**(4): p. 315-23.

11. Bayer, A.U., F. Ferrari, and C. Erb, *High occurrence rate of glaucoma among patients with Alzheimer's disease.* Eur Neurol, 2002. **47**(3): p. 165-8.

12. Abbott, N.J., et al., *Structure and function of the blood-brain barrier.* Neurobiol Dis, 2010. **37**(1): p. 13-25.

13. Villemagne, V.L., et al., *Amyloid beta deposition, neurodegeneration, and cognitive decline in sporadic Alzheimer's disease: a prospective cohort study.* Lancet Neurol, 2013. **12**(4): p. 357-67.

14. Hardy, J. and D.J. Selkoe, *The amyloid hypothesis of Alzheimer's disease: progress and problems on the road to therapeutics.* Science, 2002. **297**(5580): p. 353-6.

15. Musiek, E.S. and D.M. Holtzman, *Three dimensions of the amyloid hypothesis: time, space and 'wingmen'.* Nat Neurosci, 2015. **18**(6): p. 800-6.

16. Thal, D.R., et al., *Cerebral amyloid angiopathy and its relationship to Alzheimer's disease.* Acta Neuropathol, 2008. **115**(6): p. 599-609.

17. Selkoe, D.J. and J. Hardy, *The amyloid hypothesis of Alzheimer's disease at 25 years.* EMBO Mol Med, 2016. **8**(6): p. 595-608.

18. Estus, S., et al., *Aggregated amyloid-beta protein induces cortical neuronal apoptosis and concomitant "apoptotic" pattern of gene induction.* J Neurosci, 1997. **17**(20): p. 7736-45.

19. Mattson, M.P., et al., *beta-Amyloid peptides destabilize calcium homeostasis and render human cortical neurons vulnerable to excitotoxicity.* J Neurosci, 1992. **12**(2): p. 376-89.

20. Casley, C.S., et al., *Beta-amyloid fragment 25-35 causes mitochondrial dysfunction in primary cortical neurons.* Neurobiol Dis, 2002. **10**(3): p. 258-67.

21. Caspersen, C., et al., *Mitochondrial Abeta: a potential focal point for neuronal metabolic dysfunction in Alzheimer's disease.* FASEB J, 2005. **19**(14): p. 2040-1.

22. Palop, J.J. and L. Mucke, *Amyloid-beta-induced neuronal dysfunction in Alzheimer's disease: from synapses toward neural networks.* Nat Neurosci, 2010. **13**(7): p. 812-8.

23. Honig, L.S., et al., *Trial of Solanezumab for Mild Dementia Due to Alzheimer's Disease.* N Engl J Med, 2018. **378**(4): p. 321-330.

24. van Dyck, C.H., *Anti-Amyloid-beta Monoclonal Antibodies for Alzheimer's Disease: Pitfalls and Promise.* Biol Psychiatry, 2018. **83**(4): p. 311-319.

25. Mehta, D., et al., *Why do trials for Alzheimer's disease drugs keep failing? A discontinued drug perspective for 2010-2015.* Expert Opin Investig Drugs, 2017. **26**(6): p. 735-739.

26. Salloway, S., et al., *Two phase 3 trials of bapineuzumab in mild-to-moderate Alzheimer's disease.* N Engl J Med, 2014. **370**(4): p. 322-33.

27. Rinne, J.O., et al., *11C-PiB PET assessment of change in fibrillar amyloid-beta load in patients with Alzheimer's disease treated with bapineuzumab: a phase 2, double-blind, placebo-controlled, ascending-dose study.* Lancet Neurol, 2010. **9**(4): p. 363-72.

28. Blennow, K., et al., *Effect of immunotherapy with bapineuzumab on cerebrospinal fluid biomarker levels in patients with mild to moderate Alzheimer disease.* Arch Neurol, 2012. **69**(8): p. 1002-10.

29. Egan, M.F., et al., *Randomized Trial of Verubecestat for Prodromal Alzheimer's Disease.* N Engl J Med, 2019. **380**(15): p. 1408-1420.

30. Sevigny, J., et al., *The antibody aducanumab reduces Abeta plaques in Alzheimer's disease.* Nature, 2016. **537**(7618): p. 50-6.

31. Selkoe, D.J., *Alzheimer disease and aducanumab: adjusting our approach.* Nat Rev Neurol, 2019. **15**(7): p. 365-366.

32. Dilts, E., *Pfizer ends research for new Alzheimer's, Parkinson's drugs*, in *Reuters*. 2018.

33. Adams, B., *Eli Lilly to shutter neuroscience R&D center next year*, in *FierceBiotech*. 2019.

34. Perez-Nievas, B.G., et al., *Dissecting phenotypic traits linked to human resilience to Alzheimer's pathology.* Brain, 2013. **136**(Pt 8): p. 2510-26.

35. Barroeta-Espar, I., et al., *Distinct cytokine profiles in human brains resilient to Alzheimer's pathology.* Neurobiol Dis, 2019. **121**: p. 327-337.

36. Wood, L.B., A.R. Winslow, and S.D. Strasser, *Systems biology of neurodegenerative diseases.* Integr Biol (Camb), 2015. **7**(7): p. 758-75.

37. Patel, N.S., et al., *Inflammatory cytokine levels correlate with amyloid load in transgenic mouse models of Alzheimer's disease.* J Neuroinflammation, 2005. **2**(1): p. 9.

38. Duan, R.S., et al., *Decreased fractalkine and increased IP-10 expression in aged brain of APP(swe) transgenic mice.* Neurochem Res, 2008. **33**(6): p. 1085-9.

39. Johnstone, M., A.J. Gearing, and K.M. Miller, *A central role for astrocytes in the inflammatory response to beta-amyloid; chemokines, cytokines and reactive oxygen species are produced.* J Neuroimmunol, 1999. **93**(1-2): p. 182-93.

40. Meda, L., et al., *Proinflammatory profile of cytokine production by human monocytes and murine microglia stimulated with beta-amyloid[25-35].* J Neuroimmunol, 1999. **93**(1-2): p. 45-52.

41. Smits, H.A., et al., *Amyloid-beta-induced chemokine production in primary human macrophages and astrocytes.* J Neuroimmunol, 2002. **127**(1-2): p. 160-8.

42. Lue, L.F., D.G. Walker, and J. Rogers, *Modeling microglial activation in Alzheimer's disease with human postmortem microglial cultures.* Neurobiol Aging, 2001. **22**(6): p. 945-56.

43. Meda, L., et al., *Beta-amyloid (25-35) peptide and IFN-gamma synergistically induce the production of the chemotactic cytokine MCP-1/JE in monocytes and microglial cells.* J Immunol, 1996. **157**(3): p. 1213-8.

44. Apelt, J. and R. Schliebs, *Beta-amyloid-induced glial expression of both pro- and anti-inflammatory cytokines in cerebral cortex of aged transgenic Tg2576 mice with Alzheimer plaque pathology.* Brain Res, 2001. **894**(1): p. 21-30.

45. Wood, L.B., et al., *Identification of neurotoxic cytokines by profiling Alzheimer's disease tissues and neuron culture viability screening.* Sci Rep, 2015. **5**: p. 16622.

46. Tarkowski, E., et al., *Intrathecal inflammation precedes development of Alzheimer's disease.* J Neurol Neurosurg Psychiatry, 2003. **74**(9): p. 1200-5.

47. Wilberding, A., et al., *Multiple cytokines are involved in the early events leading to the Alzheimer's disease pathology.* Tottori Rinsho Kagaku Kenkyukai Shi, 2008. **1**(2): p. 359-373.

48. Magaki, S., et al., *Increased production of inflammatory cytokines in mild cognitive impairment.* Exp Gerontol, 2007. **42**(3): p. 233-40.

49. Butler, M.P., J.J. O'Connor, and P.N. Moynagh, *Dissection of tumor-necrosis factor-alpha inhibition of long-term potentiation (LTP) reveals a p38 mitogen-activated protein kinase-dependent mechanism which maps to early-but not late-phase LTP.* Neuroscience, 2004. **124**(2): p. 319-26.

50. Chakrabarty, P., et al., *Hippocampal expression of murine TNFalpha results in attenuation of amyloid deposition in vivo.* Mol Neurodegener, 2011. **6**: p. 16.

51. Kiyota, T., et al., *AAV serotype 2/1-mediated gene delivery of anti-inflammatory interleukin-10 enhances neurogenesis and cognitive function in APP+PS1 mice.* Gene Ther, 2012. **19**(7): p. 724-33.

52. Chakrabarty, P., et al., *IL-10 alters immunoproteostasis in APP mice, increasing plaque burden and worsening cognitive behavior.* Neuron, 2015. **85**(3): p. 519-33.

53. Wang, P., et al., *VEGF-induced angiogenesis ameliorates the memory impairment in APP transgenic mouse model of Alzheimer's disease.* Biochem Biophys Res Commun, 2011. **411**(3): p. 620-6.

54. Chakrabarty, P., et al., *Hippocampal expression of murine IL-4 results in exacerbation of amyloid deposition.* Mol Neurodegener, 2012. **7**: p. 36.

55. Lyons, A., et al., *IL-4 attenuates the neuroinflammation induced by amyloid-beta in vivo and in vitro.* J Neurochem, 2007. **101**(3): p. 771-81.

56. Wyss-Coray, T., et al., *Adult mouse astrocytes degrade amyloid-beta in vitro and in situ.* Nat Med, 2003. **9**(4): p. 453-7.

57. Shao, Y., M. Gearing, and S.S. Mirra, *Astrocyte-apolipoprotein E associations in senile plaques in Alzheimer disease and vascular lesions: a regional immunohistochemical study.* J Neuropathol Exp Neurol, 1997. **56**(4): p. 376-81.

58. Nicoll, J.A. and R.O. Weller, *A new role for astrocytes: beta-amyloid homeostasis and degradation.* Trends Mol Med, 2003. **9**(7): p. 281-2.

59. Pihlaja, R., et al., *Transplanted astrocytes internalize deposited beta-amyloid peptides in a transgenic mouse model of Alzheimer's disease.* Glia, 2008. **56**(2): p. 154-63.

60. Nagele, R.G., et al., *Astrocytes accumulate A beta 42 and give rise to astrocytic amyloid plaques in Alzheimer disease brains.* Brain Res, 2003. **971**(2): p. 197-209.

61. Thal, D.R., *The role of astrocytes in amyloid beta-protein toxicity and clearance.* Exp Neurol, 2012. **236**(1): p. 1-5.

62. Liddelow, S.A., et al., *Neurotoxic reactive astrocytes are induced by activated microglia.* Nature, 2017. **541**(7638): p. 481-487.

63. Simard, A.R., et al., *Bone marrow-derived microglia play a critical role in restricting senile plaque formation in Alzheimer's disease.* Neuron, 2006. **49**(4): p. 489-502.

64. Hickman, S.E., E.K. Allison, and J. El Khoury, *Microglial Dysfunction and Defective β-Amyloid Clearance Pathways in Aging Alzheimer's Disease Mice.* The Journal of Neuroscience, 2008. **28**(33): p. 8354-8360.

65. Krabbe, G., et al., *Functional impairment of microglia coincides with Beta-amyloid deposition in mice with Alzheimer-like pathology.* PLoS One, 2013. **8**(4): p. e60921.

66. Daneman, R. and A. Prat, *The blood-brain barrier.* Cold Spring Harb Perspect Biol, 2015. **7**(1): p. a020412.

67. Chen, Y. and L. Liu, *Modern methods for delivery of drugs across the blood-brain barrier.* Adv Drug Deliv Rev, 2012. **64**(7): p. 640-65.

68. Sweeney, M.D., A.P. Sagare, and B.V. Zlokovic, *Blood-brain barrier breakdown in Alzheimer disease and other neurodegenerative disorders.* Nat Rev Neurol, 2018. **14**(3): p. 133-150.

69. Starr, J.M., et al., *Blood-brain barrier permeability in Alzheimer's disease: a case-control MRI study.* Psychiatry Res, 2009. **171**(3): p. 232-41.

70. van de Haar, H.J., et al., *Blood-Brain Barrier Leakage in Patients with Early Alzheimer Disease.* Radiology, 2016. **281**(2): p. 527-535.

71. Iturria-Medina, Y., et al., *Early role of vascular dysregulation on late-onset Alzheimer's disease based on multifactorial data-driven analysis.* Nat Commun, 2016. **7**: p. 11934.

72. Hartz, A.M., et al., *Amyloid-beta contributes to blood-brain barrier leakage in transgenic human amyloid precursor protein mice and in humans with cerebral amyloid angiopathy.* Stroke, 2012. **43**(2): p. 514-23.

73. Anthea M, H.J., McLaughlin C W, Johnson S, Warner M Q, LaHart D, Wright J D, *Human Biology and Health*. 1993, Englewood Cliffs, New Jersey: Prentice Hall.

74. Berg JM, T.J., Stryer L., *Biochemistry. 5th edition.* 2002, New York: W H Freeman.

75. Flemmig, J., M. Zamocky, and A. Alia, *Amyloid beta and free heme: bloody new insights into the pathogenesis of Alzheimer's disease.* Neural Regen Res, 2018. **13**(7): p. 1170-1174.

76. Chuang, J.Y., et al., *Interactions between amyloid-beta and hemoglobin: implications for amyloid plaque formation in Alzheimer's disease.* PLoS One, 2012. **7**(3): p. e33120.

77. Seyfried, N.T., et al., *A Multi-network Approach Identifies Protein-Specific Co-expression in Asymptomatic and Symptomatic Alzheimer's Disease.* Cell Syst, 2017. **4**(1): p. 60-72 e4.

78. Atamna, H. and W.H. Frey, 2nd, *A role for heme in Alzheimer's disease: heme binds amyloid beta and has altered metabolism.* Proc Natl Acad Sci U S A, 2004. **101**(30): p. 11153-8.

79. Wu, C.-W., et al., *Hemoglobin promotes Aβ oligomer formation and localizes in neurons and amyloid deposits.* Neurobiology of Disease, 2004. **17**(3): p. 367-377.

80. Slemmon, J., et al., *Increased levels of hemoglobin-derived and other peptides in Alzheimer's disease cerebellum.* The Journal of Neuroscience, 1994. **14**(4): p. 2225-2235.

81. Ahn, K.C., et al., *Characterization of Impaired Cerebrovascular Structure in APP/PS1 Mouse Brains.* Neuroscience, 2018. **385**: p. 246-254.

82. Atamna, H. and K. Boyle, *Amyloid-beta peptide binds with heme to form a peroxidase: relationship to the cytopathologies of Alzheimer's disease.* Proc Natl Acad Sci U S A, 2006. **103**(9): p. 3381-6.

83. Atamna, H., W.H. Frey, 2nd, and N. Ko, *Human and rodent amyloid-beta peptides differentially bind heme: relevance to the human susceptibility to Alzheimer's disease.* Arch Biochem Biophys, 2009. **487**(1): p. 59-65.

84. Pramanik, D. and S.G. Dey, *Active site environment of heme-bound amyloid beta peptide associated with Alzheimer's disease.* J Am Chem Soc, 2011. **133**(1): p. 81-7.

85. Saha, D., et al., *Hemoglobin expression in nonerythroid cells: novel or ubiquitous?* Int J Inflam, 2014. **2014**: p. 803237.

86. Schelshorn, D.W., et al., *Expression of hemoglobin in rodent neurons.* J Cereb Blood Flow Metab, 2009. **29**(3): p. 585-95.

87. Biagioli, M., et al., *Unexpected expression of alpha- and beta-globin in mesencephalic dopaminergic neurons and glial cells.* Proc Natl Acad Sci U S A, 2009. **106**(36): p. 15454-9.

88. Richter, F., et al., *Neurons express hemoglobin alpha- and beta-chains in rat and human brains.* J Comp Neurol, 2009. **515**(5): p. 538-47.

89. Mense, S.M. and L. Zhang, *Heme: a versatile signaling molecule controlling the activities of diverse regulators ranging from transcription factors to MAP kinases.* Cell Res, 2006. **16**(8): p. 681-92.

90. Chiabrando, D., et al., *Unraveling the Role of Heme in Neurodegeneration.* Front Neurosci, 2018. **12**: p. 712.

91. Smith, A.G., E.L. Raven, and T. Chernova, *The regulatory role of heme in neurons.* Metallomics, 2011. **3**(10): p. 955-62.

92. Wang, D., et al., *Overexpression of heme oxygenase 1 causes cognitive decline and affects pathways for tauopathy in mice.* J Alzheimers Dis, 2015. **43**(2): p. 519-34.

93. Sung, H.Y., et al., *Amyloid Beta-Mediated Hypomethylation of Heme Oxygenase 1 Correlates with Cognitive Impairment in Alzheimer's Disease.* PLoS One, 2016. **11**(4): p. e0153156.

94. Xing, S., et al., *Early induction of oxidative stress in a mouse model of Alzheimer's disease with heme oxygenase activity.* Mol Med Rep, 2014. **10**(2): p. 599-604.

95. Belcher, J.D., et al., *Heme triggers TLR4 signaling leading to endothelial cell activation and vaso-occlusion in murine sickle cell disease.* Blood, 2014. **123**(3): p. 377-90.

96. Lin, S., et al., *Heme activates TLR4-mediated inflammatory injury via MyD88/TRIF signaling pathway in intracerebral hemorrhage.* J Neuroinflammation, 2012. **9**: p. 46.

97. Figueiredo, R.T., et al., *Characterization of heme as activator of Toll-like receptor 4.* J Biol Chem, 2007. **282**(28): p. 20221-9.

98. Graca-Souza, A.V., et al., *Neutrophil activation by heme: implications for inflammatory processes.* Blood, 2002. **99**(11): p. 4160-5.

99. Zhu, Y., et al., *Heme deficiency interferes with the Ras-mitogen-activated protein kinase signaling pathway and expression of a subset of neuronal genes.* Cell Growth Differ, 2002. **13**(9): p. 431-9.

100. Kim, S.H., C.J. Smith, and L.J. Van Eldik, *Importance of MAPK pathways for microglial pro-inflammatory cytokine IL-1 beta production.* Neurobiol Aging, 2004. **25**(4): p. 431-9.

101. Yao, X., et al., *Heme controls the regulation of protein tyrosine kinases Jak2 and Src.* Biochem Biophys Res Commun, 2010. **403**(1): p. 30-5.

102. Yang, X., et al., *The role of the JAK2-STAT3 pathway in pro-inflammatory responses of EMF-stimulated N9 microglial cells.* J Neuroinflammation, 2010. **7**: p. 54.

103. Shen, J., et al., *Iron metabolism regulates p53 signaling through direct heme-p53 interaction and modulation of p53 localization, stability, and function.* Cell Rep, 2014. **7**(1): p. 180-93.

104. Jayadev, S., et al., *Transcription factor p53 influences microglial activation phenotype.* Glia, 2011. **59**(10): p. 1402-13.

105. Raghuram, S., et al., *Identification of heme as the ligand for the orphan nuclear receptors REV-ERBalpha and REV-ERBbeta.* Nat Struct Mol Biol, 2007. **14**(12): p. 1207-13.

106. Yin, L., et al., *Rev-erbalpha, a heme sensor that coordinates metabolic and circadian pathways.* Science, 2007. **318**(5857): p. 1786-9.

107. Sato, S., et al., *A circadian clock gene, Rev-erbalpha, modulates the inflammatory function of macrophages through the negative regulation of Ccl2 expression.* J Immunol, 2014. **192**(1): p. 407-17.

108. Fonken, L.K., et al., *Microglia inflammatory responses are controlled by an intrinsic circadian clock.* Brain Behav Immun, 2015. **45**: p. 171-9.

109. Lam, M.T., et al., *Rev-Erbs repress macrophage gene expression by inhibiting enhancer-directed transcription.* Nature, 2013. **498**(7455): p. 511-5.

110. Gibbs, J.E., et al., *The nuclear receptor REV-ERBalpha mediates circadian regulation of innate immunity through selective regulation of inflammatory cytokines.* Proc Natl Acad Sci U S A, 2012. **109**(2): p. 582-7.

111. Silva, G., et al., *Oxidized hemoglobin is an endogenous proinflammatory agonist that targets vascular endothelial cells.* J Biol Chem, 2009. **284**(43): p. 29582-95.

112. Paine, A., et al., *Signaling to heme oxygenase-1 and its anti-inflammatory therapeutic potential.* Biochem Pharmacol, 2010. **80**(12): p. 1895-903.

113. Otterbein, L.E., et al., *Carbon monoxide has anti-inflammatory effects involving the mitogen-activated protein kinase pathway.* Nat Med, 2000. **6**(4): p. 422-8.

114. Uddin, M.J., et al., *Carbon Monoxide Inhibits Tenascin-C Mediated Inflammation via IL-10 Expression in a Septic Mouse Model.* Mediators Inflamm, 2015. **2015**: p. 613249.

115. Zhu, H., et al., *Bilirubin protects grafts against nonspecific inflammation-induced injury in syngeneic intraportal islet transplantation.* Exp Mol Med, 2010. **42**(11): p. 739-48.

116. Wu, J., et al., *Bilirubin derived from heme degradation suppresses MHC class II expression in endothelial cells.* Biochem Biophys Res Commun, 2005. **338**(2): p. 890-6.

117. Li, Q., et al., *Gene transfer of inducible nitric oxide synthase affords cardioprotection by upregulating heme oxygenase-1 via a nuclear factor-{kappa}B-dependent pathway.* Circulation, 2009. **120**(13): p. 1222-30.

118. Ricchetti, G.A., L.M. Williams, and B.M. Foxwell, *Heme oxygenase 1 expression induced by IL-10 requires STAT-3 and phosphoinositol-3 kinase and is inhibited by lipopolysaccharide.* J Leukoc Biol, 2004. **76**(3): p. 719-26.

119. Martin, D., et al., *Regulation of heme oxygenase-1 expression through the phosphatidylinositol 3-kinase/Akt pathway and the Nrf2 transcription factor in response to the antioxidant phytochemical carnosol.* J Biol Chem, 2004. **279**(10): p. 8919-29.

120. Ogawa, K., et al., *Heme mediates derepression of Maf recognition element through direct binding to transcription repressor Bach1.* EMBO J, 2001. **20**(11): p. 2835-43.

121. Abraham, N.G. and G. Drummond, *CD163-Mediated hemoglobin-heme uptake activates macrophage HO-1, providing an antiinflammatory function.* Circ Res, 2006. **99**(9): p. 911-4.

122. Moestrup, S.K. and H.J. Moller, *CD163: a regulated hemoglobin scavenger receptor with a role in the anti-inflammatory response.* Ann Med, 2004. **36**(5): p. 347-54.

123. Nielsen, M.J., H.J. Moller, and S.K. Moestrup, *Hemoglobin and heme scavenger receptors.* Antioxid Redox Signal, 2010. **12**(2): p. 261-73.

124. Hvidberg, V., et al., *Identification of the receptor scavenging hemopexin-heme complexes.* Blood, 2005. **106**(7): p. 2572-9.

125. Rajagopal, A., et al., *Haem homeostasis is regulated by the conserved and concerted functions of HRG-1 proteins.* Nature, 2008. **453**(7198): p. 1127-31.

126. Duffy, S.P., et al., *The Fowler syndrome-associated protein FLVCR2 is an importer of heme.* Mol Cell Biol, 2010. **30**(22): p. 5318-24.

127. Sankar, S.B., et al., *Heme and hemoglobin suppress amyloid beta-mediated inflammatory activation of mouse astrocytes.* J Biol Chem, 2018. **293**(29): p. 11358-11373.

128. Meda, L., P. Baron, and G. Scarlato, *Glial activation in Alzheimer's disease: the role of Abeta and its associated proteins.* Neurobiol Aging, 2001. **22**(6): p. 885-93.

129. Sofroniew, M.V., *Reactive astrocytes in neural repair and protection.* Neuroscientist, 2005. **11**(5): p. 400-7.

130. Pellerin, L., et al., *Activity-dependent regulation of energy metabolism by astrocytes: an update.* Glia, 2007. **55**(12): p. 1251-62.

131. Eroglu, C. and B.A. Barres, *Regulation of synaptic connectivity by glia.* Nature, 2010. **468**(7321): p. 223-31.

132. Lee, C.Y. and G.E. Landreth, *The role of microglia in amyloid clearance from the AD brain.* J Neural Transm (Vienna), 2010. **117**(8): p. 949-60.

133. Wang, W.Y., et al., *Role of pro-inflammatory cytokines released from microglia in Alzheimer's disease.* Ann Transl Med, 2015. **3**(10): p. 136.

134. Perry, G., et al., *Reactive Oxygen Species Mediate Cellular Damage in Alzheimer Disease.* J Alzheimers Dis, 1998. **1**(1): p. 45-55.

135. Basak, J.M., et al., *Low-density lipoprotein receptor represents an apolipoprotein E-independent pathway of Abeta uptake and degradation by astrocytes.* J Biol Chem, 2012. **287**(17): p. 13959-71.

136. Koistinaho, M., et al., *Apolipoprotein E promotes astrocyte colocalization and degradation of deposited amyloid-beta peptides.* Nat Med, 2004. **10**(7): p. 719-26.

137. Xiao, Q., et al., *Enhancing astrocytic lysosome biogenesis facilitates Abeta clearance and attenuates amyloid plaque pathogenesis.* J Neurosci, 2014. **34**(29): p. 9607-20.

138. El Khoury, J., et al., *Ccr2 deficiency impairs microglial accumulation and accelerates progression of Alzheimer-like disease.* Nat Med, 2007. **13**(4): p. 432-8.

139. Liu, C., et al., *Neuroinflammation in Alzheimer's disease: chemokines produced by astrocytes and chemokine receptors.* Int J Clin Exp Pathol, 2014. **7**(12): p. 8342-55.

140. Galimberti, D., et al., *Intrathecal chemokine synthesis in mild cognitive impairment and Alzheimer disease.* Arch Neurol, 2006. **63**(4): p. 538-43.

141. Chodobski, A., B.J. Zink, and J. Szmydynger-Chodobska, *Blood-brain barrier pathophysiology in traumatic brain injury.* Transl Stroke Res, 2011. **2**(4): p. 492-516.

142. Iadecola, C., *Dangerous leaks: blood-brain barrier woes in the aging hippocampus.* Neuron, 2015. **85**(2): p. 231-3.

143. Cullen, K.M., Z. Kocsi, and J. Stone, *Microvascular pathology in the aging human brain: evidence that senile plaques are sites of microhaemorrhages.* Neurobiol Aging, 2006. **27**(12): p. 1786-96.

144. Fernandez, P.L., et al., *Heme amplifies the innate immune response to microbial molecules through spleen tyrosine kinase (Syk)-dependent reactive oxygen species generation.* J Biol Chem, 2010. **285**(43): p. 32844-51.

145. Simoes, R.L., et al., *Proinflammatory responses of heme in alveolar macrophages: repercussion in lung hemorrhagic episodes.* Mediators Inflamm, 2013. **2013**: p. 946878.

146. Schildge, S., et al., *Isolation and culture of mouse cortical astrocytes.* J Vis Exp, 2013(71).

147. Puschmann, T.B., et al., *Bioactive 3D cell culture system minimizes cellular stress and maintains the in vivo-like morphological complexity of astroglial cells.* Glia, 2013. **61**(3): p. 432-440.

148. Lange, S.C., et al., *Primary cultures of astrocytes: their value in understanding astrocytes in health and disease.* Neurochem Res, 2012. **37**(11): p. 2569-88.

149. Sutton, E.T., et al., *Amyloid-beta peptide induced inflammatory reaction is mediated by the cytokines tumor necrosis factor and interleukin-1.* J Submicrosc Cytol Pathol, 1999. **31**(3): p. 313-23.

150. Eriksson, L., et al., *Multi-and megavariate data analysis*. 2006: Umetrics.

151. Parajuli, B., et al., *GM-CSF increases LPS-induced production of proinflammatory mediators via upregulation of TLR4 and CD14 in murine microglia.* Journal of Neuroinflammation, 2012. **9**(1): p. 268.

152. Zhang, K., et al., *CXCL1 Contributes to β-Amyloid-Induced Transendothelial Migration of Monocytes in Alzheimer's Disease.* PLOS ONE, 2013. **8**(8): p. e72744.

153. Sokolova, A., et al., *Monocyte chemoattractant protein-1 plays a dominant role in the chronic inflammation observed in Alzheimer's disease.* Brain Pathol, 2009. **19**(3): p. 392-8.

154. Shankar, G.M., et al., *Amyloid-beta protein dimers isolated directly from Alzheimer's brains impair synaptic plasticity and memory.* Nat Med, 2008. **14**(8): p. 837-42.

155. Gong, Y., et al., *Alzheimer's disease-affected brain: presence of oligomeric A beta ligands (ADDLs) suggests a molecular basis for reversible memory loss.* Proc Natl Acad Sci U S A, 2003. **100**(18): p. 10417-22.

156. Jones, R.S., et al., *Amyloid-beta-induced astrocytic phagocytosis is mediated by CD36, CD47 and RAGE.* J Neuroimmune Pharmacol, 2013. **8**(1): p. 301-11.

157. Bao, Y., et al., *CD36 is involved in astrocyte activation and astroglial scar formation.* J Cereb Blood Flow Metab, 2012. **32**(8): p. 1567-77.

158. Moore, K.J., et al., *A CD36-initiated signaling cascade mediates inflammatory effects of beta-amyloid.* J Biol Chem, 2002. **277**(49): p. 47373-9.

159. Ni, M. and M. Aschner, *Neonatal rat primary microglia: isolation, culturing, and selected applications.* Curr Protoc Toxicol, 2010. **Chapter 12**: p. Unit 12 17.

160. Nagamoto-Combs, K., J. Kulas, and C.K. Combs, *A novel cell line from spontaneously immortalized murine microglia.* Journal of Neuroscience Methods, 2014. **233**: p. 187-198.

161. Chan, W.Y., S. Kohsaka, and P. Rezaie, *The origin and cell lineage of microglia: new concepts.* Brain Res Rev, 2007. **53**(2): p. 344-54.

162. Heneka, M.T., et al., *Neuroinflammation in Alzheimer's disease.* Lancet Neurol, 2015. **14**(4): p. 388-405.

163. Hampton, D.W., et al., *Cell-mediated neuroprotection in a mouse model of human tauopathy.* J Neurosci, 2010. **30**(30): p. 9973-83.

164. Mantovani, A., et al., *The chemokine system in diverse forms of macrophage activation and polarization.* Trends in Immunology. **25**(12): p. 677-686.

165. Huang, W.-C., et al., *TGF-β1 blockade of microglial chemotaxis toward Aβ aggregates involves SMAD signaling and down-regulation of CCL5.* Journal of Neuroinflammation, 2010. **7**(1): p. 28.

166. Lee, S.C., et al., *GM-CSF promotes proliferation of human fetal and adult microglia in primary cultures.* Glia, 1994. **12**(4): p. 309-18.

167. Griffin, W.S., *Alzheimer's - Looking beyond plaques.* F1000 Med. Rep., 2011. **3**: p. 24.

168. Shaftel, S.S., et al., *Sustained hippocampal IL-1 beta overexpression mediates chronic neuroinflammation and ameliorates Alzheimer plaque pathology.* J Clin Invest, 2007. **117**(6): p. 1595-604.

169. Mills Ko, E., et al., *Deletion of astroglial CXCL10 delays clinical onset but does not affect progressive axon loss in a murine autoimmune multiple sclerosis model.* Journal of Neuroinflammation, 2014. **11**(1): p. 105.

170. Fontaine, R.H., et al., *IL-9/IL-9 receptor signaling selectively protects cortical neurons against developmental apoptosis.* Cell Death Differ, 2008. **15**(10): p. 1542-52.

171. Pulliam, L., D. Moore, and D.C. West, *Human cytomegalovirus induces IL-6 and TNF alpha from macrophages and microglial cells: possible role in neurotoxicity.* J Neurovirol, 1995. **1**(2): p. 219-27.

172. Huell, M., et al., *Interleukin-6 is present in early stages of plaque formation and is restricted to the brains of Alzheimer's disease patients.* Acta Neuropathol, 1995. **89**(6): p. 544-51.

173. Zhang, Y., et al., *An RNA-sequencing transcriptome and splicing database of glia, neurons, and vascular cells of the cerebral cortex.* J Neurosci, 2014. **34**(36): p. 11929-47.

174. Sevenich, L., *Brain-Resident Microglia and Blood-Borne Macrophages Orchestrate Central Nervous System Inflammation in Neurodegenerative Disorders and Brain Cancer.* Front Immunol, 2018. **9**: p. 697.

175. Lambert, M.P., et al., *Diffusible, nonfibrillar ligands derived from Abeta1-42 are potent central nervous system neurotoxins.* Proc Natl Acad Sci U S A, 1998. **95**(11): p. 6448-53.

176. Biron, K.E., et al., *Amyloid triggers extensive cerebral angiogenesis causing blood brain barrier permeability and hypervascularity in Alzheimer's disease.* PLoS One, 2011. **6**(8): p. e23789.

177. Philippidis, P., et al., *Hemoglobin scavenger receptor CD163 mediates interleukin-10 release and heme oxygenase-1 synthesis: antiinflammatory monocyte-macrophage responses in vitro, in resolving skin blisters in vivo, and after cardiopulmonary bypass surgery.* Circ Res, 2004. **94**(1): p. 119-26.

178. Cambos, M., et al., *The IL-12p70/IL-10 interplay is differentially regulated by free heme and hemozoin in murine bone-marrow-derived macrophages.* Int J Parasitol, 2010. **40**(9): p. 1003-12.

179. Min, H., et al., *Heme molecule functions as an endogenous agonist of astrocyte TLR2 to contribute to secondary brain damage after intracerebral hemorrhage.* Mol Brain, 2017. **10**(1): p. 27.

180. Arruda, M.A., et al., *Heme inhibits human neutrophil apoptosis: involvement of phosphoinositide 3-kinase, MAPK, and NF-kappaB.* J Immunol, 2004. **173**(3): p. 2023-30.

181. Fernandes, A., et al., *MAPKs are key players in mediating cytokine release and cell death induced by unconjugated bilirubin in cultured rat cortical astrocytes.* Eur J Neurosci, 2007. **25**(4): p. 1058-68.

182. NaveenKumar, S.K., et al., *Unconjugated Bilirubin exerts Pro-Apoptotic Effect on Platelets via p38-MAPK activation.* Sci Rep, 2015. **5**: p. 15045.

183. Ollinger, R., et al., *Bilirubin inhibits tumor cell growth via activation of ERK.* Cell Cycle, 2007. **6**(24): p. 3078-85.

184. Kaminska, B., *MAPK signalling pathways as molecular targets for anti-inflammatory therapy--from molecular mechanisms to therapeutic benefits.* Biochim Biophys Acta, 2005. **1754**(1-2): p. 253-62.

185. Rothschild, D.E., et al., *Modulating inflammation through the negative regulation of NF-kappaB signaling.* J Leukoc Biol, 2018.

186. Latacz, A., et al., *mTOR Pathway - Novel Modulator of Astrocyte Activity.* Folia Biol (Krakow), 2015. **63**(2): p. 95-105.

187. Weinstock, L.D., et al., *Fingolimod phosphate inhibits astrocyte inflammatory activity in mucolipidosis IV.* Hum Mol Genet, 2018. **27**(15): p. 2725-2738.

188. Hong, Y., et al., *Progesterone suppresses Abeta42-induced neuroinflammation by enhancing autophagy in astrocytes.* Int Immunopharmacol, 2018. **54**: p. 336-343.

189. Hanna, D.A., et al., *Heme dynamics and trafficking factors revealed by genetically encoded fluorescent heme sensors.* Proc Natl Acad Sci U S A, 2016. **113**(27): p. 7539-44.

190. Janes, K.A. and D.A. Lauffenburger, *A biological approach to computational models of proteomic networks.* Curr Opin Chem Biol, 2006. **10**(1): p. 73-80.

191. Gouveia, Z., et al., *Characterization of plasma labile heme in hemolytic conditions.* FEBS J, 2017.

192. Guo, R.X., et al., *17 beta-estradiol activates PI3K/Akt signaling pathway by estrogen receptor (ER)-dependent and ER-independent mechanisms in endometrial cancer cells.* J Steroid Biochem Mol Biol, 2006. **99**(1): p. 9-18.

193. Liang, Z., et al., *CXCR4/CXCL12 axis promotes VEGF-mediated tumor angiogenesis through Akt signaling pathway.* Biochem Biophys Res Commun, 2007. **359**(3): p. 716-22.

194. Han, X., et al., *Insulin Attenuates Beta-Amyloid-Associated Insulin/Akt/EAAT Signaling Perturbations in Human Astrocytes.* Cell Mol Neurobiol, 2016. **36**(6): p. 851-864.

195. Jiang, Z., et al., *Activation of Erk1/2 and Akt in astrocytes under ischemia.* Biochem Biophys Res Commun, 2002. **294**(3): p. 726-33.

196. Wittman, M., et al., *Discovery of a (1H-benzoimidazol-2-yl)-1H-pyridin-2-one (BMS-536924) inhibitor of insulin-like growth factor I receptor kinase with in vivo antitumor activity.* J Med Chem, 2005. **48**(18): p. 5639-43.

197. Qureshi, A.I., et al., *Spontaneous intracerebral hemorrhage.* N Engl J Med, 2001. **344**(19): p. 1450-60.

198. Li, C.Y., et al., *Inhibition of mTOR pathway restrains astrocyte proliferation, migration and production of inflammatory mediators after oxygen-glucose deprivation and reoxygenation.* Neurochem Int, 2015. **83-84**: p. 9-18.

199. Krajcovic, M., et al., *mTOR regulates phagosome and entotic vacuole fission.* Mol Biol Cell, 2013. **24**(23): p. 3736-45.

200. Heras-Sandoval, D., et al., *The role of PI3K/AKT/mTOR pathway in the modulation of autophagy and the clearance of protein aggregates in neurodegeneration.* Cell Signal, 2014. **26**(12): p. 2694-701.

201. Chen, C.H., et al., *The role of the PI3K/Akt/mTOR pathway in glial scar formation following spinal cord injury.* Exp Neurol, 2016. **278**: p. 27-41.

202. Hu, X., et al., *mTOR promotes survival and astrocytic characteristics induced by Pten/AKT signaling in glioblastoma.* Neoplasia, 2005. **7**(4): p. 356-68.

203. Banerjee, S., et al., *Neurofibromatosis-1 regulates mTOR-mediated astrocyte growth and glioma formation in a TSC/Rheb-independent manner.* Proc Natl Acad Sci U S A, 2011. **108**(38): p. 15996-6001.

204. Wu, X., et al., *PI3K/Akt/mTOR signaling regulates glutamate transporter 1 in astrocytes.* Biochem Biophys Res Commun, 2010. **393**(3): p. 514-8.

205. Garwood, C.J., et al., *Insulin and IGF1 signalling pathways in human astrocytes in vitro and in vivo; characterisation, subcellular localisation and modulation of the receptors.* Mol Brain, 2015. **8**: p. 51.

206. Logan, S., et al., *Insulin-like growth factor receptor signaling regulates working memory, mitochondrial metabolism, and amyloid-beta uptake in astrocytes.* Mol Metab, 2018. **9**: p. 141-155.

207. Drewes, G., et al., *Mitogen activated protein (MAP) kinase transforms tau protein into an Alzheimer-like state.* EMBO J, 1992. **11**(6): p. 2131-8.

208. C, O.N., *PI3-kinase/Akt/mTOR signaling: impaired on/off switches in aging, cognitive decline and Alzheimer's disease.* Exp Gerontol, 2013. **48**(7): p. 647-53.

209. Schindelin, J., et al., *Fiji: an open-source platform for biological-image analysis.* Nat Methods, 2012. **9**(7): p. 676-82.

210. Laske, C., et al., *Macrophage colony-stimulating factor (M-CSF) in plasma and CSF of patients with mild cognitive impairment and Alzheimer's disease.* Curr Alzheimer Res, 2010. **7**(5): p. 409-14.

211. Mitrasinovic, O.M., et al., *Macrophage colony stimulating factor promotes phagocytosis by murine microglia.* Neurosci Lett, 2003. **344**(3): p. 185-8.

212. Peterson, P.K., et al., *Differential production of and migratory response to beta chemokines by human microglia and astrocytes.* J Infect Dis, 1997. **175**(2): p. 478-81.

213. Deshmane, S.L., et al., *Monocyte chemoattractant protein-1 (MCP-1): an overview.* J Interferon Cytokine Res, 2009. **29**(6): p. 313-26.

214. Dominguez, F., et al., *CXCL10 and IL-6 induce chemotaxis in human trophoblast cell lines.* Mol Hum Reprod, 2008. **14**(7): p. 423-30.

215. Wang, J.M., et al., *Chemotactic activity of recombinant human granulocyte colony-stimulating factor.* Blood, 1988. **72**(5): p. 1456-60.

216. Shen, L., et al., *Synergy between IL-8 and GM-CSF in reproductive tract epithelial cell secretions promotes enhanced neutrophil chemotaxis.* Cell Immunol, 2004. **230**(1): p. 23-32.

217. Radde, R., et al., *Abeta42-driven cerebral amyloidosis in transgenic mice reveals early and robust pathology.* EMBO Rep, 2006. **7**(9): p. 940-6.

218. Oakley, H., et al., *Intraneuronal beta-amyloid aggregates, neurodegeneration, and neuron loss in transgenic mice with five familial Alzheimer's disease mutations: potential factors in amyloid plaque formation.* J Neurosci, 2006. **26**(40): p. 10129-40.

219. Kane, M.D., et al., *Evidence for seeding of beta -amyloid by intracerebral infusion of Alzheimer brain extracts in beta -amyloid precursor protein-transgenic mice.* J Neurosci, 2000. **20**(10): p. 3606-11.

220. Stepanichev, M.Y., et al., *Single intracerebroventricular administration of amyloid-beta (25-35) peptide induces impairment in short-term rather than long-term memory in rats.* Brain Res Bull, 2003. **61**(2): p. 197-205.

221. Kim, H.G., et al., *Donepezil inhibits the amyloid-beta oligomer-induced microglial activation in vitro and in vivo.* Neurotoxicology, 2014. **40**: p. 23-32.

222. Choi, C., et al., *Multiplex analysis of cytokines in the serum and cerebrospinal fluid of patients with Alzheimer's disease by color-coded bead technology.* J Clin Neurol, 2008. **4**(2): p. 84-8.

223. Krauthausen, M., et al., *CXCR3 promotes plaque formation and behavioral deficits in an Alzheimer's disease model.* J Clin Invest, 2015. **125**(1): p. 365-78.

224. Grammas, P. and R. Ovase, *Inflammatory factors are elevated in brain microvessels in Alzheimer's disease.* Neurobiol Aging, 2001. **22**(6): p. 837-42.

225. Leung, R., et al., *Inflammatory proteins in plasma are associated with severity of Alzheimer's disease.* PLoS One, 2013. **8**(6): p. e64971.

226. Koper, O.M., et al., *CXCL9, CXCL10, CXCL11, and their receptor (CXCR3) in neuroinflammation and neurodegeneration.* Adv Clin Exp Med, 2018. **27**(6): p. 849-856.

227. Yan, S.D., et al., *RAGE-Abeta interactions in the pathophysiology of Alzheimer's disease.* Restor Neurol Neurosci, 1998. **12**(2-3): p. 167-73.

228. Kremlev, S.G., et al., *Angiocidin promotes pro-inflammatory cytokine production and antigen presentation in multiple sclerosis.* J Neuroimmunol, 2008. **194**(1-2): p. 132-42.

229. Jana, M., et al., *Interleukin-12 (IL-12), but not IL-23, induces the expression of IL-7 in microglia and macrophages: implications for multiple sclerosis.* Immunology, 2014. **141**(4): p. 549-63.

230. Zhou, Y., et al., *IL-9 promotes Th17 cell migration into the central nervous system via CC chemokine ligand-20 produced by astrocytes.* J Immunol, 2011. **186**(7): p. 4415-21.

231. Lim, D., et al., *Amyloid beta deregulates astroglial mGluR5-mediated calcium signaling via calcineurin and Nf-kB.* Glia, 2013. **61**(7): p. 1134-45.

232. Ida, T., et al., *Cytokine-induced enhancement of calcium-dependent glutamate release from astrocytes mediated by nitric oxide.* Neurosci Lett, 2008. **432**(3): p. 232-6.

233. Morita, M., et al., *Dual regulation of calcium oscillation in astrocytes by growth factors and pro-inflammatory cytokines via the mitogen-activated protein kinase cascade.* J Neurosci, 2003. **23**(34): p. 10944-52.

234. Schipke, C.G., et al., *Astrocyte Ca2+ waves trigger responses in microglial cells in brain slices.* FASEB J, 2002. **16**(2): p. 255-7.

235. Liu, W., Y. Tang, and J. Feng, *Cross talk between activation of microglia and astrocytes in pathological conditions in the central nervous system.* Life Sci, 2011. **89**(5-6): p. 141-6.

236. Ramirez, G., et al., *Protection of rat primary hippocampal cultures from A beta cytotoxicity by pro-inflammatory molecules is mediated by astrocytes.* Neurobiol Dis, 2005. **19**(1-2): p. 243-54.

237. Sankar, S.B., et al., *Low cerebral blood flow is a non-invasive biomarker of neuroinflammation after repetitive mild traumatic brain injury.* Neurobiol Dis, 2019. **124**: p. 544-554.

238. Li, Y., et al., *S100beta induction of the proinflammatory cytokine interleukin-6 in neurons.* J Neurochem, 2000. **74**(1): p. 143-50.

239. Freidin, M., M.V. Bennett, and J.A. Kessler, *Cultured sympathetic neurons synthesize and release the cytokine interleukin 1 beta.* Proc Natl Acad Sci U S A, 1992. **89**(21): p. 10440-3.

240. Lenz, K.M. and L.H. Nelson, *Microglia and Beyond: Innate Immune Cells As Regulators of Brain Development and Behavioral Function.* Front Immunol, 2018. **9**: p. 698.

241. Frautschy, S.A., et al., *Microglial response to amyloid plaques in APPsw transgenic mice.* Am J Pathol, 1998. **152**(1): p. 307-17.

242. Matsumoto, Y., K. Ohmori, and M. Fujiwara, *Microglial and astroglial reactions to inflammatory lesions of experimental autoimmune encephalomyelitis in the rat central nervous system.* J Neuroimmunol, 1992. **37**(1-2): p. 23-33.

243. Ogun, A.S. and M. Valentine, *Biochemistry, Heme Synthesis*, in *StatPearls*. 2019: Treasure Island (FL).

244. Chen-Roetling, J. and R.F. Regan, *Effect of heme oxygenase-1 on the vulnerability of astrocytes and neurons to hemoglobin.* Biochem Biophys Res Commun, 2006. **350**(1): p. 233-7.

245. Chang, E.F., et al., *Heme regulation in traumatic brain injury: relevance to the adult and developing brain.* J Cereb Blood Flow Metab, 2005. **25**(11): p. 1401-17.

246. Li, R.C., et al., *Heme-hemopexin complex attenuates neuronal cell death and stroke damage.* J Cereb Blood Flow Metab, 2009. **29**(5): p. 953-64.

247. Fukuda, K., et al., *Induction of heme oxygenase-1 (HO-1) in glia after traumatic brain injury.* Brain Res, 1996. **736**(1-2): p. 68-75.

248. Zeynalov, E., et al., *Heme oxygenase 1 is associated with ischemic preconditioning-induced protection against brain ischemia.* Neurobiol Dis, 2009. **35**(2): p. 264-9.

249. Meade, R.M., D.P. Fairlie, and J.M. Mason, *Alpha-synuclein structure and Parkinson's disease - lessons and emerging principles.* Mol Neurodegener, 2019. **14**(1): p. 29.

250. Alvarez-Erviti, L., et al., *Alpha-synuclein release by neurons activates the inflammatory response in a microglial cell line.* Neurosci Res, 2011. **69**(4): p. 337-42.

251. Wu, H.Y., et al., *Amyloid beta induces the morphological neurodegenerative triad of spine loss, dendritic simplification, and neuritic dystrophies through calcineurin activation.* J Neurosci, 2010. **30**(7): p. 2636-49.